CCMS-85-05
VPI-E-85-13

VIRGINIA TECH

CENTER FOR COMPOSITE MATERIALS AND STRUCTURES

The Stress Distribution in Pin-Loaded Orthotropic Plates

E. C. Klang
M. W. Hyer

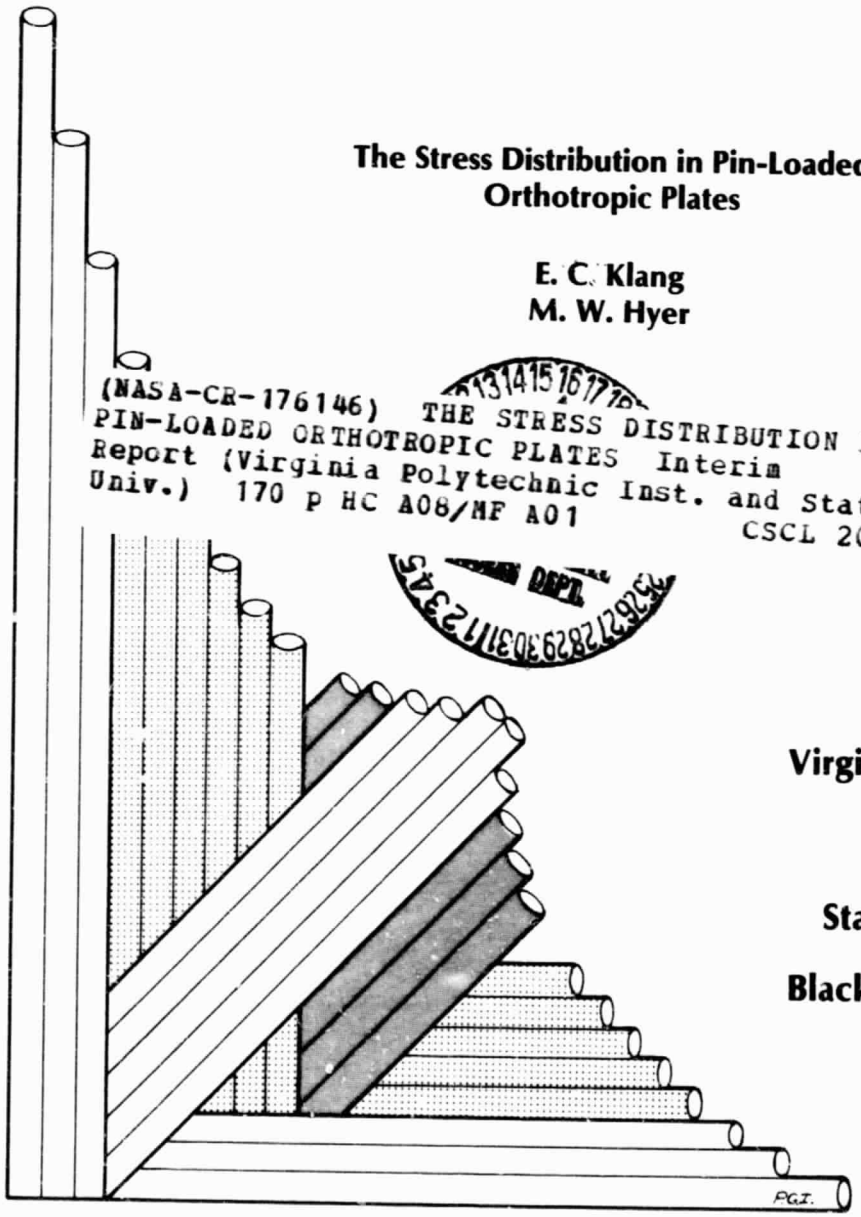

Virginia Polytechnic Institute and State University

Blacksburg, Virginia 24061

College of Engineering

Virginia Polytechnic Institute and State University

Blacksburg, VA 24061

CCMS-85-05
VPI-E-85-13

June, 1985

The Stress Distribution in Pin-Loaded Orthotropic Plates

E. C. Klang[1]
M. W. Hyer[2]

Department of Engineering Science & Mechanics

Interim Report 50
The NASA-Virginia Tech Composites Program

NASA Cooperative Agreement NAG-1-343

Prepared for: Applied Materials Branch
National Aeronautics & Space Administration
Langley Research Center
Hampton, VA 23665

[1]Former Graduate Student, Department of Engineering Science & Mechanics
[2]Professor, Department of Engineering Science & Mechanics

ABSTRACT

The performance of mechanically fastened composite joints was studied. Specifically, a single-bolt connector was modeled as a pin-loaded, infinite plate. The model that was developed used two dimensional complex variable elasticity techniques combined with a boundary collocation procedure to produce solutions for the problem. Through iteration the boundary conditions were satisfied and the stresses in the plate were calculated. Several graphite epoxy laminates were studied. In addition, parameters such as the pin modulus, coefficient of friction, and pin/plate clearance were varied.

Conclusions drawn from this study indicate: 1) The material properties (i.e., laminate configuration) of the plate alter the stress state and, for highly orthotropic materials, the contact stress deviates greatly from the cosinusoidal distribution often assumed; 2) Friction plays a major role in the distribution of stresses in the plate; 3) Reversing the load direction also greatly effects the stress distribution in the plate; 4) Clearance (or interference) fits change the contact angle and thus the location of the peak hoop stress; 5) A rigid pin appears to be a good assumption for typical material systems.

ACKNOWLEDGEMENTS

The work reported on herein constitutes the Ph.D. thesis in Engineering Mechanics at Virginia Polytechnic Institute and State University of the first author. Both authors wish to thank the personnel at the NASA Langley Research Center for their support during the study. Specifically, Mr. Gary Farley and Mr. Donald Baker are to be thanked for their help with using the NASA computing system. Thanks go to Dr. John Crews, the advisor while the first author was at NASA Langley. Finally, the financial support of the NASA-Virginia Tech Composites Program, Cooperative Agreement NCC1-15, is gratefully acknowledged.

TABLE OF CONTENTS

LIST OF TABLES

LIST OF FIGURES

Chapter 1

INTRODUCTION

Background

The joining of two composite laminates in structural applications can be accomplished using several methods. Adhesive bonding and bolted joints are by far the most common. While adhesive bonds are simple to fabricate, they have been found to be weak in shear [1] and have the further disadvantage that they cannot be readily disassembled. Mechanical (bolted) joints, on the other hand, are easy to disassemble but can lead to undesirable stress concentrations. Since mechanical joints are the only form of joining that permit disassembly, they have received much consideration in previous research work.

Figure 1a shows a simple, double-lap joint bolted joint. In this type of joint the load is transferred from the central plate, or inner lap, through a bolt to two support plates, or outer laps. Herein the total load transfered by the joint is denoted by P and it is assumed the two support plates each react one-half the load, or P/2.

The general areas of interest for bolted joints are: determining the stress distribution in the plates; determining the failure load; and determining the failure mode. Of course the answers to these questions depend on the geometry and material properties of the joint. Experimental techniques are quite costly and so various analytical techniques have been proposed in an attempt to answer these questions. To simplify the analysis, it is often assumed that a pin-loaded plate accurately represents the central plate of the joint. By symmetry of the joint, it

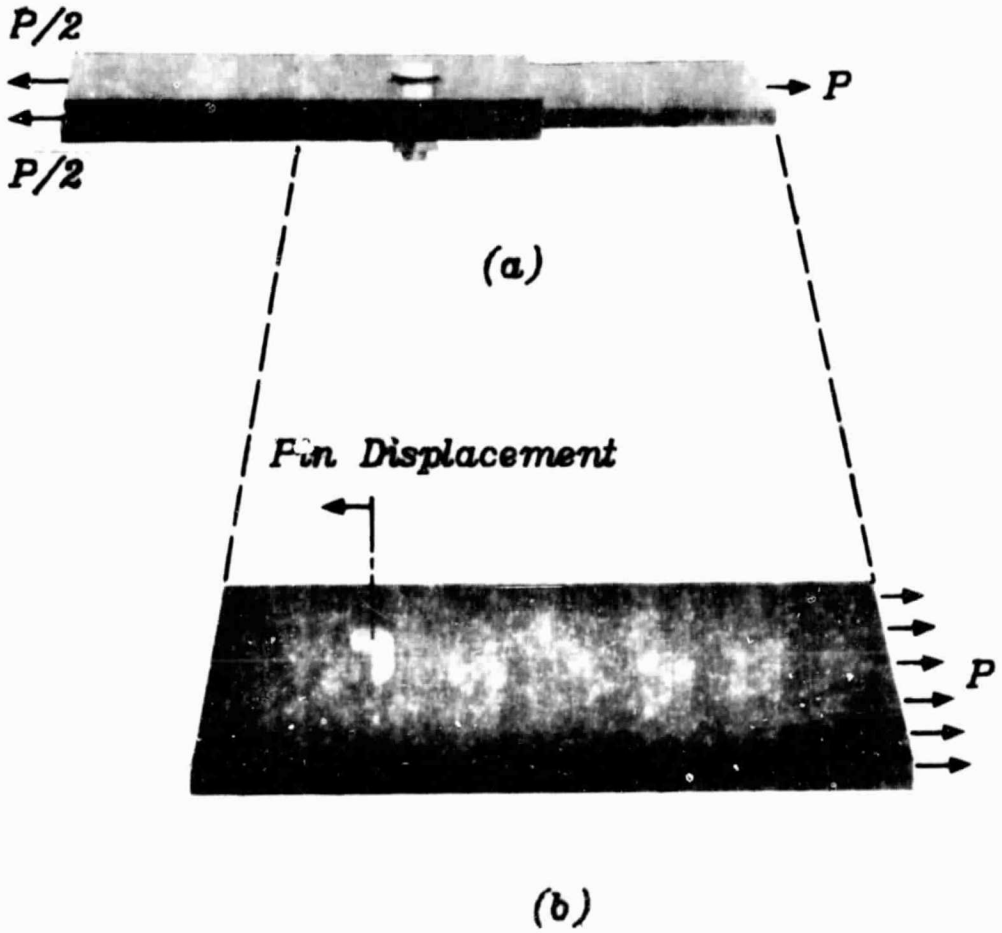

FIG. 1 MECHANICAL JOINT
a) DOUBLE-LAP JOINT
b) PIN-LOADED PLATE

is generally assumed an analysis of the central plate provides answers for the support plates. Figure 1b shows the central plate isolated from the joint. The bolt has been replaced by a simple pin. It is assumed the plate is loaded by a known pin displacement and the effects of this displacement are reacted by a far-field load P. This is the model used by several previous investigators and in the work presented here. However, even though the overall model used here is similar to that of other investigators, the details of the model to be discussed are unique and felt to represent a step forward in analysis. To substantiate this claim, and to provide a general framework for the study, it is prudent to review previous research involving bolted joints.

The analysis of bolted joints has been conducted both analytically and experimentally by many researchers. Analytical investigations have included plane-stress elasticity solutions as well as two- and three-dimensional finite-element analyses. The elasticity solutions generally assume a pinned connection rather than a bolted connection. This is due to the two dimensional limitation of the elasticity solutions. Of course with this assumption, any three-dimensional or through-the-thickness effects are not accounted for. Therefore, bolt clamping force and interlaminar effects in composites, for example, are not accounted for with any of these elasticity solutions. Recently three dimensional finite elements have been used in an attempt to account for the through-the-thickness effects of bolted joints. The following is a summary of some of the work done in the area of bolted joints.

Literature Review

One of the first analytical studies was done by Bickley in 1928 [2]. Using an isotropic elasticity approach, Bickley approximated the contact pressure caused by the pin with a sinusoidal traction applied over one-half the boundary of the hole. This approximation has been proven recently to be a good approximation for isotropic plates if friction in the contact region is neglected as shown by de Jong [3].

In an early effort to introduce finite-width effects, Theocaris [4] used an elasticity solution to model a rigid pin in contact with an isotropic plate. More recently Oplinger and Gandhi [5] used a least-squares boundary collocation technique to introduce finite geometry and multiple-hole configurations into their analysis of pin loaded orthotropic plates. Superposition of two infinite plate solutions was used by de Jong [3] to approximate the finite geometry effects of the orthotropic plates in his study. In a later report [6], de Jong used an infinite plate solution to study the effect that load direction has on orthotropic plates. When the loading direction did not coincide with one of the principle material directions, the shear-coupling effects were found to alter the stress distributions in the plates.

All of the analyses discussed so far neglected friction in the contact region. The friction between the pin and plate is a non-conservative force and is therefore difficult to include in any analysis. In one of their studies Oplinger and Gandhi [7] introduced friction into the contact regions. They produced preliminary results of the limiting cases of slip in the entire contact region and no-slip in the entire

region. Oplinger and Gandhi did find that the presence of friction altered the predicted failure locations in some of the laminates they studied.

Elsewhere, researchers at the Indian Institute of Science have introduced variables such as pin elasticity, friction, and interference (or clearance) fits into the problem for isotropic plates. In the findings of two reports [8, 9], the researchers were ultimately able to analyze an elastic pin inserted in an isotropic plate. The analysis included an interference fit and finite friction in the contact region. The analysis was taken only as far as the onset of separation for the interference fit. A large amount of information was compiled by the researchers and was presented in the form of nondimensionalized plots. In a third report [10], the researchers at the Indian Institute of Science studied the stresses in an orthotropic plate loaded by a rigid, frictionless pin. In this work the researchers focused on the effects of orthotropic elasticity rather than the details of pin/hole interaction.

The most recent elasticity approach including friction in the contact region was published by de Jong [11]. In a modification of his earlier work, de Jong included friction in the slip zone but was forced to use an empirical curve-smoothing procedure in a region which he defined as the "release area". In defining the release area, de Jong relaxed the tangential displacement boundary condition in the no-slip region and applied a smooth, antisymmetric shear stress which was a function of material properties and loading direction. With this analy-

sis de Jong showed that friction had a significant influence on the stresses in a pin-loaded composite panel.

The papers discussed so far that have included friction have done so only for monotonic loading. Reversal of the load direction (e.g., fatigue loading) reveals the nonconservative nature of friction. This complicates the problem significantly. In fact, many researchers have chosen to ignore friction entirely in an effort to make the problem mathematically tractible. In particular, finite-element models are often used without including friction.

In an early orthotropic, two-dimensional finite-element solution, Waszczak and Cruse [12] used an assumed traction boundary condition similar to that chosen by Bickley [2]. Six laminates were analyzed and a distortional energy failure criterion was used to predict failure. The researchers stated that they obtained good agreement with experimental results for the prediction of the failure mode but they found generally poor agreement for the failure load. This study accounted for finite-width and end effects but did not accurately model the tractions in the contact region.

Agarwal [13] used a displacement boundary condition to model a rigid, frictionless, pin-loaded plate. The results of the finite element model were used in conjunction with an average stress failure criterion to predict the failure of single fastener joints. Agreement between analytical and experimental results was found to be better than Waszczak and Cruse [12]. Exceptions to this were the $[\pm 45]_s$ and $[0/90]_s$

laminates. With these laminates the predicted strengths were approximately 50% of the experimentally measured values.

The finite element model by Chang et al. [14] used a traction boundary condition similar to that of Waszczak and Cruse [12]. A modified average stress failure criterion was used to predict the failure of laminates tested by other researchers [12, 13, 15]. The authors noted that all of the predictions were conservative for the $[\pm 45]_s$ and $[0/90]_s$ laminates. In papers [12-14] the stress distributions were not compared with previous solutions. In fact, two of the papers [12, 14] have used traction boundary conditions which other researchers have disputed as being valid for orthotropic materials. This may help explain the incorrect failure predictions of ref. 12 and 14 for the highly orthotropic $[\pm 45]_s$ and $[0/90]_s$ laminates. Despite this problem, improvements on the failure hypothesis seem to have been made.

Crews [16] modeled a flexible pin in an orthotropic plate using a finite element technique. By using a flexible pin the frictionless displacement boundary conditions were satisfied. In general, the results that Crews obtained agreed with those of others [5, 8]. Crews' paper primarily studied the effects of finite geometry on the stress distributions in single pin connectors. No attempt was made to predict failure.

Including friction in any finite element model is difficult and often requires a reformulation of the energy equations for the system to be analyzed. It may be possible to avoid this by using existing finite element techniques which satisfy the boundary conditions indirectly or

approximately. There are few finite element solutions which include friction. However in his Ph.D. dissertation, Wilkinson [17] included friction in his finite element model. He did not compare his solutions with any previously published solutions and many of his results seem to be inconsistent with the findings of other researchers. For example, in a paper published by Rowlands, Rahman, Wilkinson, and Chiang [18], the authors stated that the radial stress component in the contact region is only slightly changed with large changes in the coefficient of friction. This contradicts the findings of earlier researchers [7, 11].

Recently, Matthews, Wong and Chryssafitis [19] developed an isoparametric brick element to analyze the effect of bolt clamping pressure and other through-the-thickness effects. Using only one element through the thickness the authors were unable to account for interlaminar effects. A rigid pin with no friction was used to apply a load to the orthotropic plate. Matthews et al. found that bolt clamping pressure altered the stress distribution in the plate.

Several other researchers [20-23] have used finite element methods to study bolted joints. However, no one, using any method, has successfully treated the case of an elastic pin in an orthotropic plate with finite friction in the contact region. In addition, the effects of pin/hole tolerance have not been addressed for the case of an orthotropic plate. Most researchers have assumed a push-fit pin.

Where analytical methods have failed, experimental investigations have been conducted in an attempt to obtain information. Among the first attempts to experimentally determine the stresses in pin-loaded,

isotropic plates were the studies undertaken independently by Frocht and Hill. Their results were combined in a single paper appearing in 1940 [24] and later in Frocht's book on photoelasticity [25]. Frocht chose to analyze the problem using photoelastic methods while Hill used strain gages. The strain gages used had relatively large gage lengths (0.5" and 1.0") and interpolation was required to find the strains at the edge of the hole. Several diameter-to-width ratios and clearances were tested by both authors and, in general, good agreement between both investigations was found.

Nisida and Saito [26] developed an interferometric method which they used to predict the stresses in a pin-loaded isotropic plate. They presented limited results on the stresses in the plate seemingly to prove that their interferometric method was valid and could be used as a future research tool. They did note, however, that the maximum hoop stress occurred at an angle about ±85° from the loading direction. This seems to confirm the results of many analytical investigations.

Wilkinson, Fuchs, and Rowlands [27] used photomechanical (moiré and holography) techniques to obtain the response of pin-loaded holes in Sitka spruce and Balsa wood. The results were compared with previous analytical work [16, 17] at a limited number of locations in the plate. For the locations that were compared, the agreement between the analytical and experimental studies was found to be good.

Recently Prabhakaran [28] and Hyer and Liu [29] have used orthotropic photoelastic techniques to study the stress distribution in glass-fiber reinforced plastics. While the subject of orthotropic photoelas-

ticity is relatively new, Prabhakaran and Hyer and Liu are using the technique to obtain results for the case of pin-loaded holes. The results should prove invaluable in the verification of the analytical studies discussed earlier.

Several other experimental investigations have studied other aspects of mechanically fastened joints. Lambert and Brailey investigated the importance of friction between the pin and plate [30]. In their experimental analysis, Lambert and Brailey investigated the effects of slip and separation in the interference fit joints of isotropic plates. They found that a coefficient of friction equal to 0.3 existed for the Araldite specimens they used. Alterations in the coefficient of friction were obtained by coating the surfaces with a lubricant. It was found that changing the coefficient of friction significantly changed the shear stress concentration factor.

In studies involving through-the-thickness effects, Quinn and Matthews varied the stacking sequence of 8 ply, quasi-isotropic, glass-epoxy specimens [31]. Eight stacking sequences were tested and the results showed that ultimate failure was dependent on the stacking sequence. The results seemed to suggest that placing the 90° plys near the surface of the panel increased the bearing strength of the pinned joints.

Stockdale and Matthews studied the effect of clamping pressure resulting from torque applied to the bolt in a joint [32]. Two 0/90 laminate configurations were tested with various washer sizes and bolt

torques. Stockdale and Matthews found that large washers and high bolt torques led to improvements in the strength of the joints.

In a related study, Shivakumar and Crews developed an equation to describe the relaxation that occurs in resin-matrix composites where bolt torque is a factor [33]. The authors exposed several 32 ply, graphite-epoxy, bolted joints to various environments for a period of one year. Relaxation of the joints was characterized using a viscoelastic approach. The authors found moderate correlation between experiment and their viscoelastic theory.

To obtain higher performance joints, Eisenmann and Leonhardt [34] have investigated laminate tailoring concepts. By adding more 45 degree plys in the bearing region the authors were able to increase the performance of full scale composite components by as much as 62%.

Other investigators [35-40] have studied various multiple bolt geometries, performance at elevated temperatures, and other factors that effect the performance of mechanical joints in composite materials. These tests have generally been conducted to develop a data base with the hope of developing failure prediction techniques for design purposes.

One of the earliest failure prediction techniques was developed by Whitney and Nuismer for composite specimens with holes or notches [41]. Their hypothesis was based on the idea of a plastic zone found in metals. Whitney and Nuismer assumed that a characteristic dimension existed over which the laminate must be critically stressed in order for failure to occur. This theory is the average stress failure theory

already discussed in the review of the papers by Agarwal [13] and Chang et al. [14]. In these cases the stress distribution was calculated using finite-element models but Garbo and Ogonowski [15] used an elasticity solution for stress predictions. In an extensive study, Garbo and Ogonowski developed an analysis technique which predicted the failure of bolted joints in composite materials. The authors used a complex variable elasticity approach to predict the stresses and a choice of several failure criterion to obtain failure predictions. The elasticity solution, however, relied on an assumed boundary traction similar to that of Bickley [2]. This boundary traction has been shown to be inaccurate for some orthotropic materials. Both de Jong [5] and Crews [16] have shown this. This fact casts some doubt on the technique's ability to predict failure accurately.

Hart-Smith has also developed a capability to predict failure in mechanical joints [42]. Hart-Smith conducted many experimental tests with single and multiple-bolt joints. From these tests he developed a failure hypothesis based on stress concentration factors. The system that Hart-Smith developed relied heavily on a large data base and does not appear to have the flexibility required to handle joint configurations other than those already tested.

Using a somewhat different approach, Collings [43] has developed a failure prediction capability based on his experience with bolted joints. Collings chose a semi-empirical approach which used Bickley's loading on a hole [2] to calculate the contact pressure. However, rather than ignoring friction, Collings used a sinusoidal friction

distribution in the contact area. Thus, Collings' calculation of stresses would seem to be a more accurate representation of actual bolted joints than the representation of Garbo and Ogonowski who ignored friction. The reasoning for some of Collings empirical deductions seem to be based on a strength of materials approach that relies heavily on his experience in the area of bolted joints. Using tensile and compressive strength data obtained from coupon tests, Collings shows good agreement between his failure predictions and experimental results.

All of the failure predictions just discussed required some degree of empirical formulation and they lack the flexibility which is required for general design purposes. The methods do not use accurate descriptions of the stress state in bolted composite laminates. Rather, they make assumptions which are enforced independent of the particular joint geometry or material. Since an accurate description of stresses is the starting point of all failure analyses, it seems that a method dependent on the specific parameters of the joint would be more appropriate. In addition to the accurate prediction of stresses, it seems that a more flexible failure hypothesis needs to be developed. This has been pointed out in other reviews of past research. Recent reviews by Godwin and Matthews [44] as well as Oplinger [45] have been written in the area of bolted composite joints. Godwin and Matthews suggest that a factor of safety of two must be used in current designs and the review by Oplinger demonstrates the complexity of current failure prediction techniques. These reviews indicate that more work is required before a

comprehensive understanding of the performance of composite bolted joints is to be achieved.

Objective

The failure prediction techniques developed to date have lacked the flexibility required for design purposes and, in many cases, they do not predict the failure accurately (e.g., the $[0/90]_s$ and $[\pm 45]_s$ laminates of refs. 12 and 14). For accurate failure predictions for bolted joints, two steps are necessary. First it is necessary to accurately predict the stresses in the joint. Second, it is necessary to use a valid failure hypothesis. Without the first step it is unlikely that accurate failure predictions can be made. This thesis reports the development of a more accurate method for predicting the stress distribution near holes in composite joints.

From the literature review it is evident that various boundary conditions at the hole edge have been used to predict the stresses in composite joints. This is true for both the finite element approaches and the elasticity techniques. Often these boundary conditions are unjustified and may in fact be in error. Parameters such as clearance, pin flexibility, and friction are often ignored. Furthermore, there has been no analysis which includes all of these parameters for composite joints. A two-dimensional analysis of pin-loaded joints can be used to study the effects of these parameters. This avoids introducing the complexity of a three-dimensional analysis into the problem, yet new results regarding these parameters can be obtained. This is the

approach taken in the study here. In particular, it will be assumed the pin is in a state of plane strain and the plate is in a state of generalized plane stress. The plate is assumed to be infinite in extent. Using these assumptions, an analysis, based on complex variable elasticity, is developed which can accommodate pin/hole clearance, pin flexibility, and friction between the pin and the hole. By varying these effects independently, a better understanding of the problem will be possible and the importance of these often-ignored effects can be assessed.

In the succeeding five chapters the problem is formulated, the equations governing the pin, the plate, and their interaction are developed, and numerical results are presented. Chapter 2 presents the nomenclature and geometry used, and basically defines the problem. The method of solution is outlined. The problem, being a contact elasticity problem, belongs to a class of problems for which there are few closed form solutions. Numerical techniques are usually required if quantitative information is desired. Here no attempts were made to find closed-form solutions, rather it was assumed from the start that numerical techniques would be necessary. Chapter 2 outlines the numerical scheme used here, a scheme based on the collocation method and an iteration process. The elasticity solution for the pin is derived in Chapter 3 and Chapter 4 presents the details of the elasticity solution for the orthotropic plate. That a separate analysis is needed for each component will be made clear in Chapter 2. Chapter 5 discusses details of the numerical method, including convergence of both the collocation

method and the iteration procedure. Finally, Chapter 6 presents some very interesting results regarding the stress distributions around the holes. The effects of pin flexibility, pin/hole clearance, friction, and degree of plate orthotropy on the stresses are demonstrated. Chapter 7 concludes the work and presents recommendations for further studies.

Chapter 2

PROBLEM DEFINITION AND METHOD OF SOLUTION

The problem of a pin-loaded connector is a geometrically nonlinear, fourth-order boundary value problem with non-conservative forces acting between the pin and the plate. Figure 2 illustrates the nonlinear, nonconservative nature of the problem. In this figure a $[0_2/\pm 45]_s$ graphite-epoxy laminate is loaded using two different assumptions. In the first case the clearance between the pin and plate is zero and friction is neglected. The condition of zero clearance is referred to as a push fit and is an often-used assumption. This results in a linear relationship between the pin load and pin displacement. Due to the lack of friction, the load-displacement relationship is independent of loading direction. This case is compared to the nonlinear and path-dependent case of a clearance-fit pin and friction. The nonlinearity in the load-displacement relation is due to the clearance. With clearance, the contact region between the pin and the plate changes as the load increases. This changing contact region leads to the geometric nonlinearity. Friction accounts for the fact that the loading and unloading paths are different. The direction of the frictional forces depends on whether the connector is being loaded or whether it is being unloaded. Fortunately, for any given value of pin displacement, the problem is linear elastic. Through the use of the principle of superposition, a collocation procedure, and iteration, a solution to the problem can be found.

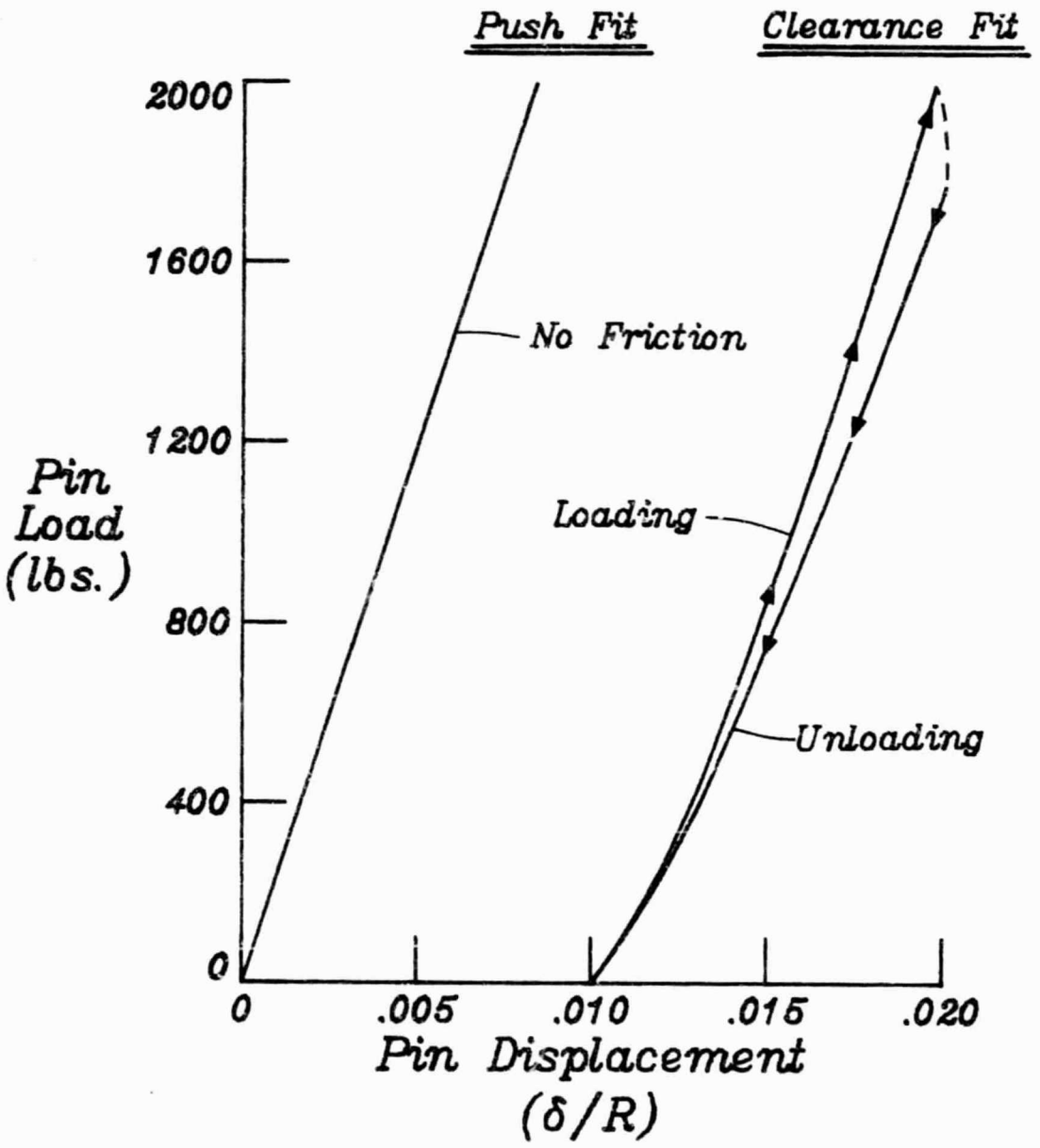

FIG. 2 ILLUSTRATION OF THE NONLINEAR, NONCONSERVATIVE NATURE OF THE PROBLEM

Plate and pin models

In modeling the plate, a two-dimensional analysis is easily justified through the assumptions of generalized plane stress theory. Generalized plane stress is consistent with classical lamination theory and therefore can be readily applied to composite materials. Of course this will mask any interlaminar effects in composite materials. However, as stated earlier, the effects of pin elasticity, clearance, and friction can be studied using two-dimensional models and the inclusion of these effects is a step forward. The use of an infinite plate greatly simplifies the elasticity analysis. Furthermore, meaningful parametric studies can be made regarding the effects of pin elasticity, friction, and clearance even for the infinite plate. It has been shown that for plate-width to hole-diameter ratios exceeding 8 or 10 and end-distance to hole-diameter ratios exceeding 4, the effects of finite geometry are negligible.

An accurate two-dimensional model of the pin is more difficult to justify. A major concern is that the pin must be in equilibrium. The reactive forces on the pin, from the plate, represent a nonequilibrating system on the pin boundary. Figure 3a shows a free-body diagram for a typical pin in a double lap joint. In this figure the load from the plate, P, is equilibrated by the forces from the two support laps. To reduce the pin to a two-dimensional problem, a disc the thickness of the inner lap is removed from the pin. A free body diagram showing only the forces acting in the plane of the disc is given in fig. 3b. It is apparent that the load from the plate is equilibrated by the shear

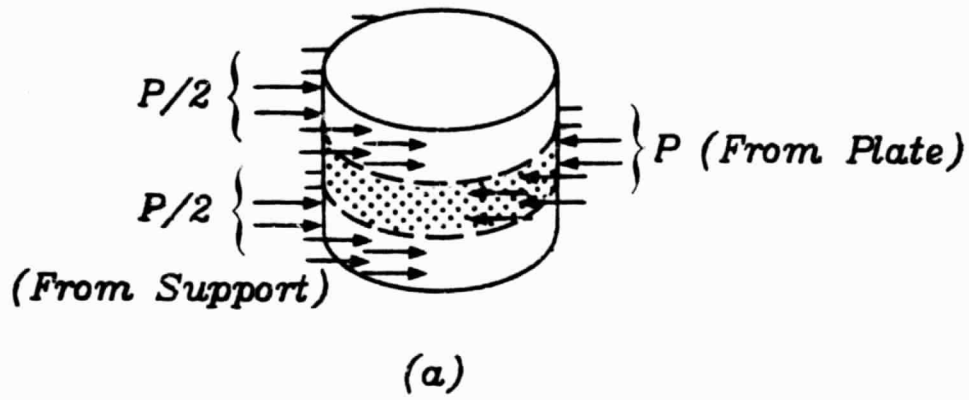

(a)

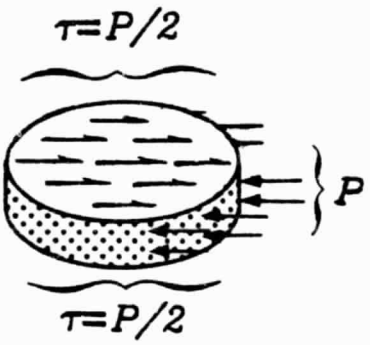

(b)

FIG. 3 PIN EQUILIBRIUM

stresses acting on the upper and lower surfaces of the disc. The distribution of these shear stresses is not known and only a three-dimensional analysis can yield this information. As a first approximation, it is assumed that the shear is uniformly distributed over the upper and lower surfaces of the disc. As the thickness of the disc is decreased, the stress distribution due to these shear stresses approaches the stress distribution caused by a uniform body force within the disc. The pin model adopted in this study therefore assumes that the tractions on the boundary of the pin are equilibrated by a constant body force within the pin. Thus, it seems that the accuracy of this model is limited only by the assumption that the shear stresses vary uniformly over the upper and lower surfaces of the disc. By using this approximation, however, the problem is reduced significantly and only the boundary tractions which generate the load P are left as unknowns.

Coordinate system and nomenclature

The coordinate systems used in this analysis are shown in fig. 4. The x-y axes coincide with the principal material axes of the orthotropic plate. In this analysis, the load is introduced into the plate by a rigid body displacement of the pin in the positive x direction. The r-θ axes are typical cylindrical coordinates, positive θ being measured counterclockwise from the +x axis. The boundary conditions at the hole edge and at the pin boundary will be written in the polar coordinate system. Numerical results will be presented using the polar coordinate system. The displacement in the x direction is denoted by u

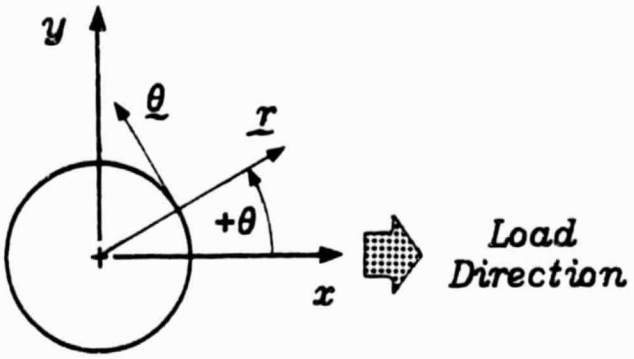

FIG. 4 GEOMETRY AND COORDINATE SYSTEMS USED FOR THE PROBLEM

while the displacement in the y direction is denoted by v. The radial displacement, which is assumed positive in the +r direction, is denoted by u_r. The tangential displacement, which is positive in the $+\theta$ direction, is denoted by u_θ. The three components of stress in the x-y and r-θ systems have the usual definitions and are denoted as σ_{xx}, σ_{yy}, τ_{xy}, and σ_{rr}, $\sigma_{\theta\theta}$, and $\tau_{r\theta}$, respectively. The strains in the two systems are: ε_{xx}, ε_{yy}, γ_{xy} and ε_{rr}, $\varepsilon_{\theta\theta}$, $\gamma_{r\theta}$. If the circle in fig. 4 represents the pin, then the boundary tractions act on the outside of the circle. If the circle represents the hole in the plate, then the boundary tractions act on the inside of the circle. Although this may be obvious and is the convention dictated by elasticity, there can be some confusion on this point when considering traction and displacement conditions at the contact region between the pin and the plate.

Figure 5 defines the pin/hole clearance, λ, and the rigid body pin displacement, δ. The clearance parameter is positive for a clearance fit, zero for a push fit, and negative for an interference fit. As will be seen, the push fit case, $\lambda = 0$, is a special case. Both the loading and unloading cases require a positive pin displacement δ. The case of loading assumes that the pin displacement has been increased from some lower value of δ, while the case of unloading assumes that the pin displacement has been decreased from some higher value of δ. For example, loading occurs if the pin displacement increases from $\delta = 0.02$ to $\delta = 0.03$. On the other hand, unloading occurs when the pin displacement decreases from $\delta = 0.04$ to $\delta = 0.03$. In both cases the

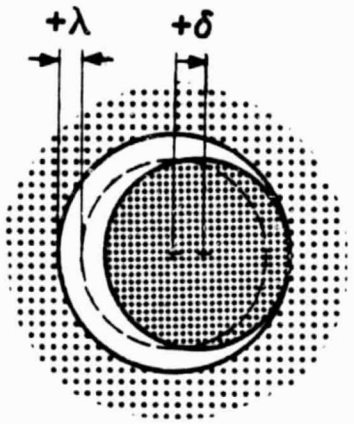

FIG. 5 ILLUSTRATION OF THE PIN CLEARANCE, λ, AND THE RIGID BODY PIN DISPLACEMENT, δ.

problem can be analyzed for $\delta = 0.03$. In the methodology here, the only difference between the two cases will be the sign on the shear stress at the pin/plate interface.

Conditions between pin and plate

Figure 6 shows the different regions of the pin/plate interface where various boundary conditions and interface conditions exist. As can be seen in the figure, three important regions exist. The regions are denoted as regions I, II and III and these are defined in the figure. The actual extent of each of the three regions depends on the pin's elastic response, the plate's elastic response, the pin clearance, the pin displacement, and the coefficient of friction, μ. However, independent of the actual extent, each region has its own unique boundary and/or interface conditions. These are as follows: Let the radial and tangential elastic displacements of the pin and plate be defined, respectively, as

$$u_{r_{pin}}, \quad u_{\theta_{pin}}, \quad u_{r_{plate}}, \quad u_{\theta_{plate}}.$$

Then in region I, referred to as the no-slip region, at the boundary:

$$u_{r_{plate}} = u_{r_{pin}} + \delta \cos\theta - \lambda \qquad (1)$$

$$-\alpha \leq \theta \leq \alpha$$

$$u_{\theta_{plate}} = u_{\theta_{pin}} - \delta \sin\theta . \qquad (2)$$

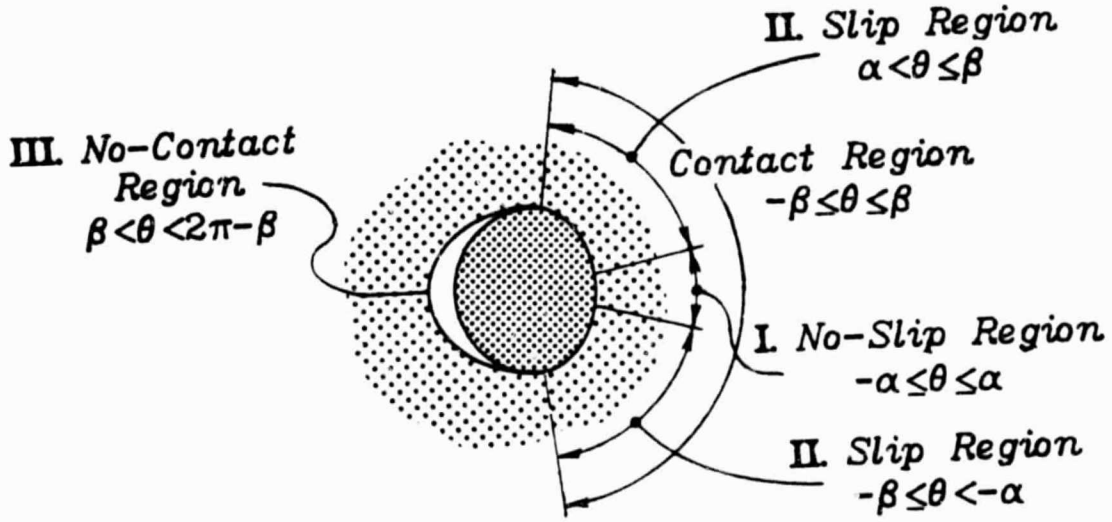

FIG. 6 REGIONS ON THE PIN/PLATE BOUNDARY

In region II, where there is slip:

$$u_{r_{plate}} = u_{r_{pin}} + \delta \cos\theta - \lambda \qquad \alpha < \theta < \beta \qquad (3)$$

and

$$\tau_{r\theta} = \mu \sigma_{rr} \; . \qquad -\beta < \theta < -\alpha \qquad (4)$$

In region III, the no-contact region:

$$\sigma_{rr} = 0 \qquad (5)$$

$$\tau_{r\theta} = 0 \; . \qquad \beta < \theta < 2\pi - \beta \qquad (6)$$

Equations 1 and 3 express continuity of radial displacements in the contact region and eq. 2 expresses continuity of tangential displacement in the no-slip region. Equation 4 is the Coulomb friction law assumed to hold in the slip region. Of course eqs. 5 and 6 express the traction- free conditions of the no-contact region. The second and third terms on the right side of eq. 1, and the second term on the right side of eq. 2 represent the effects of rigid body pin displacement and the effects of clearance. The coefficient of friction appears in region II. Therefore, the loading direction determines the sign of the shear stress in this region. For loading, $\tau_{r\theta}$ is positive (μ is negative) and for unloading, $\tau_{r\theta}$ is negative (μ is positive).

The coefficient of friction, μ, is often assumed to be only positive. However, for this report, the coefficient can change signs. This is merely a simple way of accounting for the loading/unloading cases.

Method of solution

Referring to fig. 6, the unknown boundary tractions act over regions I and II. By equilibrium considerations, the boundary tractions on the pin are identical to the boundary tractions acting on the hole in the plate. The problem reduces to finding these tractions. Once the tractions on the hole boundary are known, the stresses in the entire domain of the plate can be determined. If they are of interest, the same can be said of the stresses within the pin. Of course the elasticity of the pin, the elasticity of the plate, the pin/hole clearance, the pin displacement, and the level of friction, all couple to determine these tractions, and, as mentioned previously, the actual domains of regions I, II, and III. How can these tractions, which are the key to the problem, be found? The answer lies in the use of superposition.

To make use of superposition, the unknown tractions on the boundary of the pin and plate are taken to be represented in the form of a complex Fourier series with unknown coefficients A_k. The series is:

$$(N-iT)_{pin} = (N-iT)_{plate} = \sum_{-\infty}^{+\infty} A_k \, e^{ik\theta} \qquad (7)$$

where N = the normal traction = σ_{rr} @ the boundary

T = the tangential traction = $\tau_{r\theta}$ @ the boundary

$i \equiv \sqrt{-1}$

A_k are the unknown coefficients of the Fourier series.

There are several points regarding eq. 7 that should be discussed. First, the equation indicates normal and tangential tractions on the pin edge are equal to the normal and tangential tractions on the hole edge. Thus the same Fourier series is the driving force behind the analysis of the isotropic pin and the distinctly different analysis of the orthotropic plate. This is one of several couplings between the plate response and the pin response. Second, since the tangential traction must be an odd function of θ and the radial traction must be an even function of θ, the unknown coefficients A_k are real. Finally, the tractions around the entire circle are represented by continuous functions of θ. Therefore the coefficients A_k must be such that N and T are zero in the domain of θ corresponding to region III in fig. 6.

Since they are a legitimate boundary traction, each term $e^{ik\theta}$ in the Fourier series produces a unique set of stresses and displacements in the pin and a unique set of stresses and displacements in the plate. Through the elasticity techniques presented in the following chapters, the stresses and displacements in the pin and plate due to traction $e^{ik\theta}$ can be found in closed form. If the boundary traction is $A_k\, e^{ik\theta}$, then the components of displacement and stress will be weighted by the factor A_k. If, for example, the radial displacement due to the traction $e^{ik\theta}$ is denoted as $(u_r)_k$, then the radial displacement due to traction $A_k\, e^{ik\theta}$ is given by

$$A_k(u_r)_k \ . \tag{8}$$

Considering all terms in eq. 7, the radial displacement will be the weighted sum of the effects of the individual tractions $e^{ik\theta}$. That is,

$$u_r = \sum_{k=-\infty}^{\infty} A_k (u_r)_k \ . \tag{9}$$

If all A_k were known, then u_r could be calculated. The same can be said of the tangential displacement, namely

$$u_\theta = \sum_{k=-\infty}^{\infty} A_k (u_\theta)_k \ , \tag{10}$$

where $(u_\theta)_k$ is the tangential displacement due to traction $e^{ik\theta}$ and u_θ is the tangential displacement due to the weighted sum.

To avoid confusion, no distinction has yet been made between the plate and the pin. However, in eqs. 9 and 10 the radial and tangential responses due to traction $e^{ik\theta}$, specifically $(u_r)_k$ and $(u_\theta)_k$, are different for the plate than they are for the pin. This is obvious since a pin responds quite differently than a plate to a given set of tractions. Thus the notation

$$u_{r_{pin}} = \sum_{k=-\infty}^{\infty} A_k (u_r)_{k_{pin}} \tag{11}$$

$$u_{\theta_{pin}} = \sum_{k=-\infty}^{\infty} A_k (u_\theta)_{k_{pin}} \tag{12}$$

and

$$u_{r_{plate}} = \sum_{k=-\infty}^{\infty} A_k (u_r)_{k_{plate}} \tag{13}$$

$$u_{\theta}\Big|_{\text{plate}} = \sum_{k=-\infty}^{\infty} A_k (u_{\theta})_k\Big|_{\text{plate}} \tag{14}$$

distinguishes between pin and plate responses.

It is important to note A_k is common to the radial and tangential responses of the pin and plate. It is also important to point out that since they are a result of boundary traction $e^{ik\theta}$, $(u_r)_k\Big|_{\text{pin}}$, $(u_{\theta})_k\Big|_{\text{pin}}$, $(u_r)_k\Big|_{\text{plate}}$ and $(u_{\theta})_k\Big|_{\text{plate}}$ are known! The problem, as it is being posed here, will be reduced to finding A_k.

To continue with the formalism of the problem, the stresses in the pin and plate are given by

$$\sigma_{rr}\Big|_{\text{pin}} = \sum_{k=-\infty}^{\infty} A_k (\sigma_{rr})_k\Big|_{\text{pin}} \tag{15}$$

$$\sigma_{\theta\theta}\Big|_{\text{pin}} = \sum_{k=-\infty}^{\infty} A_k (\sigma_{\theta\theta})_k\Big|_{\text{pin}} \tag{16}$$

$$\tau_{r\theta}\Big|_{\text{pin}} = \sum_{k=-\infty}^{\infty} A_k (\tau_{r\theta})_k\Big|_{\text{pin}} \tag{17}$$

and

$$\sigma_{rr}\Big|_{\text{plate}} = \sum_{k=-\infty}^{\infty} A_k (\sigma_{rr})_k\Big|_{\text{plate}} \tag{18}$$

$$\sigma_{\theta\theta}\Big|_{\text{plate}} = \sum_{k=-\infty}^{\infty} A_k (\sigma_{\theta\theta})_k\Big|_{\text{plate}} \tag{19}$$

$$\tau_{r\theta}\Big|_{\text{plate}} = \sum_{k=-\infty}^{\infty} A_k (\tau_{r\theta})_k\Big|_{\text{plate}} . \tag{20}$$

The quantities $(\sigma_{rr})_k\Big|_{\text{pin}}$, ..., $(\tau_{r\theta})_k\Big|_{\text{plate}}$ are the stresses in the pin and plate, respectively, due to traction $e^{ik\theta}$ and they also are known. In particular, on the boundary of both the pin and the plate,

$$(\sigma_{rr} - i\tau_{r\theta})_{boundary} = N - iT = \sum_{k=-\infty}^{\infty} A_k e^{ik\theta} . \qquad (21)$$

To determine the unknown coefficients A_k, the second and third aspects of the problem solution, namely a collocation technique and iteration, are used. These aspects are explained next.

As might be expected, finite, rather than infinite sums are used in the series in eqs. 7-21. Instead of satisfying the boundary and interface conditions at each point on the circular boundary (i.e., at an infinite number of points), the boundary and interface conditions are satisfied at a finite number of points. This technique of satisfying required conditions at only a finite number of points is a numerical technique referred to as a collocation procedure. The finite number of points are referred to as collocation points. The number of terms in the finite series is then directly related to the number of collocation points. The iterative portion of the solution technique involves determining the expanse of regions I and II, i.e., determining α and β. They, like the stresses and displacements, are unknowns. However, if they are assigned values, then, since the boundary and interface conditions are specified in each region, a solution to the problem can be found. Starting with assumed values for α and β, iteration is used to obtain the correct values. The iteration procedure will be discussed shortly. First, the collocation procedure is further explained.

Assuming α and β are known, then by using finite sums in eqs. 11-21, and substituting those sums into the boundary/interface conditions

for the various regions, eqs. 1-6, the method for determining the A_k's becomes evident. Substituting the finite sums into eqs. 1-6 leads to:

For region I;

$$\sum_{k=-N}^{N} A_k (u_r)_k \Big|_{\text{plate}} = \sum_{k=-N}^{N} A_k (u_r)_k \Big|_{\text{pin}} + \delta \cos\theta - \lambda \tag{22}$$

$$\sum_{k=-N}^{N} A_k (u_\theta)_k \Big|_{\text{plate}} = \sum_{k=-N}^{N} A_k (u_\theta)_k \Big|_{\text{pin}} - \delta \sin\theta \tag{23}$$

For region II:

$$\sum_{k=-N}^{N} A_k (u_r)_k \Big|_{\text{plate}} = \sum_{k=-N}^{N} A_k (u_r)_k \Big|_{\text{pin}} + \delta \cos\theta - \lambda \tag{24}$$

$$\sum_{k=-N}^{N} A_k \left((\tau_{r\theta})_k - \mu (\sigma_{rr})_k \right) = 0 . \tag{25}$$

For region III:

$$\sum_{k=-N}^{N} A_k (\sigma_{rr})_k = 0 , \tag{26}$$

$$\sum_{k=-N}^{N} A_k (\tau_{r\theta})_k = 0 . \tag{27}$$

Here it is assumed there are 2N+1 terms in the sums. With α and β assumed to be known, everything in eqs. 22-27 is known except the A_k's. The assumed values of α and β determine over what range of θ eqs. 22 and 23 are enforced, over what other range of θ eqs. 24 and 25 are enforced, and over what range of θ eqs. 26 and 27 are enforced. Since

by equilibrium the tractions of the pin and plate edges are identical, neither the plate nor the pin has been called out specifically in eqs. 25-27. Strictly speaking,

$$\left.\begin{aligned}(\sigma_{rr})_{k\ pin} = (\sigma_{rr})_{plate} = A_k \cos(k\theta) \quad (28)\\ (\tau_{r\theta})_{k\ pin} = (\tau_{r\theta})_{k\ plate} = A_k \sin(k\theta) \quad (29)\end{aligned}\right\} \text{ at boundary}$$

Equations 25-27 could be stated alternatively as

$$\sum_{k=-N}^{N} A_k \left(\sin(k\theta) - \mu \cos(k\theta)\right) = 0 \quad (30)$$

$$\sum_{k=-N}^{N} A_k \cos(k\theta) = 0 \quad (31)$$

$$\sum_{k=-N}^{N} A_k \sin(k\theta) = 0 \quad (32)$$

Expanding eqs. 22-27 and rearranging slightly leads to

$$\{(u_r)_{o\ plate} - (u_r)_{o\ pin}\} A_o + \{(u_r)_{-1\ plate} - (u_r)_{-1\ pin}\} A_{-1} +$$

$$\{(u_r)_{1\ plate} - (u_r)_{1\ pin}\} A_1 + \ldots + \{(u_r)_{N\ plate} - (u_r)_{N\ pin}\} A_N =$$

$$\delta \cos\theta - \lambda \ , \quad (33)$$

$$\{(u_\theta)_{o\ \text{plate}} - (u_\theta)_{o\ \text{pin}}\}\, A_o + \{(u_\theta)_{-1\ \text{plate}} - (u_\theta)_{-1\ \text{pin}}\}\, A_{-1} +$$

$$\{(u_\theta)_{1\ \text{plate}} - (u_\theta)_{1\ \text{pin}}\}\, A_1 + \cdots + \{(u_\theta)_{N\ \text{plate}} - (u_\theta)_{N\ \text{pin}}\}\, A_N =$$

$$-\delta \sin\theta, \tag{34}$$

$$\{(u_r)_{o\ \text{plate}} - (u_r)_{o\ \text{pin}}\}\, A_o + \{(u_r)_{-1\ \text{plate}} - (u_r)_{-1\ \text{pin}}\}\, A_{-1} +$$

$$\{(u_r)_{1\ \text{plate}} - (u_r)_{1\ \text{pin}}\}\, A_1 + \cdots + \{(u_r)_{N\ \text{plate}} - (u_r)_{N\ \text{pin}}\}\, A_N =$$

$$\delta \cos\theta - \lambda \tag{35}$$

$$\{(\tau_{r\theta})_o - \mu(\sigma_{rr})_o\}A_o + \{(\tau_{r\theta})_{-1} - \mu(\sigma_{rr})_{-1}\}A_{-1} +$$

$$\{(\tau_{r\theta})_1 - \mu(\sigma_{rr})_1\}A_1 + \cdots + \{(\tau_{r\theta})_N - \mu(\sigma_{rr})_N\}A_N = 0 \tag{36}$$

$$\{(\sigma_{rr})_o\}A_o + \{(\sigma_{rr})_{-1}\}A_{-1} + \{(\sigma_{rr})_1\}A_1 + \cdots + \{(\sigma_{rr})_N\}A_N = 0 \tag{37}$$

$$\{(\tau_{r\theta})_o\}A_o + \{(\tau_{r\theta})_{-1}\}A_{-1} + \{(\tau_{r\theta})_1\}A_1 + \cdots + \{(\tau_{r\theta})_N\}A_N = 0 \tag{38}$$

From eqs. 33-38 it is obvious that there are 2N+1 unknown A_k's. If the equations are satisfied at 2N+1 discrete points around the circular

boundary, i.e., at 2N+1 discrete θ locations, then a set of 2N+1 linear equations can be formed from which to solve for the A_k. This is the application of the collocation procedure to the problem at hand. Since eq. 7 incorporates the proper symmetry of the problem, collocation over one-half the hole circumference, $0 \leq \theta \leq \pi$, is all that is necessary. Equation 39 illustrates, in operational form, the collocation procedure for finding A_0, A_{-1}, A_{+1}, ..., A_{-N}, A_{+N}. In eq. 39 it has been assumed that the collocation points are $\Delta\theta$ apart around the circumference of the circle.

The numerical problem now is reduced to the finding of α and β. For given values of α and β a solution to eq. 39 is found. The solution may not be realistic in terms of the stresses and displacements which result. For example, it is physically impossible to have tensile stresses between the pin and the hole. Also, the shear traction on the boundary cannot exceed μ times the normal traction. In the solution procedure here, trial values of α and β are used. The problem is solved via eq. 39 and the values of the normal and shear tractions on the boundary examined. If any physical conditions are violated, α and/or β are adjusted and eq. 39 is resolved with new values of α and/or β. Again the physical reality of the solution is examined. Within a few iterations, values of α and β are obtained that satisfy all the conditions required.

It is important to point out that with a push fit pin, $\lambda = 0$ and each element on the right-hand-side of eq. 39 changes, for example, by a factor of two when δ is doubled. Each A_k simply doubles and the spatial

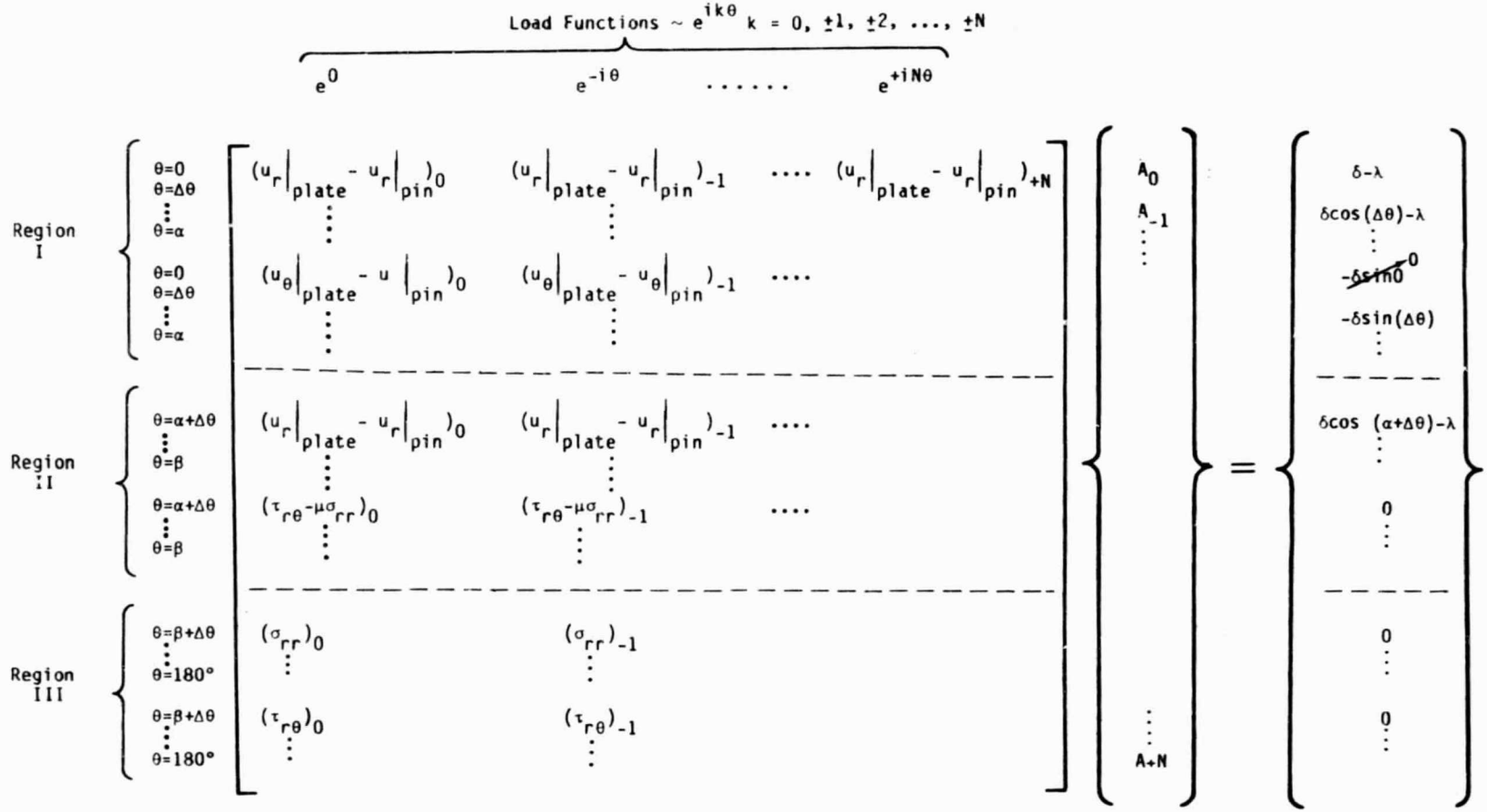
Load Functions ~ e^{ikθ} k = 0, ±1, ±2, ..., ±N
e^0
e^{-iθ}
.....
e^{+iNθ}
Region I
Region II
Region III
θ=0
θ=Δθ
θ=α
θ=α+Δθ
θ=β
θ=β+Δθ
θ=180°
(u_r|_plate - u_r|_pin)_0
(u_r|_plate - u_r|_pin)_-1
(u_r|_plate - u_r|_pin)_+N
(u_θ|_plate - u_θ|_pin)_0
(u_θ|_plate - u_θ|_pin)_-1
(τ_rθ-μσ_rr)_0
(τ_rθ-μσ_rr)_-1
(σ_rr)_0
(σ_rr)_-1
(τ_rθ)_0
(τ_rθ)_-1
A_0
A_-1
A+N
δ-λ
δcos(Δθ)-λ
-δsinθ
0
-δsin(Δθ)
δcos (α+Δθ)-λ
0
0
0
=

Equation (39)

variation of N-iT, with θ, remains unchanged. Thus α and β are unaffected by δ. With $\lambda \neq 0$, doubling δ does not result in a doubling of each element of the right-hand-side of eq. 39. Each A_k changes by a different amount and thus the spatial variation of N-iT varies. This translates into δ directly affecting α and β. The push fit case is therefore quite special and is often referred to as the linear case.

Chapter 5 will discuss details of the numerical procedure. That chapter will discuss, among other things, the specific manner in which α and β were determined. The next two chapters are devoted to finding the response of the isotropic pin and the orthotropic plate to the boundary traction $e^{ik\theta}$. Chapter 3 examines the pin while Chapter 4 presents the analysis of the plate. Both solutions use complex variable elasticity. Several books exist on this subject [46-49] but, in general, the details of these types of analyses are not as familiar as analyses with real variables. Therefore, some of the details of the analyses will be discussed.

Chapter 3

PIN ANALYSIS

For the complete solution to an elasticity problem, three sets of equations, in addition to the appropriate boundary conditions, must be satisfied. The equations are the equilibrium, constitutive, and compatibility equations. The strain-displacement equations can be considered as definitions but certainly they must be satisfied. The boundary conditions can be known displacement conditions, known stress conditions, or a combination of both. In the solution of the problem for both the pin and the plate, the governing equations can be simplified and combined into one governing biharmonic differential equation. The dependent variable in this equation is the Airy stress function. The boundary conditions for the problem are satisfied through the use of various integrated forms of the solutions of the biharmonic equation. This simplifies the solution because after the boundary conditions are satisfied, the solution automatically satisfies the governing differential equation. The key to both the pin and plate analyses here is the development of the stress functions in terms of complex variables. This is presented below for the pin.

The pin is assumed to be isotropic and in a state of plane strain. The governing equations are therefore reduced to the following: equilibrium:

$$\frac{\partial \sigma_{xx}}{\partial x} + \frac{\partial \tau_{xy}}{\partial y} = b_x$$

$$\frac{\partial \tau_{xy}}{\partial x} + \frac{\partial \sigma_{yy}}{\partial y} = b_y \ , \qquad (40)$$

constitutive:

$$\begin{aligned}\varepsilon_{xx} &= \frac{1}{E}\left[(1-\nu^2)\sigma_{xx} - \nu(1+\nu)\sigma_{yy}\right]\\ \varepsilon_{yy} &= \frac{1}{E}\left[(1-\nu^2)\sigma_{yy} - \nu(1+\nu)\sigma_{xx}\right]\\ \gamma_{xy} &= \frac{1}{G}\tau_{xy}\ ,\end{aligned} \tag{41}$$

compatibility:

$$\frac{\partial^2\varepsilon_{xx}}{\partial y^2} + \frac{\partial^2\varepsilon_{yy}}{\partial x^2} = \frac{\partial^2\gamma_{xy}}{\partial x\partial y}\ , \tag{42}$$

strain-displacement:

$$\varepsilon_{xx} = \frac{\partial u}{\partial x};\quad \varepsilon_{yy} = \frac{\partial v}{\partial y};\quad \gamma_{xy} = 2\varepsilon_{xy} = \frac{\partial u}{\partial y} + \frac{\partial v}{\partial x}\ . \tag{43}$$

Here b_x and b_y are the x and y component of the body force. The material properties E, ν, and G have their usual definitions and fig. 4 defines the coordinate system. The strains may be substituted into the compatibility equation to yield

$$\begin{aligned}&(1-\nu^2)\frac{\partial^2\sigma_{xx}}{\partial y^2} - \nu(1+\nu)\frac{\partial^2\sigma_{yy}}{\partial y^2} + (1-\nu^2)\frac{\partial^2\sigma_{yy}}{\partial x^2} - \nu(1+\nu)\frac{\partial^2\sigma_{xx}}{\partial x^2}\\ &= 2(1+\nu)\frac{\partial^2\tau_{xy}}{\partial x\partial y}\ .\end{aligned} \tag{44}$$

The stresses in this equation can be written in terms of a stress function F and a scalar body potential V. The body forces b_x and b_y are

related to V by

$$b_x = \frac{\partial V}{\partial x} \tag{45a}$$

$$b_y = \frac{\partial V}{\partial y} , \tag{45b}$$

and are used here, as mentioned in Chapter 2, to represent the pin loading from the outer laps. By considering the equilibrium equations, the stresses are defined as

$$\sigma_{xx} \equiv \frac{\partial^2 F}{\partial y^2} + V \tag{46a}$$

$$\sigma_{yy} \equiv \frac{\partial^2 F}{\partial x^2} + V \tag{46b}$$

$$\tau_{xy} \equiv - \frac{\partial^2 F}{\partial x \partial y} . \tag{46c}$$

With these definitions, the equilibrium equations are automatically satisfied. Substitution of these definitions into eq. 44 yields

$$\nabla^4 F + \frac{1-2\nu}{1-\nu} \nabla^2 V = 0 . \tag{47}$$

For all cases where the body forces are derivable from a potential, the potential V can be written as

$$V = \nabla^2 Q . \tag{48}$$

Here Q is another scalar function. The redefinition of V further simplifies the biharmonic equation to

$$\nabla^4(F + \kappa Q) = 0 \ , \tag{49}$$

where $\kappa \equiv \frac{1-2\nu}{1-\nu}$.

It is convenient to take advantage of the biharmonic nature of the governing differential equation by using a complex variable approach. In this approach the ∇^4 operator is written in terms of the complex variable z and its conjugate $\bar{z}$. Here z and $\bar{z}$ are defined by

$$z = x + iy \tag{50a}$$

$$\bar{z} = x - iy. \tag{50b}$$

In what follows, the overbar will be used to denote complex conjugate. Using eqs. 50, the following differential operators may be defined:

$$D_1 = \frac{\partial}{\partial z} = \frac{1}{2}\left(\frac{\partial}{\partial x} - i\,\frac{\partial}{\partial y}\right) \tag{51a}$$

$$D_2 = \frac{\partial}{\partial \bar{z}} = \frac{1}{2}\left(\frac{\partial}{\partial x} + i\,\frac{\partial}{\partial y}\right) \ . \tag{51b}$$

By using these operators, the biharmonic equation, eq. 49, can be written as

$$16\, D_1 D_2 D_1 D_2 (F + \kappa Q) = 16\, \frac{\partial}{\partial z}\frac{\partial}{\partial \bar{z}}\frac{\partial}{\partial z}\frac{\partial}{\partial \bar{z}}(F + \kappa Q) = \nabla^4(F + \kappa Q) = 0 \tag{52}$$

Despite the use of complex variables, by eq. 46 F is real. In addition, V and Q are real. The form of F can be found by integrating eq. 52. First the equation is integrated once with respect to z and then once with respect to $\bar{z}$. Integrating with respect to z results in

$$\frac{\partial}{\partial \bar{z}} \frac{\partial}{\partial z} \frac{\partial}{\partial \bar{z}} (F + \kappa Q) = \overline{F_1(\bar{z})} , \tag{53}$$

where $\overline{F_1(\bar{z})}$ is an arbitrary function of $\bar{z}$ and any constant of integration is incorporated into $\overline{F_1(\bar{z})}$. Integrating eq. 53 with respect to $\bar{z}$ gives

$$\frac{\partial}{\partial z} \frac{\partial}{\partial \bar{z}} (F + \kappa Q) = \overline{\int F_1(\bar{z})} + F_2(z) . \tag{54}$$

Here $F_2(z)$ is an arbitrary function of z, including any constant of integration, and

$$\overline{\int F_1(\bar{z})} \equiv \int \overline{F_1(\bar{z})}\, d\bar{z} . \tag{55}$$

Realizing

$$\frac{\partial}{\partial z} \frac{\partial}{\partial \bar{z}} \equiv \frac{1}{4} \left(\frac{\partial^2}{\partial x^2} + \frac{\partial^2}{\partial y^2}\right) \tag{56}$$

is a real operator, and knowing $(F + \kappa Q)$ is real, the right hand side of eq. 54 must be real. Thus $\overline{\int F_1(\bar{z})}$ and $F_2(z)$ must be conjugate functions,

i.e.,

$$F_2(z) = W(z) \tag{57}$$

$$\overline{F_1(\overline{z})} = \overline{W(\overline{z})} \ . \tag{58}$$

Then eq. 54 becomes

$$\frac{\partial}{\partial z}\frac{\partial}{\partial \overline{z}}(F + \kappa Q) = W(z) + \overline{W(\overline{z})} \ . \tag{59}$$

The equation above can also be obtained by noting that every harmonic function (here W(z) is harmonic) is also biharmonic. In addition, the conjugate harmonic function is required to insure that the stresses remain real valued.

Two more integrations are required. Integrating eq. 59 with respect to $\overline{z}$ yields

$$\frac{\partial}{\partial z}(F + \kappa Q) = \overline{z}W(z) + \overline{W(\overline{z})} + F_3(z) \ , \tag{60}$$

where $F_3(z)$ is an arbitrary function of z and

$$\overline{W(\overline{z})} = \int \overline{W(\overline{z})}\, d\overline{z} \ . \tag{61}$$

Finally, integrating eq. 60 with respect to z leads to

$$F + \kappa Q = \overline{z}W(z) + z\overline{W(\overline{z})} + F_3(z) + \overline{F_4(\overline{z})} \ , \tag{62}$$

$\overline{F_4(\bar{z})}$ being an arbitrary function of $\bar{z}$ and $\breve{F}_3(z)$ being defined similar to eqs. 55 and 61. Again, making use of the fact that $F + \kappa Q$ is real, the right side of eq. 62 must be real. The first two terms are conjugate functions and therefore their sum is real. Obviously $\breve{F}_3(z)$ and and $\overline{F_4(\bar{z})}$ must also be conjugate functions. Equation 62 can now be written as the familiar Goursat equation (see ref. 46) for isotropic materials. That equation is

$$F = \frac{1}{2}\left[\bar{z}\phi(z) + z\overline{\phi(\bar{z})} + \chi(z) + \overline{\chi(\bar{z})}\right] - \kappa Q \ . \tag{63}$$

Here

$$\phi(z) = 2\,\breve{W}(z) \tag{64a}$$

$$\overline{\phi(\bar{z})} = 2\,\overline{\breve{W}(\bar{z})} \tag{64b}$$

$$\chi(z) = 2\,\breve{F}_3(z) \tag{64c}$$

$$\overline{\chi(\bar{z})} = 2\,\overline{F_4(\bar{z})} \ . \tag{64d}$$

The stress function F has now been expressed in terms of two complex functions, ϕ and χ, and their conjugates. This, at first, may seem to be a step backward, i.e., we have increased the number of stress functions. However it will now be shown that this simplifies the steps necessary to satisfy the boundary conditions.

To illustrate, consider the case of traction boundary conditions. For the pin, σ_{rr} and $\tau_{r\theta}$ are known to be N and T, respectively, on the boundary. It is convenient to use the fundamental stress combinations introduced by Kolosov (see ref. 46). These combinations are defined as:

$$4\, D_1 D_2 F = \sigma_{yy} + \sigma_{xx} - 2V \tag{65}$$

$$4\, D_1 D_1 F = \sigma_{yy} - \sigma_{xx} + 2i\, \tau_{xy} \tag{66}$$

Taking the appropriate derivatives produces

$$\sigma_{yy} + \sigma_{xx} = 2\left(\phi'(z) + \overline{\phi'(\bar{z})}\right) - 4\kappa \frac{\partial^2 Q}{\partial z \partial \bar{z}} + 8 \frac{\partial^2 Q}{\partial z \partial \bar{z}} \tag{67}$$

$$\sigma_{yy} - \sigma_{xx} + 2i\, \tau_{xy} = 2\left(\bar{z}\phi'(z) + \chi''(z)\right) - 4\kappa \frac{\partial^2 Q}{\partial z^2} . \tag{68}$$

These variables are often defined as:

$$\phi(z) \equiv \chi'(z) \tag{69a}$$

$$\Phi(z) \equiv \phi'(z) \tag{69b}$$

$$\Psi(z) \equiv \phi'(z) . \tag{69c}$$

This is merely a change in notation that has been used by several

authors. Using eq. 69 leads to following fundamental stress combinations:

$$\sigma_{yy} + \sigma_{xx} = 2(\Phi(z) + \overline{\Phi(\bar{z})}) + (8 - 4\kappa) \frac{\partial^2 Q}{\partial z \partial \bar{z}} \tag{70}$$

$$\sigma_{yy} - \sigma_{xx} + 2i\ \tau_{xy} = 2(\bar{z}\Phi'(z) + \Psi(z)) - 4\kappa \frac{\partial^2 Q}{\partial z^2}\ . \tag{71}$$

The first stress combination is the trace of the stress tensor and is invariant under coordinate transformation. Therefore the stresses in polar coordinates remain unchanged, i.e.,

$$\sigma_{\theta\theta} + \sigma_{rr} = \sigma_{yy} + \sigma_{xx} = 2(\Phi(z) + \overline{\Phi(\bar{z})}) + (8 - 4\kappa) \frac{\partial^2 Q}{\partial z \partial \bar{z}}\ . \tag{72}$$

The second stress combination is not an invariant quantity and can be shown to transform as

$$\sigma_{\theta\theta} - \sigma_{rr} + 2i\ \tau_{r\theta} = (\sigma_{yy} - \sigma_{xx} + 2i\ \tau_{xy})\ \sigma^2, \tag{73}$$

where

$$\sigma = e^{i\theta}. \tag{74}$$

It is interesting to note that the magnitude of the left hand side of eqs. 68 and 73 are related to the maximum shear stress.

The stress combinations rewritten in terms of polar coordinates r and θ are

$$\sigma_{\theta\theta} + \sigma_{rr} = 2\left(\Phi(z) + \overline{\Phi(\bar{z})}\right) + (8 - 4\kappa)\frac{\partial^2 Q}{\partial z \partial \bar{z}} \tag{75}$$

$$\sigma_{\theta\theta} - \sigma_{rr} + 2i\,\tau_{r\theta} = 2\sigma^2\left(\bar{z}\Phi'(z) + \Psi(z) - 2\kappa\frac{\partial^2 Q}{\partial z^2}\right) . \tag{76}$$

Subtracting the second equation from the first yields a complex stress expression which involves those stresses which are known on the boundary, namely σ_{rr} and $\tau_{r\theta}$. The expression is

$$\sigma_{rr} - i\,\tau_{r\theta} = \Phi(z) + \overline{\Phi(\bar{z})} - \sigma^2\left(\bar{z}\Phi'(z) + \Psi(z)\right) + (4-2\kappa)\frac{\partial^2 Q}{\partial z \partial \bar{z}} + 2\sigma^2\kappa\frac{\partial^2 Q}{\partial z^2} . \tag{77}$$

In Chapter 2 eqs. 7 and 21, the stresses on the boundary were defined in terms of a complex fourier series, i.e.,

$$(\sigma_{rr} - i\tau_{r\theta})_{boundary} = N - iT = \sum_{k=-\infty}^{\infty} A_k e^{ik\theta} . \tag{21}R$$

Therefore, the right hand side of eq. 77 evaluated on the boundary is the complex series involving A_k. This equation ties the boundary conditions directly to the stress function.

Having illustrated the convenience of using complex stress functions and having expressed the traction boundary conditions of interest here directly in terms of these stress functions, it remains to find the specific forms of Φ, Ψ and Q for the pin. First the form of the body force potential, Q, will be found.

In Chapter 2 it was assumed that a constant body force acts in the x direction. Denote this constant as C. By eqs. 48 and 51, the potential V is related to Q by

$$4 \frac{\partial^2 Q}{\partial z \partial \bar{z}} = V \ . \tag{78}$$

By definition,

$$b_x = C = \frac{\partial V}{\partial x} \quad \text{and} \quad b_y = 0 = \frac{\partial V}{\partial y} \ . \tag{79a,b}$$

Equation 51a yields

$$\frac{\partial V}{\partial z} = \frac{1}{2} \left(\frac{\partial V}{\partial x} - i \frac{\partial V}{\partial y} \right) = \frac{1}{2} (C - i0) = \frac{1}{2} C \tag{80}$$

Integrating once leads to

$$V = \frac{1}{2} Cz + \overline{g_1(\bar{z})} \ , \tag{81}$$

where $g_1(\bar{z})$ is an arbitrary function of $\bar{z}$.

But by eq. 51b,

$$\frac{\partial V}{\partial \bar{z}} = \overline{g_1'(\bar{z})} = \frac{1}{2} \left(\frac{\partial V}{\partial x} + i \frac{\partial V}{\partial y} \right) = \frac{1}{2} (C + i0) \ . \tag{82}$$

Therefore, integrating with respect to $\bar{z}$ gives

$$g_1(\bar{z}) = \frac{1}{2} C \bar{z} + B, \tag{83}$$

B being a constant. Combining eqs. 81 and 83 results in

$$V = \frac{1}{2} C z + \frac{1}{2} C \bar{z} + B . \tag{84}$$

Since concern is with the derivatives of V (see eq. 45) the constant B can be set to zero. Therefore

$$V = \frac{1}{2} C (z + \bar{z}). \tag{85}$$

Substituting this into eq. 78 and integrating once with respect to $\bar{z}$ yields

$$4 \frac{\partial Q}{\partial z} = \frac{1}{2} C(z\bar{z} + \frac{\bar{z}^2}{2}) + g_2(z) , \tag{86}$$

where $g_2(z)$ is an arbitrary function of z. Integrating once more, with respect to z, results in

$$4Q = \frac{1}{2} C(\frac{z^2}{2} \bar{z} + \frac{\bar{z}^2}{2} z) + \grave{g}_2(z) + \overline{\overline{g_3(\bar{z})}} , \tag{87}$$

where

$$\grave{g}_2(z) = \int g_2(z)\, dz \tag{88}$$

and $\overline{\overline{g_3(\bar{z})}}$ is an arbitrary function of $\bar{z}$. Substituting for Q in eq. 77 results in the following expression:

$$\sigma_{rr} - i\tau_{r\theta} = \Phi(z) + \overline{\Phi(\bar{z})} - \sigma^2(\bar{z}\Phi'(z) + \Psi(z) - \frac{C\kappa}{4}\bar{z}) + \frac{C}{4}(2-\kappa)(z+\bar{z}) \quad (89)$$

Attention can now be focused on the form of the stress functions Φ and Ψ. Since the functions Φ and Ψ are analytic in the domain of the pin, they may each be expanded in Laurent series. These series can be written as

$$\Phi(z) = \sum_{-\infty}^{\infty} a_n z^n \quad (90a)$$

and

$$\Psi(z) = \sum_{-\infty}^{\infty} b_n z^n \ , \quad (90b)$$

a_n and b_n being complex constants. If the stresses are to remain bounded at the origin of the pin, the negative powers of z must be eliminated. This leaves the following form for the stress functions:

$$\Phi(z) = \sum_{0}^{\infty} a_n z^n = \sum_{0}^{\infty} a_n r^n \sigma^n \quad (91a)$$

$$\Psi(z) = \sum_{0}^{\infty} b_n z^n = \sum_{0}^{\infty} b_n r^n \sigma^n, \quad (91b)$$

where

$$z \equiv re^{i\theta} = r\sigma \ , \quad (92a)$$

$$r = \sqrt{x^2 + y^2} \quad (92b)$$

$$\theta = \tan^{-1}(y/x) \ . \quad (92c)$$

These equations define the functional forms of Φ and Ψ used in the pin analysis. The stress combination in eq. 89 can now be written explicitly in terms of z.

In the following chapter, the radius of the hole in the plate will be assumed to be unity. If pin/hole clearance (or interference) is to be included in the solution, it must be accounted for in the analysis of the pin. Since the clearance has been defined as $+\lambda$ in Chapter 2, the pin must have a radius

$$R = 1 - \lambda. \tag{93}$$

An interference fit is obtained by selecting a negative value of λ. If the functional forms for Ψ and Φ from eq. 91 are substituted into eq. 89, and the result is evaluated on the pin boundary, $z = R\sigma$, the result is

$$N - iT = \sum_{-\infty}^{\infty} A_n \sigma^n = \sum_{n=0}^{\infty} a_n R^n \sigma^n + \sum_{n=0}^{\infty} \overline{a}_n R^n \sigma^{-n} - \sum_{n=1}^{\infty} n a_n R^n \sigma^n + \\ - \sum_{n=2}^{\infty} b_{n-2} R^{n-2} \sigma^n + \frac{C(2-\kappa)}{4} (R\sigma + R\sigma^{-1}) + \frac{C\kappa}{4} R\sigma . \tag{94}$$

Here eq. 21 has been used.

The exact solution for the stress in the pin due to boundary traction $N - iT = e^{ik\theta}$ can now be determined from eq. 94. This can be done by setting $A_n = 1$, $n = k$, and all other $A_n = 0$ in that equation. To solve for the coefficients a_n and b_n which give the stress functions for

this state of stress, it becomes a simple matter of comparing terms of like powers of σ in eq. 94. Table 1 lists the results of this procedure. Using eqs. 91, the coefficients in Table 1 completely define the stress functions Φ and Ψ anywhere in the pin. Using the fundamental stress combinations, the stresses may be calculated anywhere within the pin, if so desired.

The solution technique discussed in Chapter 2, however, requires the displacements as well as the stresses. Specifically, the displacements on the boundary are required. For this reason the method of determining the displacements will now be discussed.

To begin the displacement analysis, first recall the constitutive relations given in eq. 41. Forming the combination $\varepsilon_{yy} - \varepsilon_{xx} + i\gamma_{xy}$ results in

$$\varepsilon_{yy} - \varepsilon_{xx} + i\gamma_{xy} = \frac{1+\nu}{E} [\sigma_{yy} - \sigma_{xx} + 2i\tau_{xy}] . \tag{95}$$

The bracketed quantity on the right side of eq. 95 is the second fundamental stress combination, eq. 66. The strains may thus be written in terms of simple derivatives of the stress function F, i.e.,

$$\varepsilon_{yy} - \varepsilon_{xx} + i\gamma_{xy} = \frac{1+\nu}{E} \left[4 \frac{\partial^2 F}{\partial z^2}\right] . \tag{96}$$

In addition, using the strain-displacement relations, the strains can be rewritten in terms of spatial derivatives of the displacements, i.e.,

Table 1

Coefficients of the Stress Functions Φ and Ψ for the Pin.

A_k	a_n	b_n
$A_o = 1$	$a_o = 1$	$b_n = 0$
$A_{-1} = 1$	$a_1 = \frac{1}{R}$	$b_n = 0$
$A_1 = 1$	$a_1 = \frac{\kappa-2}{2R}$ *	$b_n = 0$
$A_{-2} = 1$	$a_2 = \frac{1}{R^2}$	$b_o = -1$
$A_2 = 1$	$a_n = 0$	$b_o = -1$
$A_{-3} = 1$	$a_3 = \frac{1}{R^3}$	$b_1 = -\frac{2}{R}$
$A_3 = 1$	$a_n = 0$	$b_1 = -\frac{1}{R}$
$\vdots$	$\vdots$	$\vdots$
$A_{-k} = 1$	$a_k = \frac{1}{R^k}$	$b_{k-2} = -\frac{(k-1)}{R^{k-2}}$
$A_{+k} = 1$	$a_n = 0$	$b_{k-2} = -\frac{1}{R^{k-2}}$

* $\kappa \equiv \frac{1-2\nu}{1-\nu}$

$$\frac{\partial v}{\partial y} - \frac{\partial u}{\partial x} + i\left(\frac{\partial u}{\partial x} + \frac{\partial u}{\partial y}\right) = \frac{1+\nu}{E}\left[4\,\frac{\partial^2 F}{\partial z^2}\right] . \tag{97}$$

Using eq. 51, eq. 97 may be written as

$$2\,\frac{\partial(u-iv)}{\partial z} = -\,\frac{1+\nu}{E}\left[4\,\frac{\partial^2 F}{\partial z^2}\right] . \tag{98}$$

Integrating eq. 98 with respect to z yields

$$G(u-iv) = -\,\frac{\partial F}{\partial z} + \overline{h_1(\overline{z})} . \tag{99}$$

The function $\overline{h_1(\overline{z})}$ in eq. 99 is an arbitrary function of $\overline{z}$ and is to be determined through the use of the first fundamental stress combination. This follows.

Proceeding in a manner similar to that presented above, the following equation is obtained by using the first fundamental stress combination:

$$(1-2\nu)\left[4\,\frac{\partial^2 F}{\partial z \partial \overline{z}} + 2V\right] = 2G(\varepsilon_{xx} + \varepsilon_{yy}) . \tag{100}$$

Again, the strain-displacement relations and eq. 51 can be used to rewrite eq. 100 as

$$(1-2\nu)\left[4\,\frac{\partial^2 F}{\partial z \partial \overline{z}} + 2V\right] = 2G\left[\frac{\partial(u+iv)}{\partial z} + \frac{\partial(u-iv)}{\partial \overline{z}}\right] . \tag{101}$$

Making use of eq. 99 and its conjugate leads to

$$(1-2\nu)\left[2\frac{\partial^2 F}{\partial z \partial \bar{z}} + V\right] = -\frac{\partial^2 F}{\partial z \partial \bar{z}} + h_1'(z) - \frac{\partial^2 F}{\partial z \partial \bar{z}} + \overline{h_1'(\bar{z})} \ . \quad (102)$$

Combining terms and using the relation between V and Q results in

$$h_1'(z) + \overline{h_1'(\bar{z})} = 4(1-\nu)\left[\frac{\partial^2 F}{\partial z \partial \bar{z}} + \kappa \frac{\partial^2 Q}{\partial z \partial \bar{z}}\right] . \quad (103)$$

Using previous definitions,

$$h_1'(z) + \overline{h_1'(\bar{z})} = 2(1-\nu)\left[\Phi(z) + \overline{\Phi(\bar{z})}\right] , \quad (104)$$

or

$$h_1'(z) = 2(1-\nu)\,\overline{\Phi(\bar{z})} \ . \quad (105)$$

Integrating eq. 105 with respect to $\bar{z}$ leads to the form of $\overline{h_1(\bar{z})}$ needed in eq. 99, namely

$$\overline{h_1(\bar{z})} = 2(1-\nu)\,\overline{\phi(\bar{z})} + D \ , \quad (106)$$

D being a constant. D is related to a rigid body displacement of the pin. Since only the elastic response of the pin is required here, D is set to zero.

Everything is now available to determine the displacements in terms of the stress functions. This relation is

$$u - iv = \frac{1}{2G}\left[(3-4\nu)\overline{\phi} - \overline{z}\Phi - \psi + \frac{C\kappa}{4}\left(z\overline{z} + \frac{\overline{z}^2}{2}\right)\right] . \qquad (107)$$

A simple coordinate transformation yields the displacements in the r,θ coordinate system:

$$u_r - iu_\theta = \sigma^{-1}(u - iv) . \qquad (108)$$

With this result the tractions and displacements at any point within the pin can be determined. These equations will be combined with those of Chapter 4 to solve the problem.

Chapter 4

PLATE ANALYSIS

This chapter will discuss the development of the solution technique for an orthotropic plate. The techniques for analyzing the pin and plate are similar, but the material properties for each case alter the specific forms of the solutions. In addition to this, the plate is not simply connected. This complicates the solution by placing constraints on the displacements which did not appear in the pin analysis of Chapter 3. Fortunately, there is no body force in the analysis of the plate. This is a simplification relative to the pin analysis. The following discussion explains the analysis of the plate.

The plate is assumed to be in a state of generalized plane stress. For the plate, the equilibrium equations, the strain-displacement equations, and the compatibility equations are the same as those given for the pin analysis, eqs. 40, 42, and 43. The constitutive equations for the plate are different than those of the pin and are given by

$$\begin{Bmatrix} \varepsilon_x \\ \varepsilon_y \\ \gamma_{xy} \end{Bmatrix} = \begin{bmatrix} \frac{1}{E_x} & -\frac{\nu_{xy}}{E_x} & 0 \\ -\frac{\nu_{yx}}{E_y} & \frac{1}{E_y} & 0 \\ 0 & 0 & \frac{1}{G_{xy}} \end{bmatrix} \begin{Bmatrix} \sigma_x \\ \sigma_y \\ \tau_{xy} \end{Bmatrix} , \tag{109}$$

where

$E_x \equiv$ plate modulus in the x direction

$E_y \equiv$ plate modulus in the y direction

$G_{xy} \equiv$ plate shear modulus

$\nu_{xy} \equiv$ plate Poisson ratio.

Proceeding in a manner analogous to that of the isotropic case, the stresses are written in terms of the stress function F:

$$\sigma_{xx} = \frac{\partial^2 F}{\partial y^2}$$

$$\sigma_{yy} = \frac{\partial^2 F}{\partial x^2} \tag{110}$$

$$\tau_{xy} = -\frac{\partial^2 F}{\partial x \partial y} .$$

Substituting these stresses into the constitutive equations and defining the strains in terms of the stress function, the nontrivial compatibility equation becomes

$$\frac{1}{E_x}\frac{\partial^4 F}{\partial y^4} + \left(\frac{1}{G_{xy}} - 2\frac{\nu_{xy}}{E_x}\right)\frac{\partial^4 F}{\partial x^2 \partial y^2} + \frac{1}{E_y}\frac{\partial^4 F}{\partial x^4} = 0 . \tag{111}$$

This governing differential equation is referred to as a generalized biharmonic equation. The characteristic equation of this differential equation is

$$\frac{1}{E_x}\mu^4 + \left(\frac{1}{G_{xy}} - 2\frac{\nu_{xy}}{E_x}\right)\mu^2 + \frac{1}{E_y} = 0 \ . \tag{112}$$

Due to energy considerations, the roots of this equation cannot be real valued [48]. In addition, the roots will occur in conjugate pairs. Therefore, the four roots of eq. 112 can be written as

$$\begin{aligned} \mu_1 &= \bar{\mu}_3 \\ \mu_2 &= \bar{\mu}_4 \ . \end{aligned} \tag{113}$$

Equation 112 is obtained by assuming

$$F = F(x + \mu y) \ . \tag{114}$$

If this assumption had been made for the isotropic case and this form for F had been substituted into eq. 44, with Q = 0, the result would have been repeated roots of $\mu = \pm i$. With this, the argument of F would be $x + iy$ or $x - iy$. Thus the motivation for using complex variables to aid in the solution of the biharmonic equation for the isotropic case.

As in the isotropic case it is convenient to use complex variables to aid in the solution of the generalized biharmonic equation. Four complex variables can be defined as

$$z_k = x + \mu_k y, \quad k = 1, 2, 3, 4 \ . \tag{115}$$

By eq. 113

$$\bar{z}_3 = z_1 \text{ and } \bar{z}_4 = z_2 \ . \tag{116}$$

With the definition of z_k in eq. 115,

$$z_1 = \gamma_1 z + \delta_1 \bar{z} \quad \text{and} \quad z_2 = \gamma_2 z + \delta_2 \bar{z} \ , \tag{117a,b}$$

where

$$\gamma_k = \frac{1-i\mu_k}{2} \quad \text{and} \quad \delta_k = \frac{1+i\mu_k}{2} \quad k = 1, 2 \ . \tag{118,119}$$

Differential operators can be defined as

$$D_k \equiv \frac{\partial}{\partial y} - \mu_k \frac{\partial}{\partial x} \ , \quad k = 1, 2, 3, 4 \ . \tag{120}$$

The generalized biharmonic equation can thus be written as

$$D_1 D_2 D_3 D_4 F = 0 \ . \tag{121}$$

Integrating eq. 121 four times yields the following equation:

$$F = \frac{1}{4} \left(W_1(x+\mu_1 y) + W_2(x+\mu_2 y) + W_3(x+\mu_3 y) + W_4(x+\mu_4 y) \right) \tag{122}$$

The stress function F must be real. Thus, by eq. 113, the four functions W_k, k = 1-4 must be related through complex conjugates. The solution for F thus assumes the form

$$F = \frac{1}{4}\left(W_1(z_1) + W_2(z_2) + \overline{W_1(\bar{z}_1)} + \overline{W_2(\bar{z}_2)}\right) \tag{123}$$

This is the Goursat equation for the orthotropic case.

Equation 123 will play a fundamental role in finding equations for the boundary conditions, just as in the isotropic case. It is convenient at this time however, to introduce some notation which was not required for the isotropic case. The following identities will be useful when using the Goursat equation:

$$\frac{\partial}{\partial x} = \frac{\partial}{\partial z_1} + \frac{\partial}{\partial \bar{z}_1} \qquad \frac{\partial}{\partial x} = \frac{\partial}{\partial z_2} + \frac{\partial}{\partial \bar{z}_2}$$

$$\frac{\partial}{\partial y} = \mu_1 \frac{\partial}{\partial z_1} + \bar{\mu}_1 \frac{\partial}{\partial \bar{z}_1} \qquad \frac{\partial}{\partial y} = \mu_2 \frac{\partial}{\partial z_2} + \bar{\mu}_2 \frac{\partial}{\partial \bar{z}_2}$$

$$\frac{\partial}{\partial z} = \frac{1}{2}\left(\frac{\partial}{\partial x} - i\,\frac{\partial}{\partial y}\right) \qquad \frac{\partial}{\partial \bar{z}} = \frac{1}{2}\left(\frac{\partial}{\partial x} + i\,\frac{\partial}{\partial y}\right) \tag{124}$$

$$(\mu_1 - \bar{\mu}_1)\frac{\partial}{\partial z_1} = -\bar{\mu}_1 \frac{\partial}{\partial x} + \frac{\partial}{\partial y}$$

$$(\mu_1 - \bar{\mu}_1)\frac{\partial}{\partial \bar{z}_1} = \mu_1 \frac{\partial}{\partial x} - \frac{\partial}{\partial y}$$

$$(\mu_2 - \bar{\mu}_2)\frac{\partial}{\partial z_2} = -\bar{\mu}_2 \frac{\partial}{\partial x} + \frac{\partial}{\partial y}$$

$$(\mu_2 - \bar{\mu}_2) \frac{\partial}{\partial \bar{z}_2} = \mu_2 \frac{\partial}{\partial x} - \frac{\partial}{\partial y} .$$

Using the definitions of eq. 124, the fundamental stress combinations can be found. Recall from Chapter 3 the following stress combinations:

$$\sigma_{xx} + \sigma_{yy} \equiv 4 \frac{\partial^2 F}{\partial z \partial \bar{z}} \tag{125a}$$

$$\sigma_{yy} - \sigma_{xx} + 2i\tau_{xy} \equiv 4 \frac{\partial^2 F}{\partial z^2} \tag{125b}$$

Taking the appropriate derivations of the stress function F, and recombining eq. 121, the following equations for the stresses are found:

$$\sigma_{xx} = \frac{1}{4} [\mu_1^2 W_1'' + \mu_2^2 W_2'' + \bar{\mu}_1^2 \bar{W}_1'' + \bar{\mu}_2^2 \bar{W}_2''] \tag{126a}$$

$$\sigma_{yy} = \frac{1}{4} [W_1'' + W_2'' + \bar{W}_1'' + \bar{W}_2''] \tag{126b}$$

$$\tau_{xy} = -\frac{1}{4} [\mu_1 W_1'' + \mu_2 W_2'' + \bar{\mu}_1 \bar{W}_1'' + \bar{\mu}_2 \bar{W}_2''] \tag{126c}$$

where

$$W_1'' \equiv \frac{\partial^2 W_1}{\partial z_1^2} \tag{127a}$$

$$W_2'' \equiv \frac{\partial^2 W_2}{\partial z_2^2} . \tag{127b}$$

Unfortunately these equations are not useful in their present form. This is because the stress functions W_1 and W_2 must be found through boundary condition requirements. The boundary conditions N-iT act on the boundary $z = e^{i\theta}$. However, the stress functions are written in terms of the variables z_1 and z_2. In other words, the analysis has been mapped from the z plane to two planes; z_1 and z_2. The boundary conditions have not been defined in the z_1 and z_2 planes. To remedy this problem, a second mapping is required. This mapping maps z_1 to ζ_1 and z_2 to ζ_2. In these mappings, ζ_1 and ζ_2 will be forced to transform such that at the hole boundary $\zeta_1 = \zeta_2 = z$. Under these transformations, the hole in the plate is mapped from an ellipse in the z_1 and z_2 planes to a circle in the ζ_1 and ζ_2 planes. Figure 7 shows the transformations used in this analysis. These transformations require a different approach in the development of the traction boundary conditions in terms of the stress functions. The relationship between the traction boundary condition and the stress function will now be derived.

First consider a line element, ds, in the z plane. Figure 8a shows this element along with its unit normal vector n. From the geometry of fig. 8a, the following equations relate $d\bar{z}$ to the line element ds:

$$dx = ds \cos\left(\frac{\pi}{2} + \alpha\right)$$

$$dy = ds \sin\left(\frac{\pi}{2} + \alpha\right)$$

$$dz = dx + idy$$

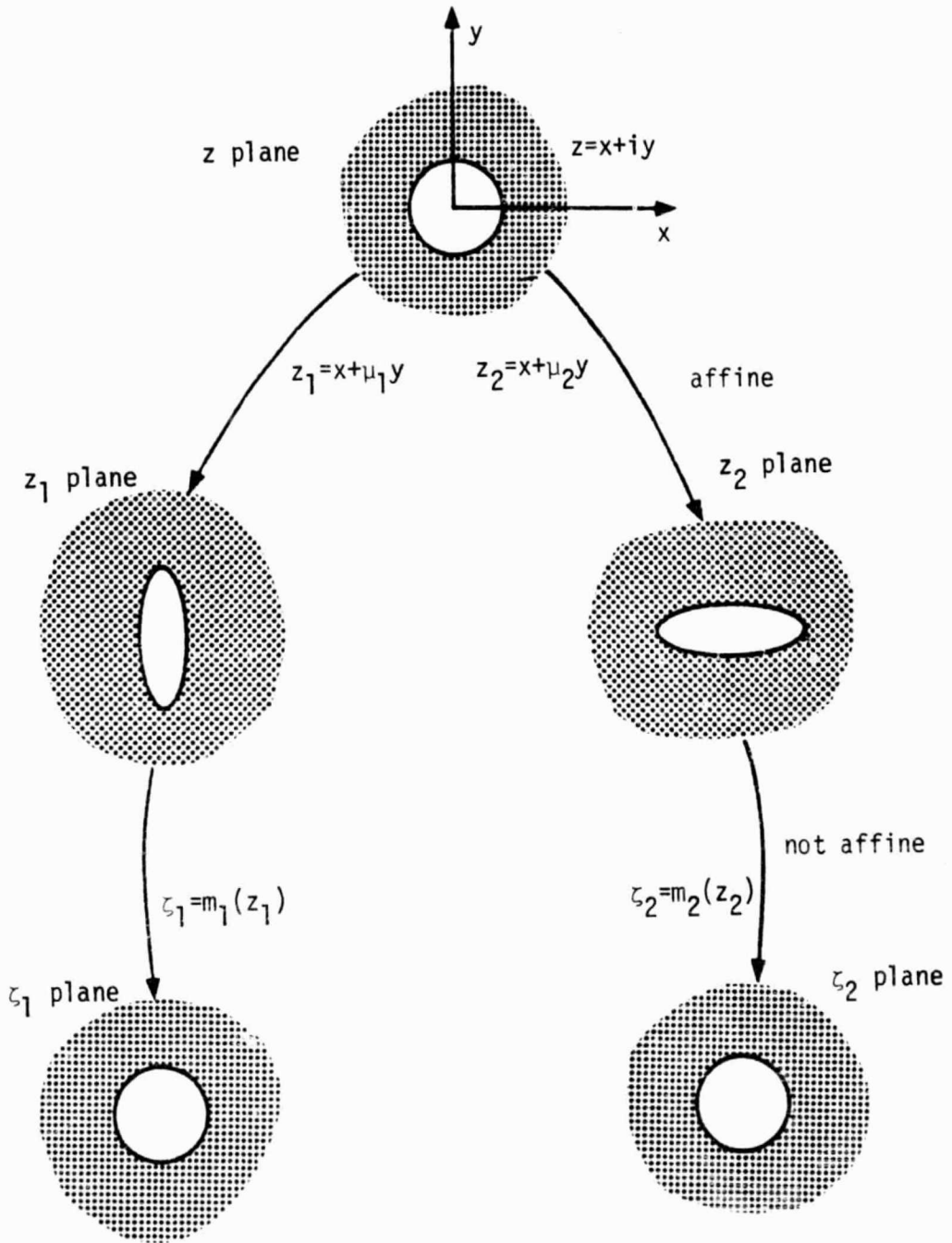

FIG. 7 TRANSFORMATIONS REQUIRED FOR THE ORTHOTROPIC SOLUTION.

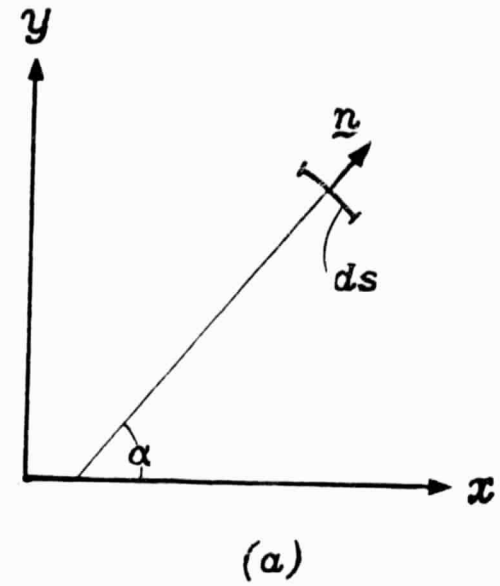

FIG. 8 BOUNDARY TRACTIONS

$$dz = ds[\cos\left(\frac{\pi}{2} + \alpha\right) + i \sin\left(\frac{\pi}{2} + \alpha\right)]$$

$$dz = ie^{i\alpha}ds$$

or

$$d\bar{z} = -ie^{-i\alpha}ds \ . \tag{128}$$

Now consider the tractions T_x and T_y acting on line element ds, fig. 8b. These tractions can be related to the normal and tangential tractions through the following equation:

$$T_x - iT_y = e^{-i\alpha}(N - iT) \ . \tag{129}$$

To find the total force acting on a portion of the circular boundary, the tractions acting on line element ds are integrated along the arc from the value of s denoting the beginning of the arc to value of s denoting the end of the arc. Defining the total forces acting on the arc in the x direction as X and in the y direction at Y, the following equation is obtained:

$$X - iY = \int (T_x - iT_y)ds \ . \tag{130}$$

Using eq. 129, the integral car be written as

$$Y - iY = \int (N - iT)e^{-i\alpha}ds \ . \tag{131}$$

Finally, using equation 128 to write the surface integral in terms of $\bar{z}$, the following equation is obtained:

$$X - iY = i \int (N - iT)\, d\bar{z} \,. \tag{132}$$

Returning to eq. 124, the tractions can be rewritten in terms of the stress function F, by using the following equation:

$$T_i = \sigma_{ij}\, n_j, \quad i, j = 1, 2 \tag{133}$$

where n_j are the direction cosines between the normal to ds and the x and y directions. Here

$$n_1 = \frac{\partial y}{\partial s} \text{ and } n_2 = -\frac{\partial x}{\partial s} \,. \tag{134}$$

Using eqs. 110 and 128 in eq. 133, the tractions on ds become

$$T_x - iT_y = \frac{\partial^2 F}{\partial y^2}\frac{\partial y}{\partial s} + \frac{\partial^2 F}{\partial x \partial y}\frac{\partial x}{\partial s} - i\left(-\frac{\partial^2 F}{\partial x \partial y}\frac{\partial y}{\partial s} - \frac{\partial^2 F}{\partial x^2}\frac{\partial x}{\partial s}\right) \,. \tag{135}$$

This equation is obtained when the chain rule is used to differentiate

$$T_x - iT_y = i\,\frac{\partial}{\partial s}\left(\frac{\partial F}{\partial x} - i\,\frac{\partial F}{\partial y}\right) \,,$$

i.e.,

$$T_x - iT_y = i\,\frac{\partial}{\partial s}\left(2\,\frac{\partial F}{\partial z}\right) \,. \tag{136}$$

Using this result in eq. 130, the total forces acting on the arc of arbitrary length can be written as:

$$X - iY = i \int \frac{\partial}{\partial s} \left(2 \frac{\partial F}{\partial z}\right) ds$$

$$= i \, 2 \frac{\partial F}{\partial z} \, . \tag{137}$$

Combining eqs. 132 and 137, a relation between the boundary condition and the stress function is obtained, namely,

$$2 \frac{\partial F}{\partial z} = \int (N - iT) \, d\bar{z} \, . \tag{138}$$

Differentiating the stress function with respect to z yields:

$$\frac{1}{2} \left[\bar{\delta}_1 \frac{\partial \bar{W}_1}{\partial \bar{z}_1} + \bar{\delta}_2 \frac{\partial \bar{W}_2}{\partial \bar{z}_2} + \gamma_1 \frac{\partial W_1}{\partial z_1} + \gamma_2 \frac{\partial W_2}{\partial z_2}\right] = \int (N - iT) \, d\bar{z} \, . \tag{139}$$

Note that the stress functions W_1 and W_2 are functions of z_1 and z_2, but the boundary tractions are a function of z. Therefore, the stress functions must be transformed to the ζ_1 and ζ_2 planes. This will now be done.

The coordinates z_1 and z_2 were previously related to z by

$$z_1 = \gamma_1 z + \delta_1 \bar{z} \tag{117a)R}$$

$$z_2 = \gamma_2 z + \delta_2 \bar{z} \tag{117b)R}$$

On the hole boundary in the plate, $z = e^{i\theta} \equiv \sigma$. Therefore, eqs. 117 take the following forms on the boundary:

$$z_1 = \gamma_1\sigma + \delta_1/\sigma \tag{140a}$$

$$z_2 = \gamma_2\sigma + \delta_2/\sigma \, . \tag{140b}$$

The mappings from the z_1 to the ζ_1 planes and from the z_2 to ζ_2 planes require $\zeta_1 = \zeta_2 = z = \sigma$ on the boundary. This motivates the transformations from the z_1 and z_2 planes to the ζ_1 and ζ_2 planes to be

$$z_1 = \gamma_1\zeta_1 + \delta_1/\zeta_1 \tag{141a}$$

$$z_2 = \gamma_2\zeta_2 + \delta_2/\zeta_2 \, . \tag{141b}$$

Solving eqs. 141 for ζ_1 and ζ_2 yields:

$$\zeta_1 = \frac{z_1 + \sqrt{z_1^2 - 4\gamma_1\delta_1}}{2\gamma_1} \tag{142a}$$

$$\zeta_2 = \frac{z_2 + \sqrt{z_2^2 - 4\gamma_2\delta_2}}{2\gamma_2} \, . \tag{142b}$$

The positive signs in front of the radicals have been chosen to insure that the mappings put the ζ_1 and ζ_2 domains outside the unit circle (i.e., the mappings give a plate with a hole, not a disk. A disk is obtained with a negative sign).

The derivatives $\frac{\partial \zeta_1}{\partial z_1}$ and $\frac{\partial \zeta_2}{\partial z_2}$ will be required later. These derivatives are found by differentiating eqs. 142. These derivatives are

$$\frac{\partial}{\partial z_1}\left(z_1 = \gamma_1 \zeta_1 + \delta_1/\zeta_1\right)$$

$$\frac{\partial}{\partial z_1}\left(\gamma_1 \zeta_1^{\,2} - \zeta_1 z_1 + \delta_1\right) = 0$$

$$2\gamma_1 \zeta_1 \frac{\partial \zeta_1}{\partial z_1} - z_1 \frac{\partial \zeta_1}{\partial z_1} - \zeta_1 = 0$$

$$\left(2\gamma_1 \zeta_1 - z_1\right) \frac{\partial \zeta_1}{\partial z_1} = \zeta_1 \,. \tag{143a}$$

Similarly,

$$\left(2\gamma_2 \zeta_2 - z_2\right) \frac{\partial \zeta_2}{\partial z_2} = \zeta_2 \,. \tag{143b}$$

The definitions for ζ_1 and ζ_2 which appear in eqs. 142 can be substituted into eqs. 143 to yield:

$$\left[2\gamma_1 \left(\frac{z_1 + \sqrt{z_1^{\,2} - 4\gamma_1 \delta_1}}{2\gamma_1}\right) - z_1\right] \frac{\partial \zeta_1}{\partial z_1} = \zeta_1$$

or

$$\frac{\partial \zeta_1}{\partial z_1} = \frac{\zeta_1}{\sqrt{z_1^{\,2} - 4\gamma_1 \delta_1}} \,, \tag{144a}$$

and similarly

$$\frac{\partial \zeta_2}{\partial z_2} = \frac{\zeta_2}{\sqrt{z_2^{\,2} - 4\gamma_2 \delta_2}} \,. \tag{144b}$$

With these results, it is now possible to define the stress functions of eq. 139 in terms of the new coordinates ζ_1 and ζ_2, i.e.,

$$\frac{\partial W_1}{\partial z_1} \equiv 2\phi_1(\zeta_1)$$
$$\frac{\partial W_2}{\partial z_2} \equiv 2\phi_2(\zeta_2) \ . \tag{145}$$

The specific forms of the stress functions $\phi_1(\zeta_1)$ and $\phi_2(\zeta_2)$ will now be defined.

Each component of stress has been defined by eqs. 126. In these equations, the second derivative of W_1 and W_2 are required. Equation 145 has defined the first derivatives of W_1 and W_2 in terms of the new stress functions $\phi_1(\zeta_1)$ and $\phi_2(\zeta_2)$. Equations 145 must therefore be differentiated to find the forms of W_1'' and W_2'' in terms of the new stress functions. This differentiation leads to:

$$\frac{\partial^2 W_1}{\partial z_1^2} = \frac{\partial}{\partial z_1}\left(\frac{\partial W_1}{\partial z_1}\right)$$
$$= \frac{\partial}{\partial z_1}\left(2\phi_1(\zeta_1)\right)$$
$$= 2\,\frac{\partial \phi_1}{\partial \zeta_1}\,\frac{\partial \zeta_1}{\partial z_1} \ . \tag{146a}$$

Similarly,

$$\frac{\partial^2 W_2}{\partial z_2^2} = 2\,\frac{\partial \phi_2}{\partial \zeta_2}\,\frac{\partial \zeta_2}{\partial z_2} \ . \tag{146b}$$

The partial derivatives $\frac{\partial \zeta_1}{\partial z_1}$ and $\frac{\partial \zeta_2}{\partial z_2}$ have been defined by eqs. 144. This leaves $\frac{\partial \phi_1}{\partial \zeta_1}$ and $\frac{\partial \phi_2}{\partial \zeta_2}$ to be defined. Since any analytic function can be represented by a Laurent series, these derivatives will be represented in the following forms:

$$\frac{\partial \phi_1}{\partial \zeta_1} = \sum_{-\infty}^{\infty} \alpha_n \zeta_1^n \tag{147a}$$

$$\frac{\partial \phi_2}{\partial \zeta_2} = \sum_{-\infty}^{\infty} \beta_n \zeta_2^n \,. \tag{147b}$$

Equations 146 now become

$$\frac{\partial^2 W_1}{\partial z_1^2} = 2 \left(\sum_{-\infty}^{\infty} \alpha_n \zeta_1^n \right) \frac{\zeta_1}{\sqrt{z_1^2 - 4\gamma_1\delta_1}} \tag{148a}$$

$$\frac{\partial^2 W_2}{\partial z_2^2} = 2 \left(\sum_{-\infty}^{\infty} \beta_n \zeta_2^n \right) \frac{\zeta_2}{\sqrt{z_2^2 - 4\gamma_2\delta_2}} \,. \tag{148b}$$

The boundary conditions for the plate exist on the inside of the hole and at the ends of the plate. The conditions at the inside of the hole will be satisfied using the method described in Chapter 2. The other conditions are placed on the stress distribution at $z = \infty$. These conditions are:

1) The stresses at $z = \infty$ are bounded, and

2) The plate must remain in equilibrium.

The geometry of the plate (i.e., infinite dimensions) and condition (2) above, require the stresses at infinity to not only be bounded, but they must be zero in magnitude. From eqs. 142 it is apparent that

if $z_1 = \infty$ and $z_2 = \infty$, then $\zeta_1 = \infty$ and $\zeta_2 = \infty$. When infinite values of ζ_1 and ζ_2 are substituted into eq. 148 it is evident that some of the coefficients α_n and β_n must be zero if the stresses at infinity are to be zero. These coefficients are:

$$\alpha_n = 0 \qquad \text{for } n \geq 0 \,. \tag{149}$$
$$\beta_n = 0 \,.$$

This leaves the following forms for the derivatives $\frac{\partial \phi_1}{\partial \zeta_1}$ and $\frac{\partial \phi_2}{\partial \zeta_2}$:

$$\frac{\partial \phi_1}{\partial \zeta_1} = \left(\frac{a_0}{\zeta_1} - \sum_{n=1}^{\infty} n \frac{a_n}{\zeta_1^{n+1}}\right) \tag{150a}$$

$$\frac{\partial \phi_2}{\partial \zeta_2} = \left(\frac{b_0}{\zeta_2} - \sum_{n=1}^{\infty} n \frac{b_n}{\zeta_2^{n+1}}\right) , \tag{150b}$$

where

$$a_0 \equiv \alpha_{-1}$$
$$b_0 \equiv \beta_{-1}$$
$$-n a_n \equiv \alpha_{-(n+1)} \quad n \geq 1$$
$$-n b_n \equiv \beta_{-(n+1)} \quad n \geq 1 \,.$$

Integration of eqs. 150 yields the stress functions required in eq. 139. These stress functions are

$$\frac{\partial W_1}{\partial z_1} \equiv 2\phi_1(\zeta_1) = 2\left(a_0 \ln \zeta_1 + \sum_{n=1}^{\infty} \frac{a_n}{\zeta_1^n}\right) \tag{151a}$$

$$\frac{\partial W_2}{\partial z_2} \equiv 2\phi_2(\zeta_2) = 2\left(b_o \ln \zeta_2 + \sum_{n=1}^{\infty} \frac{b_n}{\zeta_2^n}\right) . \qquad (151b)$$

Equation 139 is now fully defined in the ζ_1 and ζ_2 planes and takes the form

$$[\overline{\delta_1}\overline{\phi_1(\zeta_1)} + \overline{\delta_2}\overline{\phi_2(\zeta_2)} + \gamma_1\phi_1(\zeta_1) + \gamma_2\phi_2(\zeta_2)] = \int (N-iT)d\overline{z} . \qquad (152)$$

It is important to realize that the right-hand-side of eq. 152 is integrated along the boundary arc to some particular value of s. The left hand side is evaluated at the value of $z = x + iy$ on the boundary arc which corresponds to the end point of the arc of length s.

Recalling that $\zeta_1 = \zeta_2 = z = e^{i\theta}$ on the boundary, it is now possible to define eq. 152 in terms of a common variable $\sigma \equiv e^{i\theta}$. For example, on the boundary the stress functions ϕ_1 and ϕ_2 become:

$$\phi_1(\sigma) = a_o \ln \sigma + \sum_{n=1}^{\infty} \frac{a_n}{\sigma^n} \qquad (153a)$$

$$\phi_2(\sigma) = b_o \ln \sigma + \sum_{n=1}^{\infty} \frac{b_n}{\sigma^n} \qquad (153b)$$

Differentiating eq. 152 with respect to $\overline{\sigma}$ ($= \overline{z}$ on the boundary) now yields

$$\overline{\delta}_1 \frac{\partial \overline{\phi}_1}{\partial \overline{\sigma}} + \overline{\delta}_2 \frac{\partial \overline{\phi}_2}{\partial \overline{\sigma}} + \gamma_1 \frac{\partial \phi_1}{\partial \sigma}\frac{\partial \sigma}{\partial \overline{\sigma}} + \gamma_2 \frac{\partial \phi_2}{\partial \sigma}\frac{\partial \sigma}{\partial \overline{\sigma}} = N - iT . \qquad (154)$$

The derivative $\frac{\partial \sigma}{\partial \overline{\sigma}}$ is equal to $-\sigma^2$, thus eq. 154 becomes

$$\bar{\delta}_1 \frac{\partial \bar{\phi}_1}{\partial \bar{\sigma}} + \bar{\delta}_2 \frac{\partial \bar{\phi}_2}{\partial \bar{\sigma}} - \sigma^2 \gamma_1 \frac{\partial \phi_1}{\partial \sigma} - \sigma^2 \gamma_2 \frac{\partial \phi_2}{\partial \sigma} = N - iT \ . \tag{155}$$

The derivatives $\frac{\partial \phi_1}{\partial \zeta_1}$ and $\frac{\partial \phi_2}{\partial \zeta_2}$ were defined in eq. 150. Upon substitution of σ for ζ_1 and ζ_2, these derivatives become:

$$\frac{\partial \phi_1}{\partial \sigma} = \frac{1}{\sigma} \left(a_0 - \sum_{n=1}^{\infty} n \frac{a_n}{\sigma^n} \right) \tag{156a}$$

$$\frac{\partial \phi_2}{\partial \sigma} = \frac{1}{\sigma} \left(b_0 - \sum_{n=1}^{\infty} n \frac{b_n}{\sigma^n} \right) \ . \tag{156b}$$

Substituting eqs. 156 into eq. 155 results in

$$\begin{aligned} &- \gamma_1 \left(a_0 \sigma - \sum_{n=1}^{\infty} n \, a_n \sigma^{-(n-1)} \right) - \gamma_2 \left(b_0 \sigma - \sum_{n=1}^{\infty} n \, b_n \sigma^{-(n-1)} \right) + \\ &\bar{\delta}_1 \left(\bar{a}_0 \sigma - \sum_{n=1}^{\infty} n \, \bar{a}_n \sigma^{n+1} \right) + \bar{\delta}_2 \left(\bar{b}_0 \sigma - \sum_{n=1}^{\infty} n \, \bar{b}_n \sigma^{n+1} \right) = N - iT \ . \end{aligned} \tag{157}$$

Just as in the isotropic case, N - iT is expanded in a Fourier series and like powers of σ are compared to obtain the coefficients a_n and b_n. This procedure is summarized in Table 2. The coefficients a_0, b_0, $\bar{a}_0$, and $\bar{b}_0$ require special consideration. This is as follows.

Comparing the coefficients multiplying σ^{+1} yields two equations for the four unknowns a_0, b_0, $\bar{a}_0$ and $\bar{b}_0$. To obtain two more equations, a restriction on the displacement field in the plate must be imposed. Mathematically, the logarithmic terms in eqs. 151 are multivalued. If this were left as such, the displacements in the plate would also be multivalued. It is necessary, therefore, to impose restrictions on the

Table 2

Coefficients for the Stress Functions ϕ_1 and ϕ_2.

A_n	a_n	b_n
A_o	$a_1 = 1/(\gamma_1 - \frac{\delta_1}{\delta_2}\gamma_2)$	$b_1 = 1/(\gamma_2 - \frac{\delta_2}{\delta_1}\gamma_1)$
A_{-1}	$a_2 = 1/[2(\gamma_2 - \frac{\delta_2}{\delta_1}\gamma_1)]$	$b_2 = 1/[2(\gamma_1 - \frac{\delta_1}{\delta_2}\gamma_2)]$
A_{+1}	*	*
A_{-2}	$a_3 = 1/[3(\gamma_2 - \frac{\delta_2}{\delta_1}\gamma_1)]$	$b_3 = 1/[3(\gamma_1 - \frac{\delta_1}{\delta_2}\gamma_2)]$
A_{+2}	$a_1 = 1/(\delta_2\frac{\gamma_1}{\gamma_2} - \delta_1)$	$b_1 = 1/(\delta_1\frac{\gamma_2}{\gamma_1} - \delta_2)$
. . . .	. . . .	. . . .
A_{-k}	$a_{(k+1)} = 1/[(k+1)(\gamma_1 - \frac{\delta_1}{\delta_2}\gamma_2)]$	$b_{(k+1)} = 1/[(k+1)(\gamma_1 - \frac{\delta_1}{\delta_2}\gamma_2)]$
A_{+k}	$a_{(k-1)} = 1/[(k-1)(\delta_2\frac{\gamma_1}{\gamma_2} - \delta_1)]$	$b_{(k-1)} = 1/[(k-1)(\delta_1\frac{\gamma_2}{\gamma_1} - \delta_2)]$

*See text for explanation

coefficients a_o and b_o which will force the displacements to be single-valued. In this process, two more equations involving these coefficients are generated. There are then four equations with which to solve for a_o, b_o, $\bar{a}_o$, and $\bar{b}_o$. The equations needed to enforce the single valued displacements will now be developed.

To begin, it is necessary to develop an equation which relates the displacements to the complex stress functions. The procedure for the orthotropic case follows that of the isotropic case exactly. Specific differences arise due to the forms of the constitutive relations for each case. Due to the complexity of the algebra involved in the orthotropic case, the derivation of the displacement equations will not be presented here. Instead, an outline of the method is presented below.

1) Write the strains in terms of the displacements

$$\varepsilon_x = \frac{\partial u}{\partial x} \qquad \varepsilon_y = \frac{\partial v}{\partial y} \qquad \gamma_{xy} = \frac{\partial u}{\partial y} + \frac{\partial v}{\partial x} .$$

2) Use the stresses of eqs. 126 in the constitutive relations to find the derivatives of the displacements in terms of the stress functions $W_1(z_1)$ and $W_2(z_2)$.

3) Combine these equations and integrate with respect to z to obtain the displacement equation.

The following equation is the result of this procedure:

$$4(u + iv) = p_1 W_1' + p_2 W_2' + \bar{q}_1 \bar{W}_1' + \bar{q}_2 \bar{W}_2' , \qquad (158)$$

where

$$p_1 \equiv -\frac{\nu_{xy}}{E_x} + \frac{1}{E_x}\mu_1^2 + \frac{i}{\mu_1}\left(\frac{1}{E_y} - \frac{\nu_{xy}}{E_x}\mu_1^2\right) \tag{159a}$$

$$p_2 \equiv -\frac{\nu_{xy}}{E_x} + \frac{1}{E_x}\mu_2^2 + \frac{i}{\mu_2}\left(\frac{1}{E_y} - \frac{\nu_{xy}}{E_x}\mu_2^2\right) \tag{159b}$$

$$\bar{q}_1 \equiv -\frac{\nu_{xy}}{E_x} + \frac{1}{E_x}\bar{\mu}_1^2 + \frac{i}{\bar{\mu}_1}\left(\frac{1}{E_y} - \frac{\nu_{xy}}{E_x}\bar{\mu}_1^2\right) \tag{159c}$$

$$\bar{q}_2 \equiv -\frac{\nu_{xy}}{E_x} + \frac{1}{E_x}\bar{\mu}_2^2 + \frac{i}{\bar{\mu}_2}\left(\frac{1}{E_y} - \frac{\nu_{xy}}{E_x}\bar{\mu}_2^2\right) . \tag{159d}$$

Recall from eqs. 151 the following definitions:

$$W_1' = \frac{\partial W_1}{\partial z_1} = 2\left(a_o \ln \zeta_1 + \sum_{n=1}^{\infty} \frac{a_n}{\zeta_1^n}\right) \tag{160a}$$

$$W_2' = \frac{\partial W_2}{\partial z_2} = 2\left(b_o \ln \zeta_2 + \sum_{n=1}^{\infty} \frac{b_n}{\zeta_1^n}\right) . \tag{160b}$$

When transversing the boundary $z = e^{i\theta}$ from $\theta = 0$ to $\theta = 2\pi$, it is evident that each term of the stress functions W_1' and W_2' returns to their original value except the logarithmic terms. These terms increase by a factor of $2\pi i$. The displacements at $\theta = 2\pi$ and $\theta = 0$ are therefore related through the following equation:

$$(u + iv)_{\theta=2\pi} = 2\pi i(p_1 a_o + p_2 b_o - \bar{q}_1 \bar{a}_o - \bar{q}_2 \bar{b}_o) + (u + iv)_{\theta=0} \tag{161}$$

Thus, if the displacements are to be single valued,

$$p_1 a_o + p_2 b_o - \bar{q}_1 \bar{a}_o - \bar{q}_2 \bar{b}_o = 0 \qquad (162a)$$

and its conjugate

$$\bar{p}_1 \bar{a}_o + \bar{p}_2 \bar{b}_o - q_1 a_o - q_2 b_o = 0 \ . \qquad (162b)$$

Using these two equations and the equations obtained by comparing like powers of σ in eq. 157, a_o, b_o, $\bar{a}_o$ and $\bar{b}_o$ can be found. This will be done numerically in the computer program developed for this study.

With the analysis of the orthotropic plate complete, the results can be combined with the reults of Chapter 3 to implement the solution scheme described in Chapter 2.

Chapter 5

DETAILS OF THE NUMERICAL SCHEME

As described in Chapter 2, the various coefficients multiplying the unknowns A_k in eq. 39 are computed by the closed-form complex variable techniques described in the previous two chapters. The constants a_k and b_k tabulated in Tables 1 and 2 are used to compute the stresses and displacements of the plate and pin due to the traction $e^{ik\theta}$. Once all the quantities have been computed, they are assembled into the system of linear equations, eq. 39. The system is solved using a standard linear equation solver.

Modifying the system of equations

Operationally, eq. 39 had to be modified in order to effect a solution. As they are stated, the system of equations in eq. 39 cannot be solved. The reason is as follows: The elasticity solution for the displacement of the pin and the displacement of the plate to the traction $N\text{-}iT = e^{ik\theta}$ automatically yields

$$(u_\theta)_{k\ \text{pin}} = (u_\theta)_{k\ \text{plate}} = 0 \quad @\ \theta = 0\ ,\ k = 0, \pm 1, \ldots \pm N\ . \tag{163}$$

This is due to the antisymmetric nature of the functional dependence on θ of the tangential pin and plate displacements to traction $N\text{-}iT = e^{ik\theta}$. Also due to the nature of the solution, the conditions

$$(\tau_{r\theta})_{k\ \text{pin}} = (\tau_{r\theta})_{k\ \text{plate}} = 0 \quad \text{at}\ \theta = \pi,\ k = 0, \pm 1, \ldots, \pm N\ . \tag{164}$$

are automatically satisfied. The collocation procedure included the points $\theta = 0$ and $\theta = \pi$. This is necessary because there is one other condition at each point that must be enforced. These conditions are

$$(u_r)_{pin} = (u_r)_{plate} \quad @\ \theta = 0 \text{ and } \sigma_{rr} = 0 \quad @\ \theta = \pi. \quad (165, 166)$$

The conditions

$$u_{\theta}{}_{pin} - u_{\theta}{}_{plate} = 0 \quad @\ \theta = 0 \quad \text{and} \quad (\tau_{r\theta}) = 0 \quad @\ \theta = \pi (167,168)$$

were eliminated from eq. 39. To include them would result in two rows being identically zero and producing a singular matrix. Thus the number of equations solved and the number of A_k's was 2N-2.

Finding α and β

As has been mentioned previously, actually solving the reduced set of linear equations required having numerical values for α and β. A specific set of values were chosen for α, β, and δ, the rigid body pin displacement. The system of equations was then solved. In all likelihood the values of α and β chosen were not the correct values for the specified value of δ. As a consequence, one or more of the physical realities of the problem, expressed as what will be termed auxiliary boundary conditions, were violated. Subsequently, an iteration process was used to find values of α and β which satisfied all the conditions.

The iteration processes was divided into two parts, 1) the finding of β, and, 2), the finding of α. The two parameters were not found to be strongly dependent on one another.

The key to the iteration process for finding α and β was the satisfaction of the auxiliary boundary conditions. These auxiliary boundary conditions are the combination of a restatement of the conditions stipulated by eqs. 1-6, and statements of the physics of the problem. Specifically, the auxiliary boundary conditions are:

$$N = T = 0 \ @ \ \theta = \beta \tag{169}$$

$$N = T = 0, \ \beta < \theta < \pi \tag{170}$$

$$N < 0 \text{ all } \theta \tag{171}$$

$$T = \mu N \ @ \ \theta = \alpha \tag{172}$$

$$T < \mu N \ 0 < \theta < \alpha \tag{173}$$

Equations 169 and 172 are written explicitly because these were the most powerful indicators of convergence to the correct values of α and β. These above five equations express the fact that the normal traction must remain compressive everywhere and that it must be zero at the value of θ corresponding to the loss of pin/plate contact. Also, in the region of no slip, the friction-induced shear traction, must be less than or equal to the normal traction. At the end of the no-slip region the shear traction must be exactly equal to μ times the normal traction.

Figure 9 diagrams the procedure used in the iteration process to determine the half-contact angle, β. In this figure, a typical stress

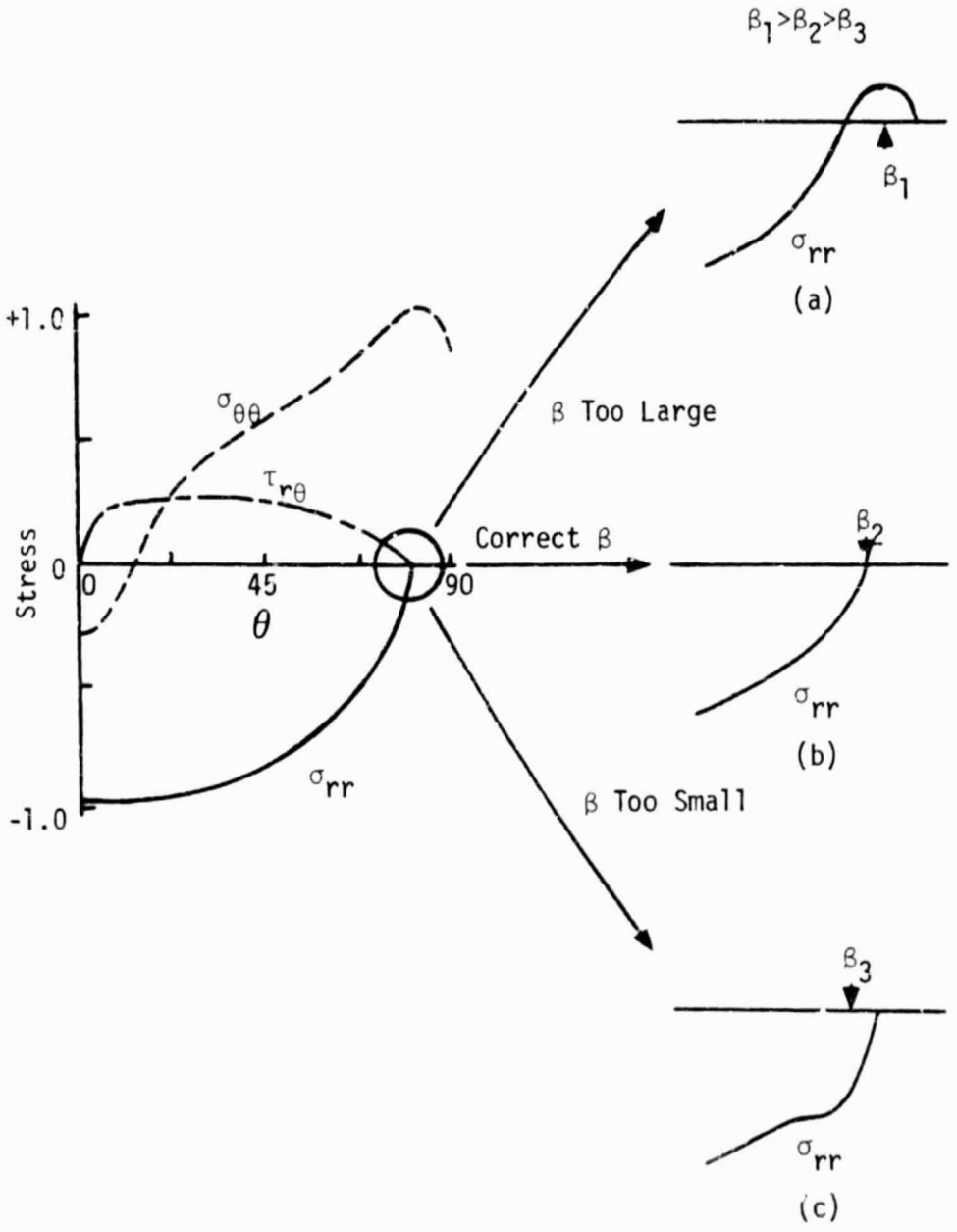

FIG. 9 ITERATION PROCEDURE FOR THE HALF-CONTACT ANGLE, β.

distribution for the plate at R = 1 is shown for $0° < \theta < 90°$. The normal stress, σ_{rr}, in the region of $\theta = \beta$ is shown for three choices of β. As shown in fig. 9a, if β is too great, the normal stress becomes tensile -- a physical impossibility in the contact region. If β is too small, however, as shown in fig. 9c, the normal stress is compressive but not zero as required by the boundary condition at $\theta = \beta$. The correct choice of β, fig. 9b, yields a zero value for the normal stress at $\theta = \beta$. All cases considered have followed this description of the iterative procedure exactly, and each solution appears to be unique.

A similar iterative procedure for determining the region of no-slip, $-\alpha < \theta < \alpha$, is shown in fig. 10. In this case, the shear stress, $\tau_{r\theta}$, at $\theta = \alpha$ is analyzed. If the shear stress at $\theta = \alpha$ is greater than $|\mu\sigma_{rr}|$, as in fig. 10a, then the no slip angle is too large. On the other hand, if $\tau_{r\theta} < |\mu\sigma_{rr}|$, as in fig. 10c, then the no slip angle is too small. When the correct choice of α is made, as in fig. 10b, then the boundary condition at $\theta = \alpha$ (i.e., $\tau_{r\theta} = |\mu\sigma_{rr}|$) is satisfied. As in the case of the contact angle, this procedure was found to be general, and all solutions to date appear to be unique.

The procedure for finding α and β was to set α to a value corresponding to the angular location of the first collocation point away from $\theta = 0$. With this value of α, the value of β was found by the iteration method discussed in fig. 9. Once a value of β was found, the iteration procedure focused on finding the value of α. When this was done, β was checked. There generally was little coupling between the two variables.

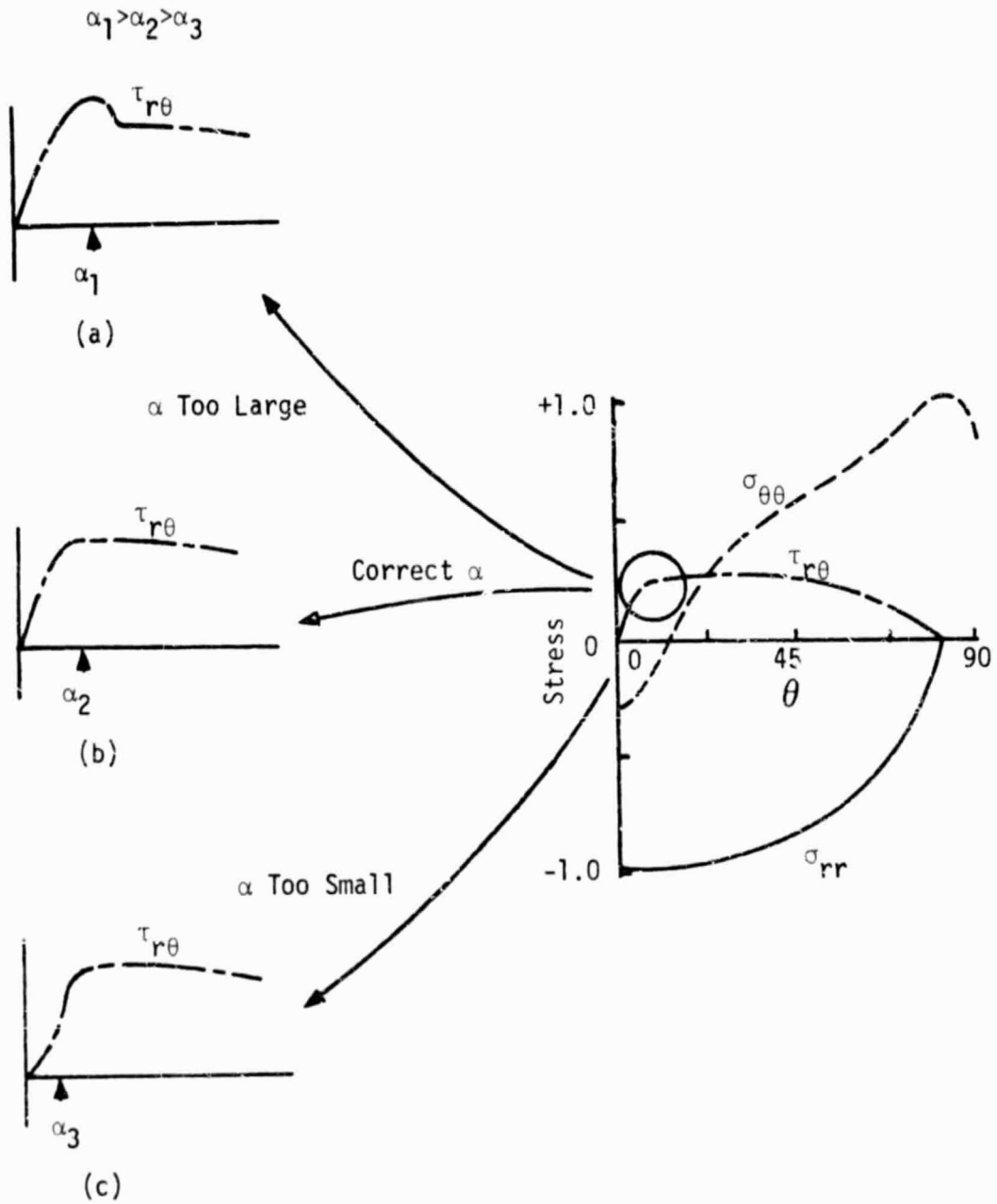

FIG. 10 ITERATION PROCEDURE FOR THE NO-SLIP ANGLE, α.

For lower values of the coefficient of friction (e.g., $\mu = 0.2$), the no-slip region was found to be small. Often times the angle α was less than the spacing between $\theta = 0°$ and the first collocation point. In these cases, the no-slip boundary condition was satisfied at only one point i.e., $\theta = 0°$. Larger values of the coefficient of friction (e.g., $\mu = 0.4$) enlarged the no slip region. For these cases, the number of points at which the no-slip boundary conditions was satisfied were increased. Due to the limited size of the no-slip region, it was found to be very simple to iterate to the correct value of α. The half-contact angle, β, on the other hand, varied greatly from case to case and generally took more iterations to converge to the correct solution.

Collocation points

Overall, however, the convergence of the solution was found to be dependent on the location and number of points used to satisfy the boundary conditions (i.e., the collocation points). As mentioned in Chapter 2, two boundary conditions were enforced at each point. In earlier stages of programming, each boundary condition was enforced at a different point. This arrangement proved to have poor convergence characteristics and was abandoned in favor of enforcing two boundary conditions at each point.

Additional convergence problems were encountered when the spacing between the collocation points was not uniform. The analysis requires that the number of points in the contact region and those outside the contact region be specified separately. It is quite possible that the

point spacing in one region could be quite different than in the other region. In such cases, the solution was found to oscillate in the region with the widest spacing. This problem was easily overcome, however, by ensuring that the point spacing was as uniform as possible for the entire region $0 < \theta < \pi$.

It was found that if fewer than ten points were used to satisfy the boundary conditions, the solutions were inaccurate. Twenty to thirty points along the boundary gave reasonable results. Forty points were used to obtain the results presented in this report. Forty points was close to the upper limit of the interactive capability of the computer used in this analysis.

The solutions presented here all have 78 unknown A_k's in the series representation of the boundary traction. The 78 terms were divided evenly between negative k terms and positive k terms. The solutions were forced to satisfy a total of 78 boundary conditions at 40 points around the half-circle. This means the boundary conditions are met at roughly every 4.6° around the circumference of the hole.

Computer programs

The computer programs were written at NASA Langley Research Center, Hampton, Virginia. The machines that were available for this work were Control Data Corporation Cyber 173's. Control Data's Fortran, version 5, language was used throughout the analysis. Due to the finite memory limitations of these machines and the extensive use of complex variables

in the analysis, it was necessary to use single precision accuracy. Single precision accuracy for the Cyber 173 is 14 digits.

Run times were typically 12-15 seconds. This made interactive analysis practical. In fact, one of the goals of the numerical scheme was to make it efficient enough so that convergence to α and β could be effected by means of interactive computing. A "human in the loop" made the scheme more attractive than imbedding the stress analysis in an iteration loop with convergence criteria. With graphics and short run times, the program was ideal for interactive usage. With some practice, a solution could be found in as little as four iterations.

Chapter 6

NUMERICAL RESULTS

Comparison with past work

To build confidence in the present technique, numerical results obtained from it were compared with the results of other researchers. The results of previous researchers generally include more restrictive assumptions than were used in this study and were often more restricted in overall scope. However, they from a basis with which to compare the current results.

The studies which are most similar to the present work were produced by de Jong [3, 11] and Crews [16]. Recall that de Jong's work represented a rigid pin in an infinite orthotropic plate. This work included friction and only considered loading, not unloading. In addition, de Jong studied only the linear, push-fit case. Crews, on the other hand, studied elastic pin-loaded plates of various widths. His study did not include friction and the clearance was not varied. Nonethe-less, the papers by de Jong and Crews offer good results for comparison with the present study. One of the comparisons is presented in figs. 11-12. This comparison is for the frictionless case of a rigid pin-loaded isotropic plate. The contact stresses and the hoop stress are shown for the region $0 \leq \theta \leq 90°$ in these plots. Symmetry and antisymmetry conditions can be used to find the stresses in the region $-90° \leq \theta \leq 0$. Outside these regions the contact stresses are zero and the hoop stress decays steadily to a near zero value at $\theta = 180^0$. This display of results will be used throughout the rest of this report.

Figure 11 shows a comparison of the normal stress, σ_{rr}, as computed by de Jong [3], Crews [16] and the present investigation. Figure 12 shows a comparison of the hoop stress, $\sigma_{\theta\theta}$. As can be seen, there is excellent agreement among the three studies. There is a difference among the three, however, at the end of the contact region ($\theta = \beta$). This is not surprising since neither de Jong nor Crews iterated to find the value of β. In contrast, iteration to find the correct value of β was a key step in the present analysis.

Another comparison with previous results is shown in figs. 13 and 14. These figures display the contact and hoop stresses as a function of circumferential location. The results are for a rigid pin-loaded quasi-isotropic plate. Friction is included in both de Jong's [11] and the present study. The agreement between the two solutions is good except in the no-slip region, near ($\theta = 0$), and at the end of the contact region. Recall, de Jong assumed boundary conditions in the no-slip region. Also, de Jong did not iterate to find β. The boundary conditions were not approximated in the present study, hence differences might be expected. The following discussion demonstrates the analysis' flexibility by presenting the results of a limited parametric study. This parametric study was designed to show the influence of the various parameters on the response of the plate. As such, the parametric study presents new and interesting results regarding the stress in pin-loaded orthotropic plates.

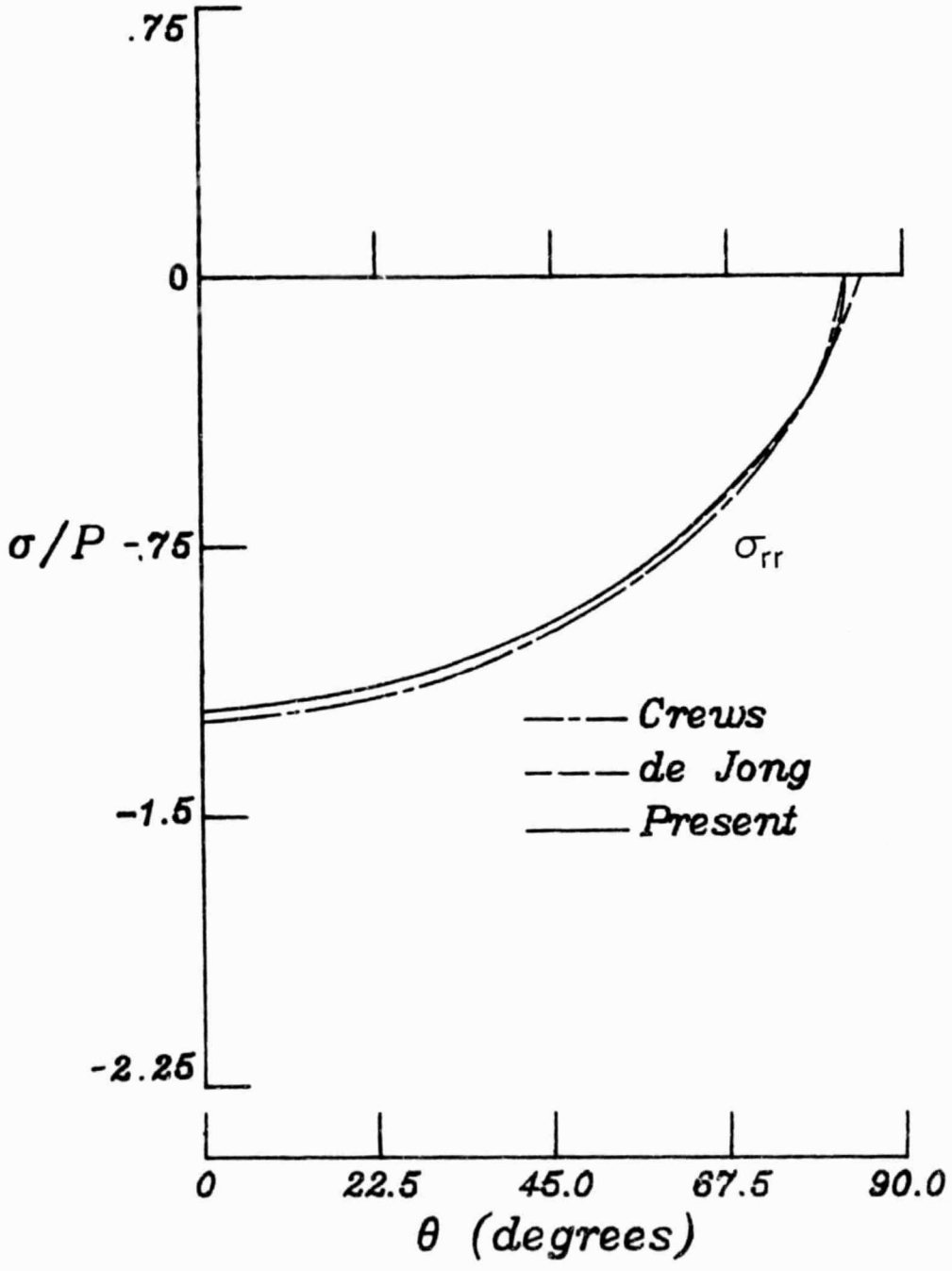

FIG. 11 COMPARISON OF THE CONTACT STRESSES FOR AN ISOTROPIC PLATE LOADED BY A RIGID, FRICTIONLESS PIN. (CREWS - REF. 16, DE JONG - REF. 3)

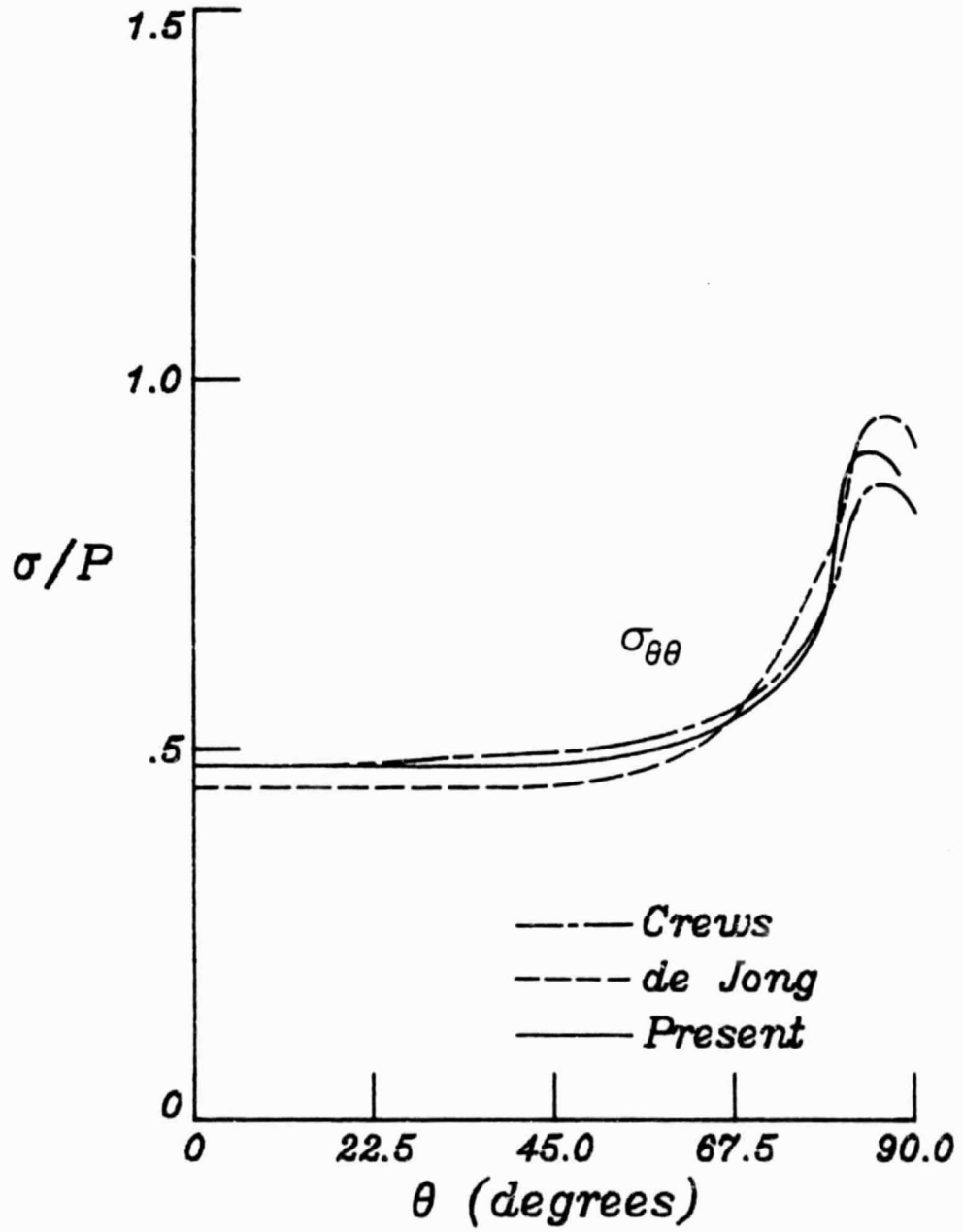

FIG. 12 COMPARISON OF THE HOOP STRESSES FOR AN ISOTROPIC PLATE LOADED BY A RIGID, FRICTIONLESS PIN. (CREWS - REF. 16, DE JONG - REF. 3)

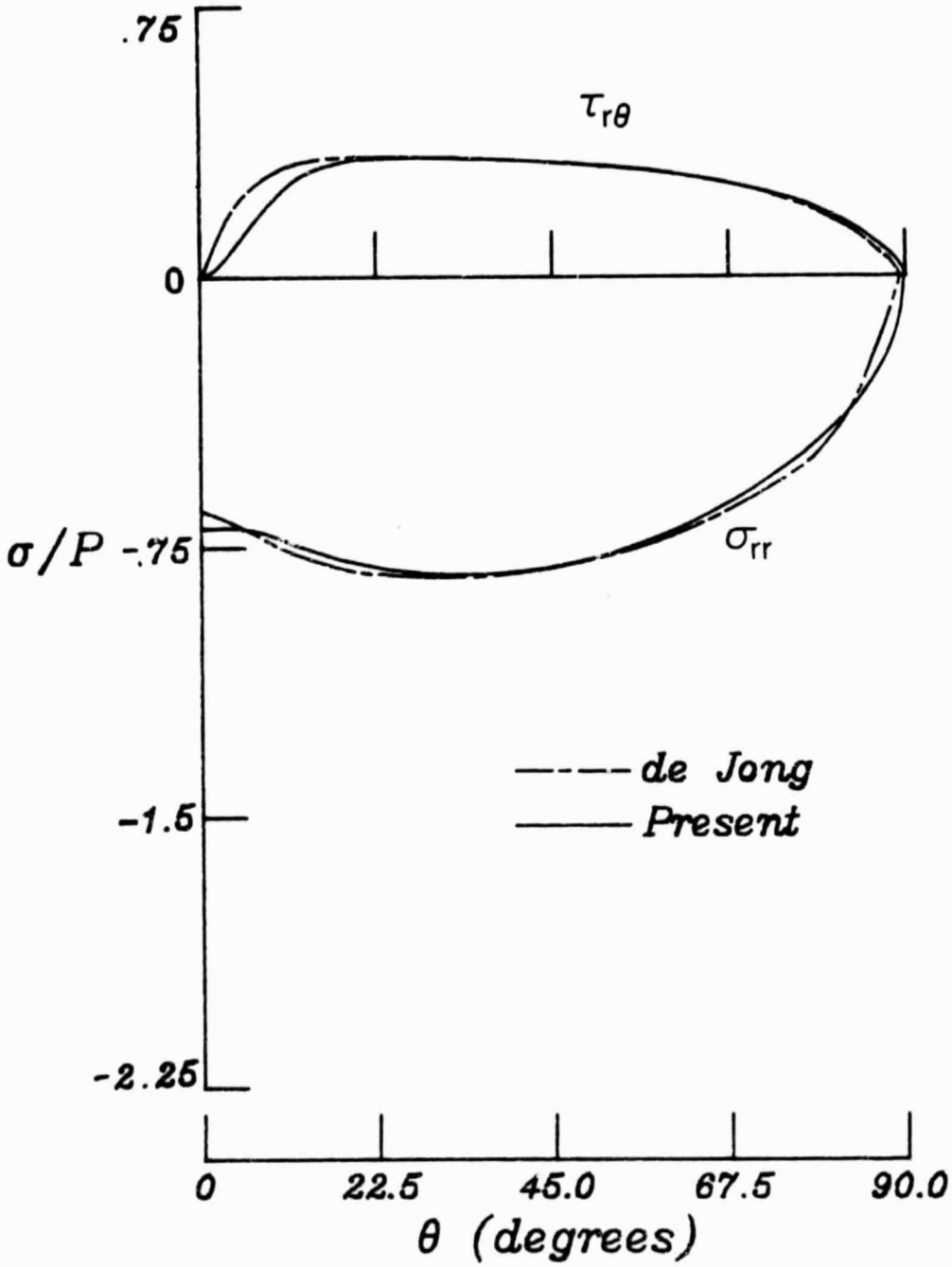

FIG. 13 COMPARISON OF THE CONTACT STRESSES FOR A QUASI - ISOTROPIC PLATE LOADED BY A RIGID PIN WITH A FRICTION COEFFICIENT OF 0.2 (DE JONG - REF. 11)

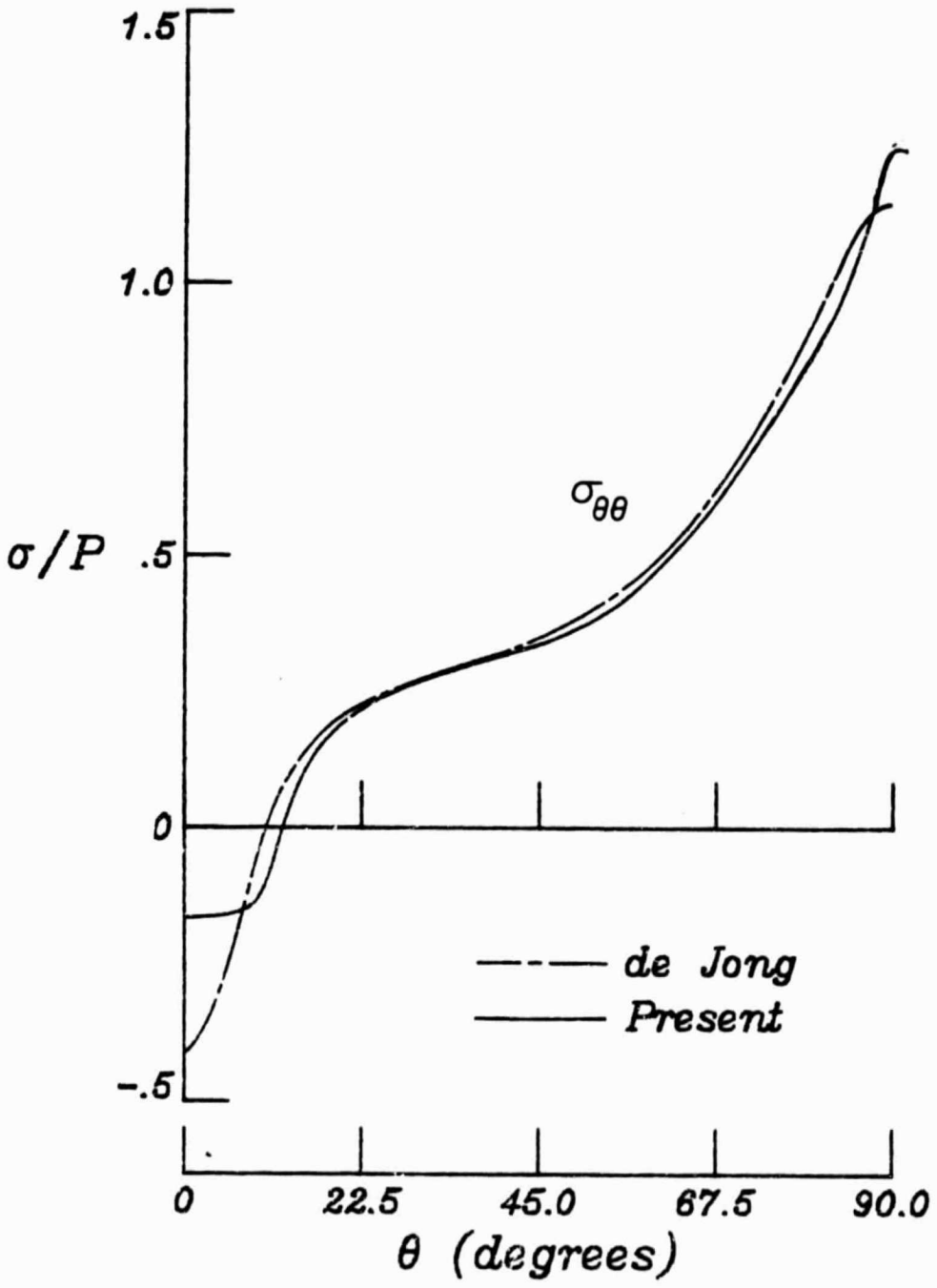

FIG. 14 COMPARISON OF THE HOOP STRESSES FOR A QUASI - ISOTROPIC PLATE LOADED BY A RIGID PIN WITH A FRICTION COEFFICIENT OF 0.2 (DE JONG - REF. 11)

Parametric studies

A standard case has been adopted to show which parameters have the greatest effect on the problem. The parameters for the standard case are

pin - steel,

friction coefficient - 0.2,

loading direction - positive (i.e., $\mu = -0.2$)

clearance - $\lambda = 0.01$,

rigid body pin displacement - $\delta = 0.07$.

A steel pin ($E = 30 \times 10^6$ psi, $\nu = .25$) was chosen to simulate steel bolts commonly used to join composite panels. Various values of the coefficient of friction between steel and graphite epoxy have been found, but $\mu = 0.2$ seems to be the most widely accepted value and will therefore be used as the standard case in this report. A clearance of 1% has also been found to be reasonable for typical joints tested in a laboratory environment. The parametric study will begin by varying the plate properties. Various laminates of graphite epoxy will be used to study the effects of plate properties on the stress distributions. The properties were chosen from the report by Crews [16]. They are listed in Table 3. As can be seen, these laminates represent a wide variation in plate properties.

These properties were used along with the other parameters in the standard case to compute stresses. The numerical results appear in

Table 3

Plate Properties

Laminate	$E_x \cdot 10^{-6}$(psi)	$E_y \cdot 10^{-6}$(psi)	ν_{xy}	$G_{xy} \cdot 10^{-6}$(psi)
$[0/\pm45/90]_s$	8.40	8.40	0.310	3.20
$[0]_8$	21.31	1.58	0.380	.93
$[90]_8$	1.58	21.31	0.028	.93
$[0/90]_{2s}$	11.53	11.53	0.052	.93
$[\pm45]_{2s}$	3.26	3.26	0.735	5.47
$[0/\pm45]_s$	9.31	4.09	0.699	3.96

figures which occur in pairs according to the plate material. The first figure of each pair gives the normal and shear contact stresses, σ_{rr} and $\tau_{r\theta}$, and the hoop stresses, $\sigma_{\theta\theta}$, for the plate at the hole edge. This is similar to the presentation of results for comparison with other investigators. The second figure of each pair gives the net-section and shear-out stresses for each plate. The net-section and shear-out planes are shown in fig. 15. The stresses along these planes are typically studied when the prediction of the failure mode is required. Often in design studies, the net-section failure mode is suppressed. This, however, can lead to shear-out failures. The stresses along each plane are therefore presented in an attempt to describe the overall response of each layup. In each figure the stresses have been nondimensionalized by F, which for a plate of unit thickness, is the bearing stress on the hole. In addition, since the hole in the plate has a unit radius, i.e., equals 1.0 in., the parameters δ and λ are effectively nondimensionalized by the hole radius.

Figure 16 shows the stresses at the hole-edge for a quasi-isotropic laminate. This laminate is quite popular in current applications of composite materials. As can be seen, the hoop stress is compressive at $\theta = 0$ and becomes tensile as θ increases. The maximum hoop stress occurs near the end of the contact region. The negative hoop stress at $\theta = 0$ is due to the effects of friction. The net-section and shear-out stresses, shown in fig. 17, are as could be expected. It is interesting to note that the shear-out stress peaks within a hole radius of the net-section.

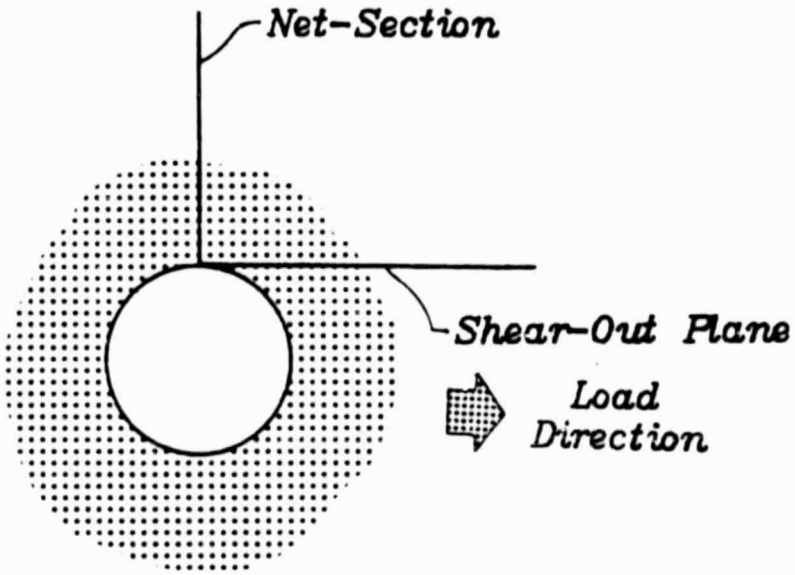

FIG. 15 NET-SECTION AND SHEAR-OUT PLANES

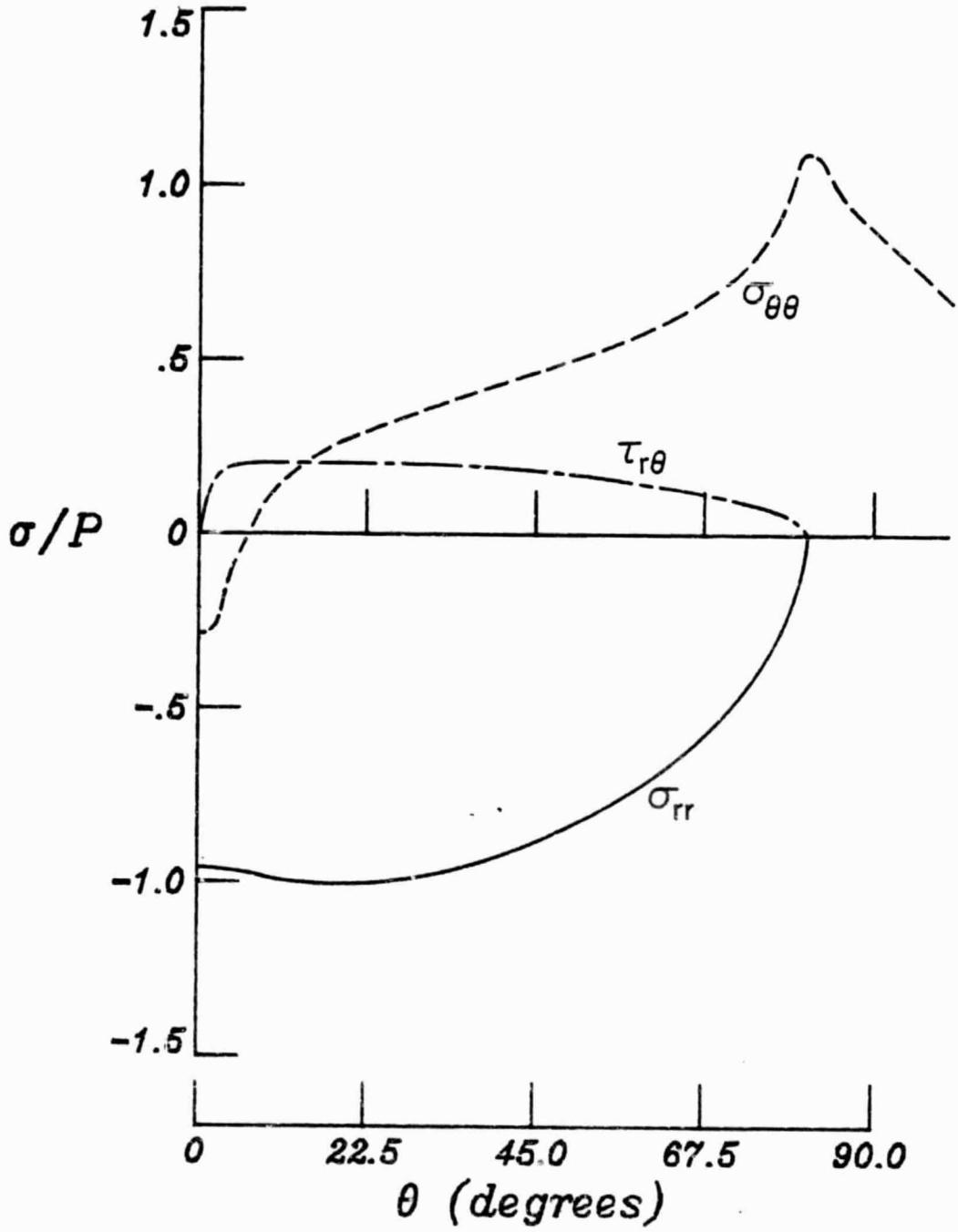

FIG. 16 STRESSES AT R = 1 FOR A $[0/\pm45/90]_s$ LAMINATE UNDER STANDARD CASE CONDITIONS.

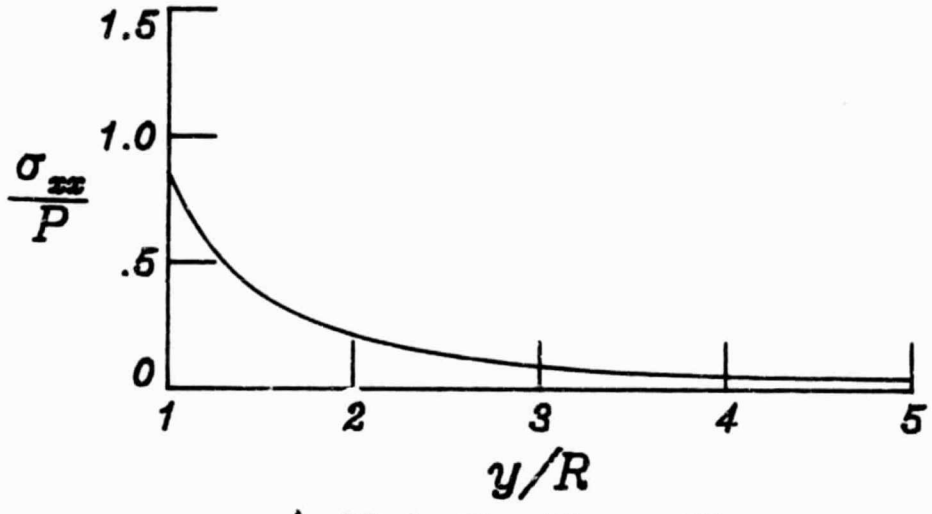

a) Net-Section Stress

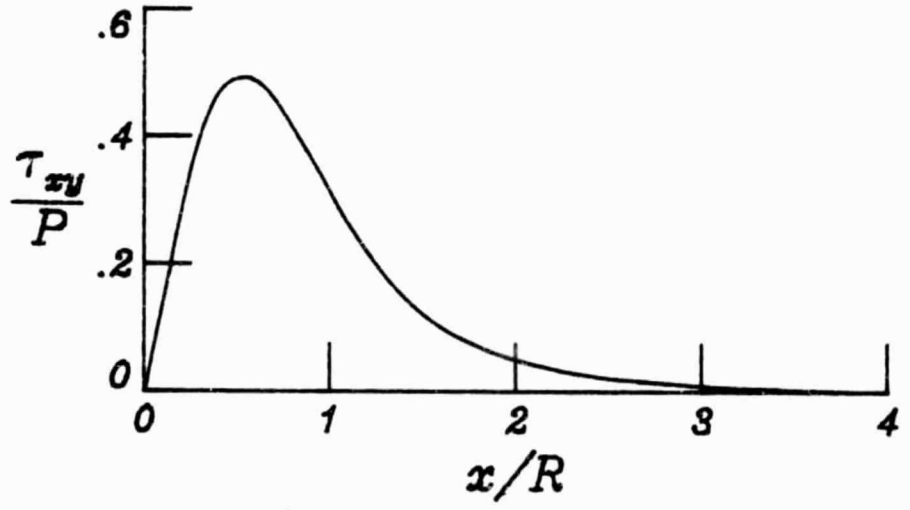

b) Shear-Out Stress

FIG. 17 NET-SECTION AND SHEAR-OUT STRESSES FOR A $[0/\pm45/90]_s$ LAMINATE UNDER STANDARD CASE CONDITIONS.

Figure 18 shows the contact and hoop stresses for a $[0]_8$ laminate while fig. 19 shows the net-section and shear-out stresses. This case is an extreme example of the effects of orthotropicity. There are several unusual features for the stress distributions illustrated here. One of the most prominent features is the distribution of the normal stress, σ_{rr}. Many analyses assume that a sinusoidal distribution is valid independent of laminate. It is clear from fig. 18 that such an assumption for a highly orthotropic laminate is in error. Another prominent feature is the peak in the hoop stress near $\theta = 90°$. Not only is the magnitude of the peak greater than that of the quasi-isotropic case, but the peak occurs outside the contact region. It is interesting to note that the hoop stress changes sign several times within the contact region. The net-section stress for the $[0]_8$ laminate, fig. 19a, looks similar to the net-section stress of the quasi-isotropic laminate, but the magnitude at the hole edge is considerably greater. On the other hand, the spatial dependence of the shear-out stress is considerably different than the quasi-isotropic case. The magnitude of the shear-out stress for the $[0]_8$ laminate is less, but the shear strength of this laminate is considerably less than that of the quasi-isotropic laminate. It can be expected that a $[0]_8$ laminate would fail in shear-out.

Figures 20 and 21 document the stresses for a $[90]_8$ laminate. This laminate represents the other extreme in orthotropicity. In practice, such a laminate would never be used. The hoop stress in fig. 20 has two peaks of roughly the same magnitude. The hoop stress shows very little

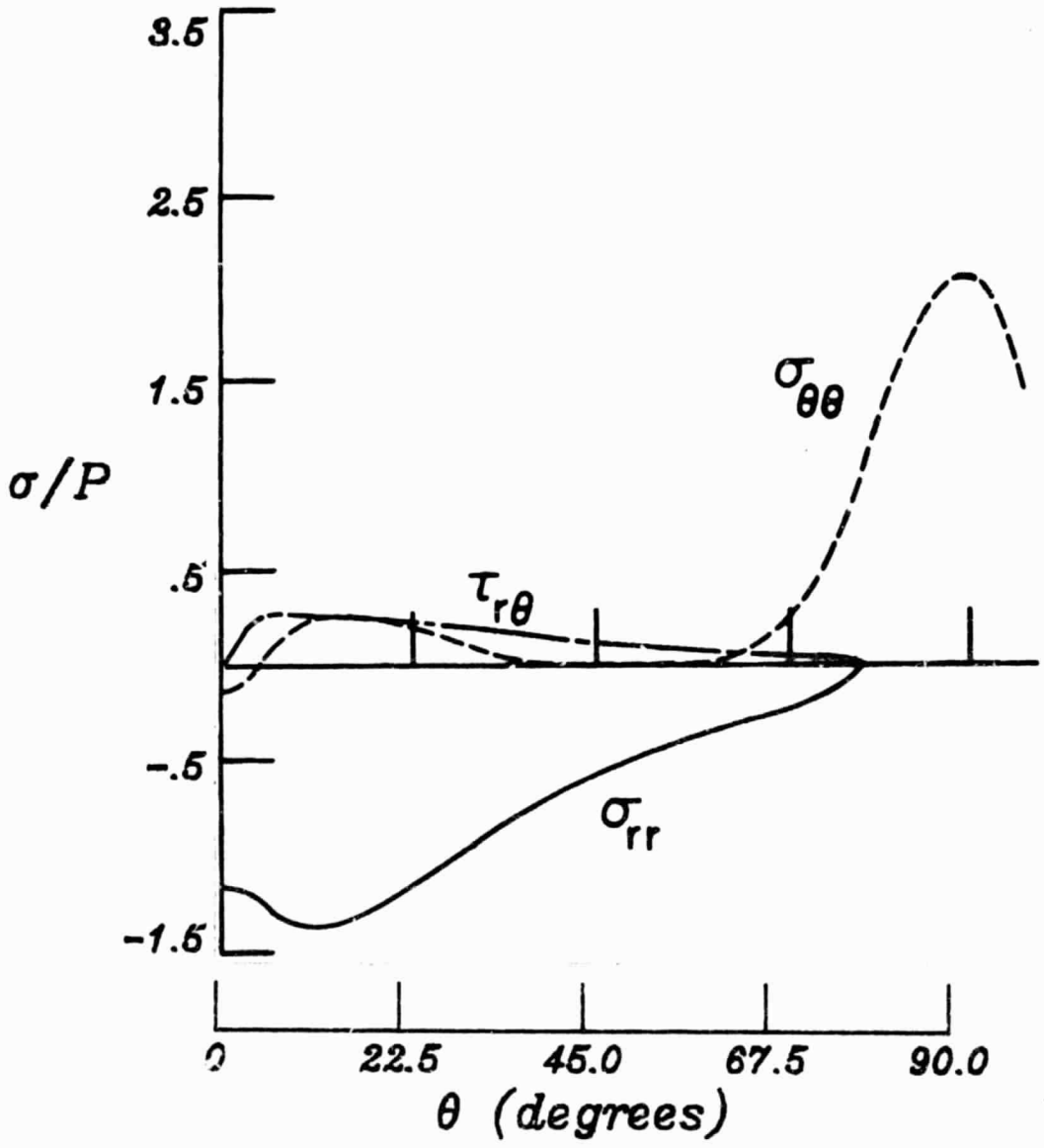

FIG. 18 STRESSES AT R = 1 FOR A $[0]_8$ LAMINATE UNDER STANDARD CASE CONDITIONS.

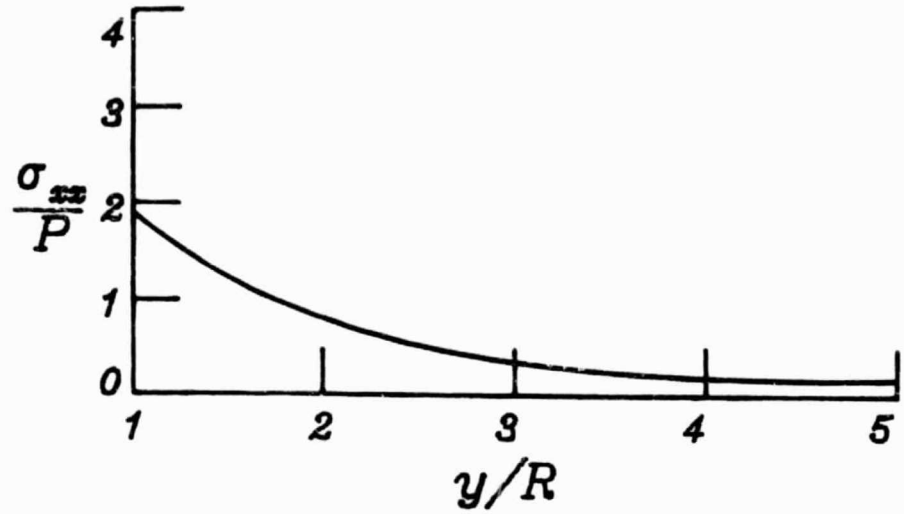

a) Net-Section Stress

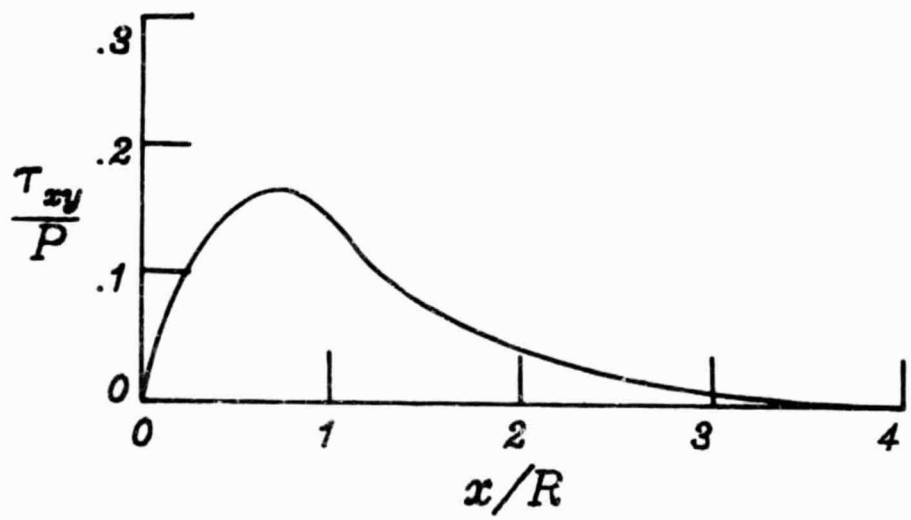

b) Shear-Out Stress

FIG. 19 NET-SECTION AND SHEAR-OUT STRESSES FOR A $[0]_8$ LAMINATE UNDER STANDARD CASE CONDITIONS.

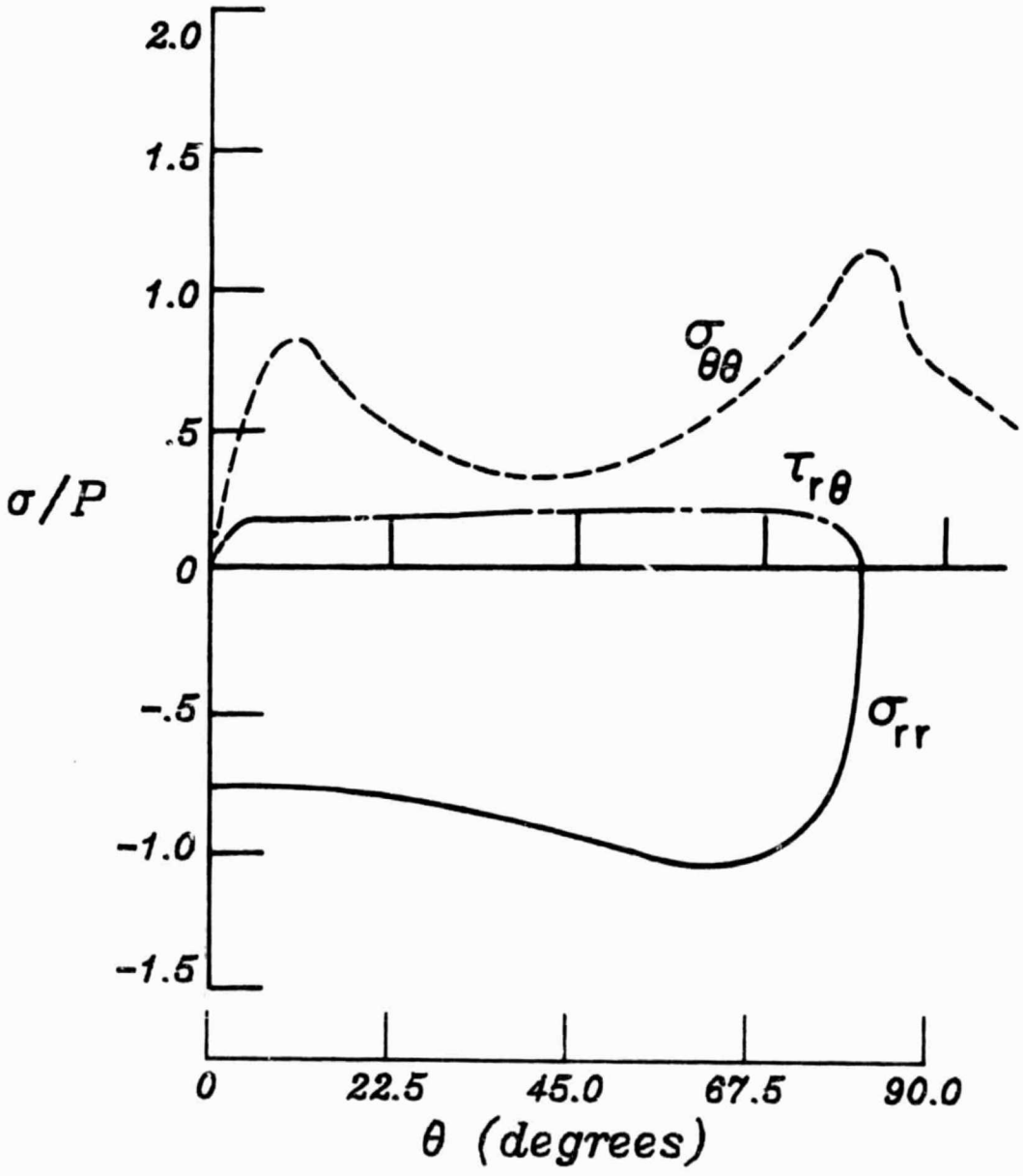

FIG. 20 STRESSES AT R = 1 FOR A $[90]_8$ LAMINATE UNDER STANDARD CASE CONDITIONS.

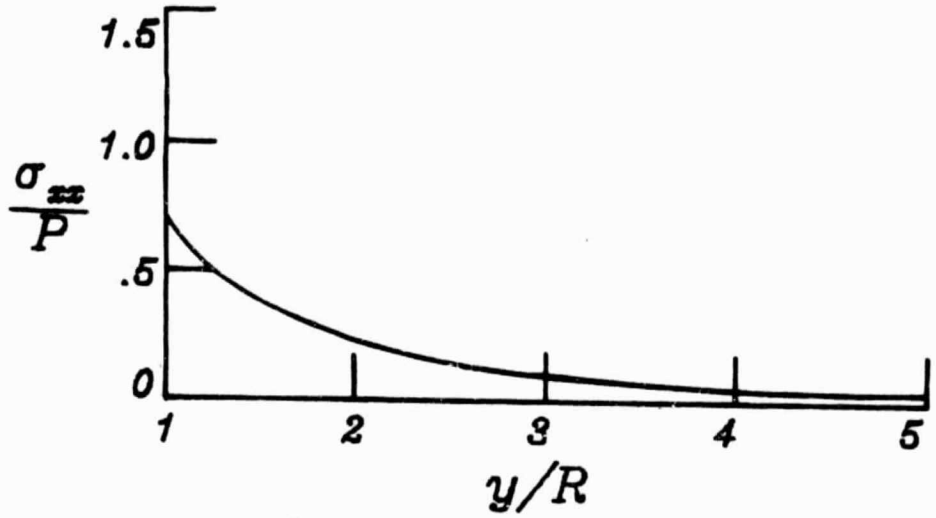

a) Net-Section Stress

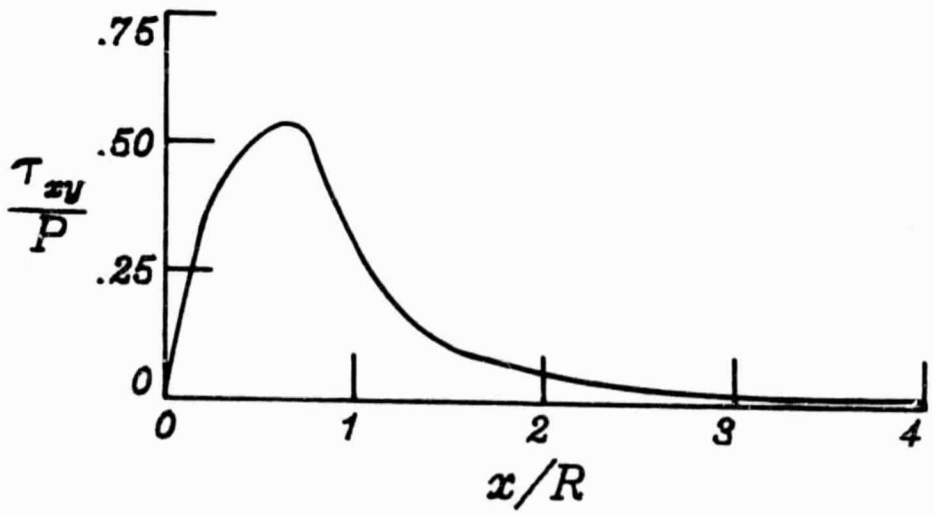

b) Shear-Out Stress

FIG. 21 NET-SECTION AND SHEAR-OUT STRESSES FOR A $[90]_8$ LAMINATE UNDER STANDARD CASE CONDITIONS.

similarity with the previous two cases. Note that $\sigma_{\theta\theta}$ is compressive over about half the contact region. The normal stress, σ_{rr}, is radically different than the previous two cases. A sinusoidal approximation would be very much in error for this case. The shear-out and net-section stresses for the $[90]_8$ laminate are nominally the same as the quasi-isotropic case (fig. 17). However, the net-section stress is no doubt the failure producing stress for the $[90]_8$ laminate.

Figures 22 and 23 illustrate the stresses for a $[0/90]_{2s}$ laminate. This laminate, though not as popular as the quasi-isotropic laminate, does have some applications. As with the $[90]_8$ laminate, there are two peaks in the hoop stress. The magnitude of the peak nearest $\theta = 0$, however, is less than the peak near $\theta = 90°$. This is no doubt due to the influence of the 0° laminae. As with the $[0]_8$ case, the maximum hoop stress occurs outside the contact region. It should be pointed out that the maximum hoop stress at $\theta = 90°$ is not too much less than the maximum stress for the $[0]_8$ laminate. This is due to the fact that the 0° laminae, rather than the 90° laminae are responsible for transmitting the load past the net-section. Thus, similarity with the $[0]_8$ laminate might be expected in this region. The net-section and shear-out stresses, for the $[0/90]_{2s}$ laminate, fig. 23, show no unexpected results.

Figures 24 and 25 show the numerical results for a $[\pm 45]_{2s}$ laminate. Such a laminate can be used where high shear strength and/or stiffness is required. Tailoring studies [34] have suggested that, for higher performance joints, the region near the pin should contain a high

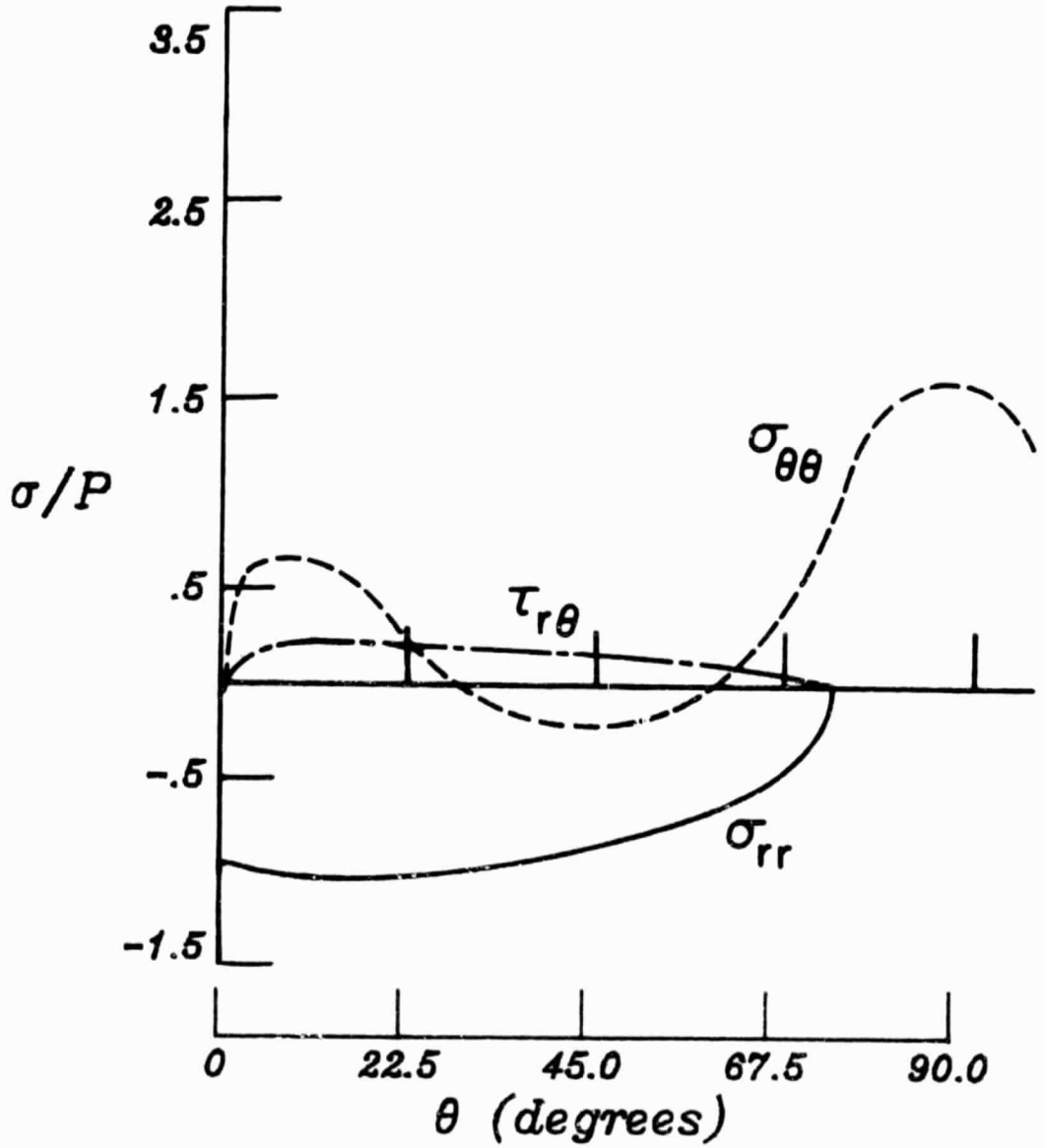

FIG. 22 STRESSES AT R = 1 FOR A $[0/90]_{2S}$ LAMINATE UNDER STANDARD CASE CONDITIONS.

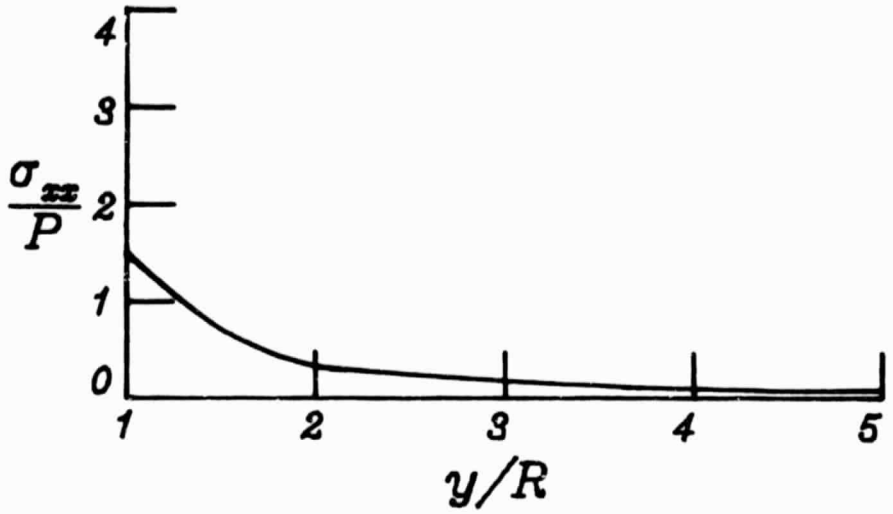

a) Net-Section Stress

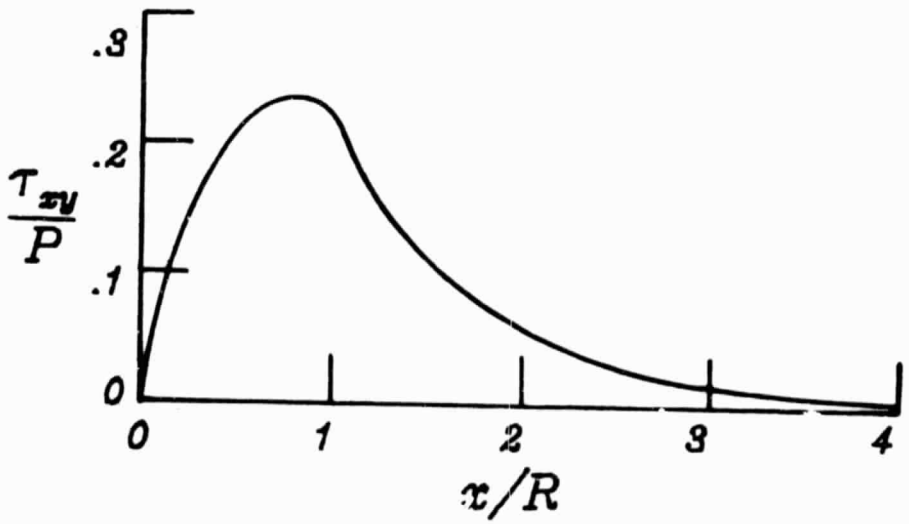

b) Shear-Out Stress

FIG. 23 NET-SECTION AND SHEAR-OUT STRESSES FOR A $[0/90]_{2S}$ LAMINATE UNDER STANDARD CASE CONDITIONS.

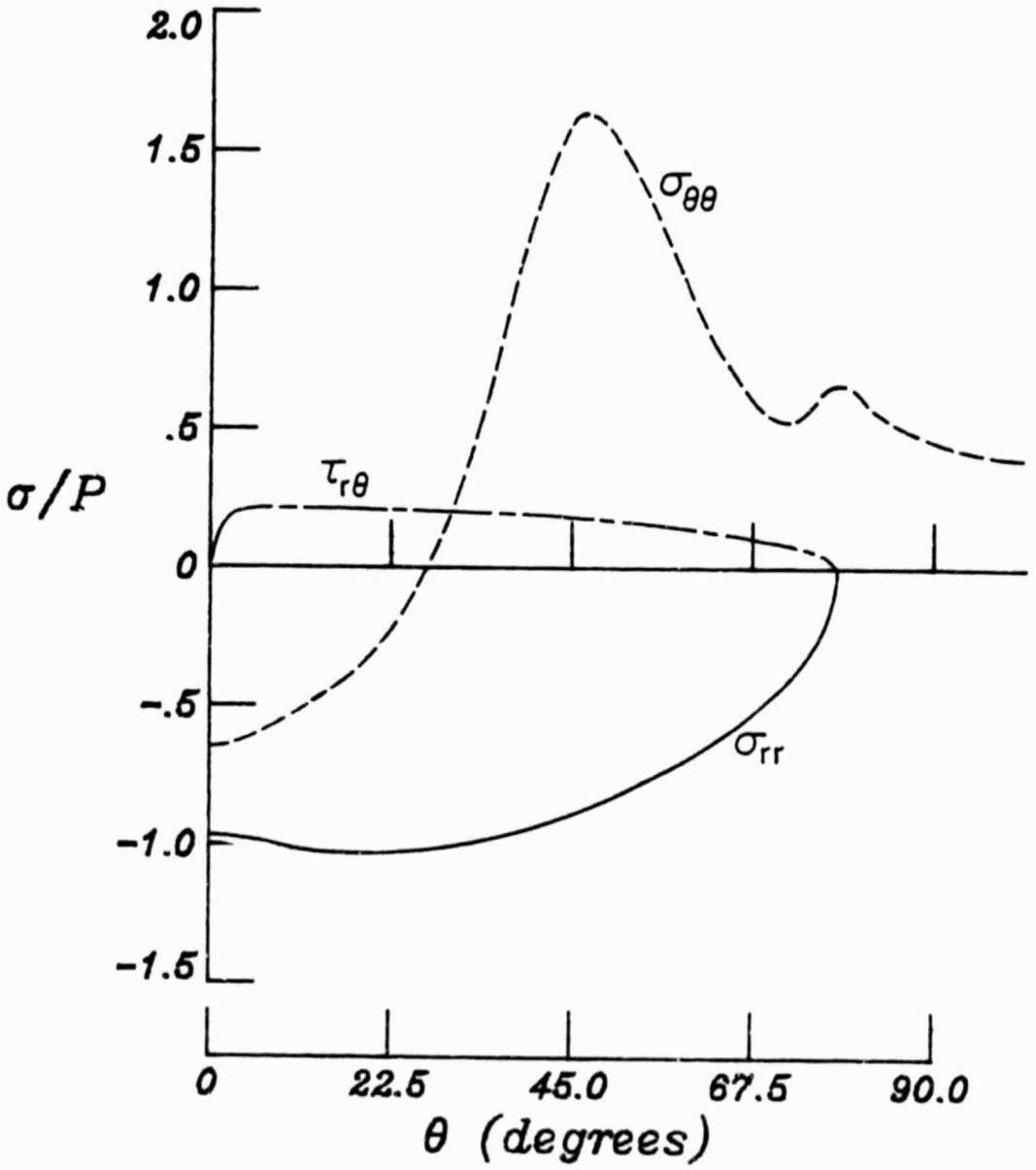

FIG. 24 STRESSES AT R = 1 FOR A $[\pm 45]_{2S}$ LAMINATE UNDER STANDARD CASE CONDITIONS.

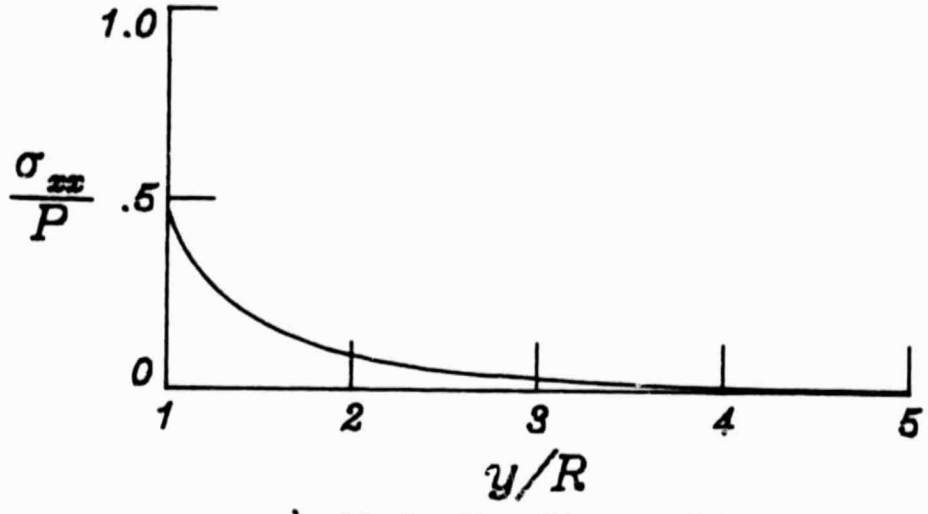

a) Net-Section Stress

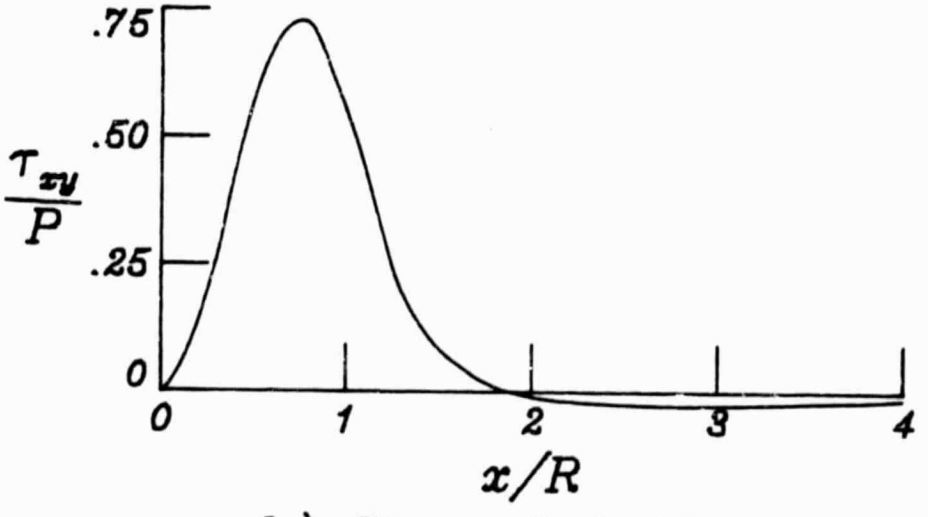

b) Shear-Out Stress

FIG. 25 NET-SECTION AND SHEAR-OUT STRESSES FOR A $[\pm 45]_{2S}$ LAMINATE UNDER STANDARD CASE CONDITIONS.

percentage of ±45 plys. The most obvious feature of the hole edge stresses in the $[\pm 45]_{2s}$ laminate is the maximum hoop stress occurring at $\theta = 45°$. This should be put in context because the maximum strength of the laminate is also at $\theta = 45°$. The magnitude of the peak stress at $\theta = 45°$ is comparable with the peak stress at the net-section of the quasi-isotropic laminate. The other components of stress for the $[\pm 45]_{2s}$ laminate are similar to that of the quasi-isotropic case.

Finally, figs. 26 and 27 show the stress distribution for a $[0/\pm 45]_s$ laminate. This laminate has many applications. The differences between the results for this laminate and the quasi-isotropic case are small. The hoop stress, however, is higher near $\theta = 45°$ for the $[0/\pm 45]_s$ laminate than it is for the $[0/\pm 45/90]_s$ laminate. This may be due to slightly higher percentage of 45° laminae in the $[0/\pm 45]_s$ case.

The results presented in these figures have shown that the plate properties have a significant effect on pin-loaded joints. Other parameters affect the stress distributions as well. Therefore, the plate properties will now be held constant and the pin modulus, friction coefficient, and clearance will be varied. A $[0_2/\pm 45]_s$ laminate was chosen for this portion of the parameter study because it represents a moderately orthotropic material which is commonly used in the aerospace industry. The properties for this layup were selected from de Jong's report [11]. This was done because de Jong presented results of a parametric study which complement the current research effort. The properties used by de Jong were

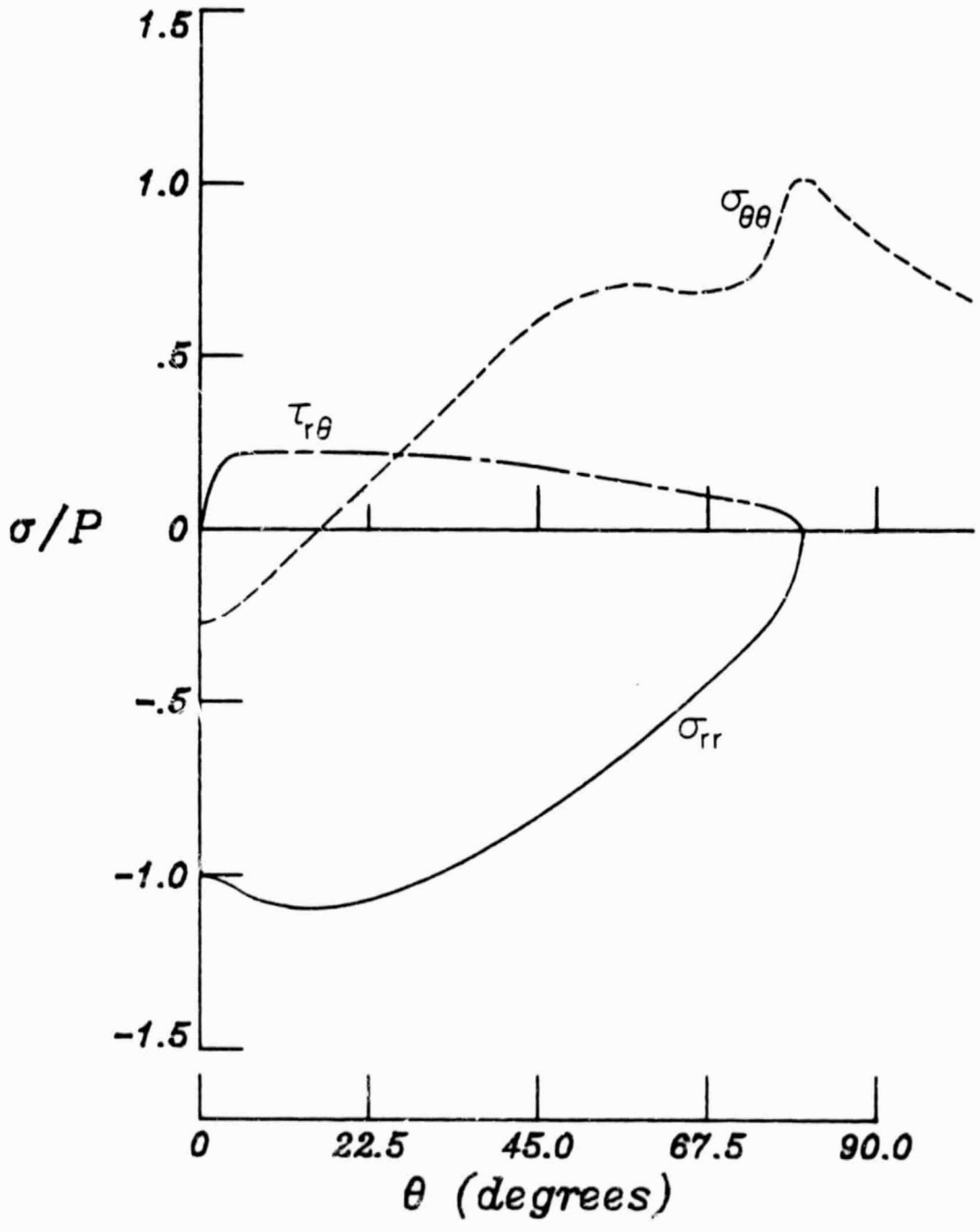

FIG. 26 STRESSES AT R = 1 FOR A $[0/\pm45]_S$ LAMINATE UNDER STANDARD CASE CONDITIONS.

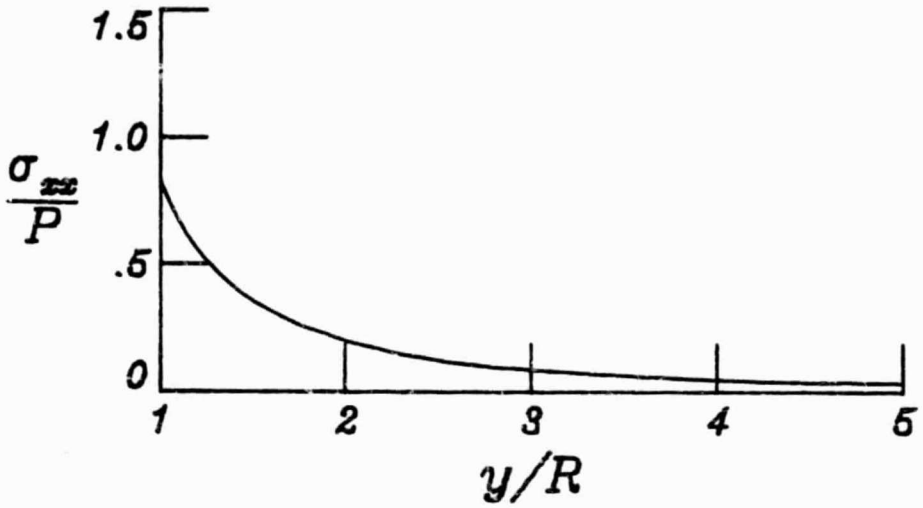

a) Net-Section Stress

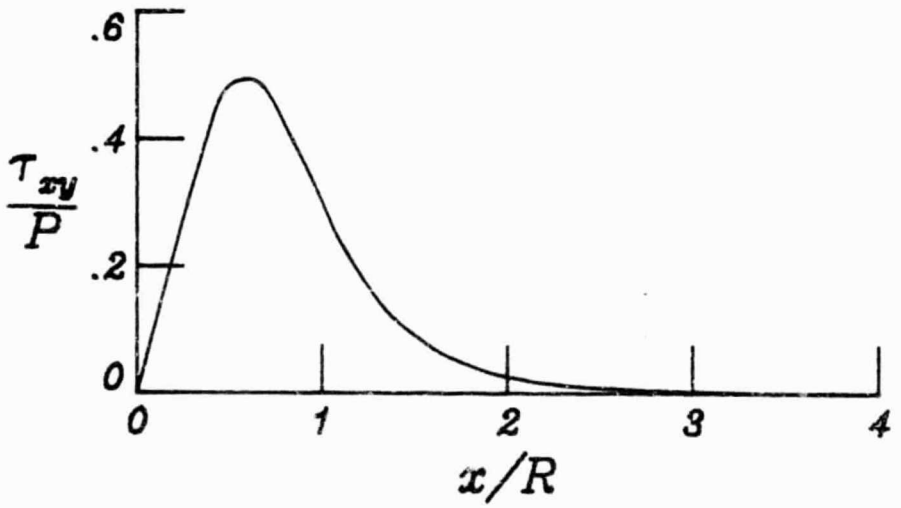

b) Shear-Out Stress

FIG. 27 NET-SECTION AND SHEAR-OUT STRESSES FOR A $[0/\pm45]_S$ LAMINATE UNDER STANDARD CASE CONDITIONS.

$$E_x = 11.61 \times 10^6 \text{ psi}$$
$$E_y = 3.43 \times 10^6 \text{ psi}$$
$$\nu_{xy} = .662 \qquad (174)$$
$$G_{xy} = 2.40 \times 10^6 \text{ psi}$$

The format used to illustrate the effects of pin modulus, clearance, and friction will be the same as has been used in presenting all results so far. Here, however, each situation studied will involve four figures. This was done primarily to emphasize the effect of these variables on certain stresses and to avoid cluttering the figures. The first two figures of each set illustrate the effect of parameter variation on the normal and the shear stresses. The second figure illustrates the effect on the hoop stress. The third and fourth figures show the effects on the shear-out and net-section stresses.

Using the laminate elastic properties given by eq. 174 along with the values given for the parameters of the standard case, the pin modulus is now varied to see what effect this has on the stresses. Three values of pin modulus are studied: a perfectly rigid pin, a steel pin, and an aluminum pin. The stresses for these cases are presented in figs. 28-31. It is evident from these plots that the pin modulus plays a very small role in this problem. Apparently a rigid pin assumption can be made without introducing any significant error in the problem.

In figs. 32-35, the standard case with variable clearance, λ, is shown. In these plots, the rigid body pin displacement is held constant. The nonlinear nature of the problem under these conditions is

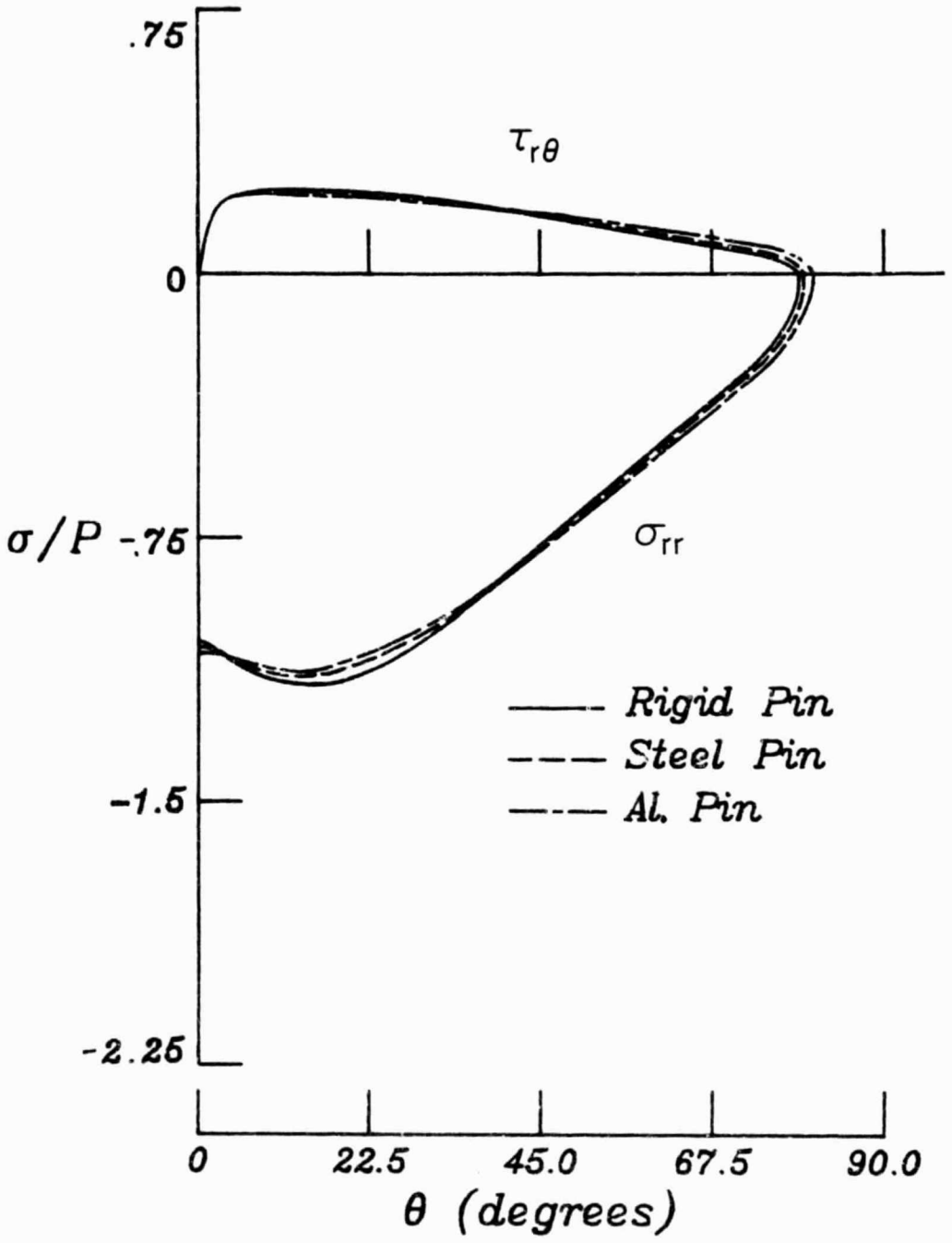

FIG. 28 CONTACT STRESSES AT R = 1 FOR THE STANDARD CASE WITH VARIABLE PIN MODULII.

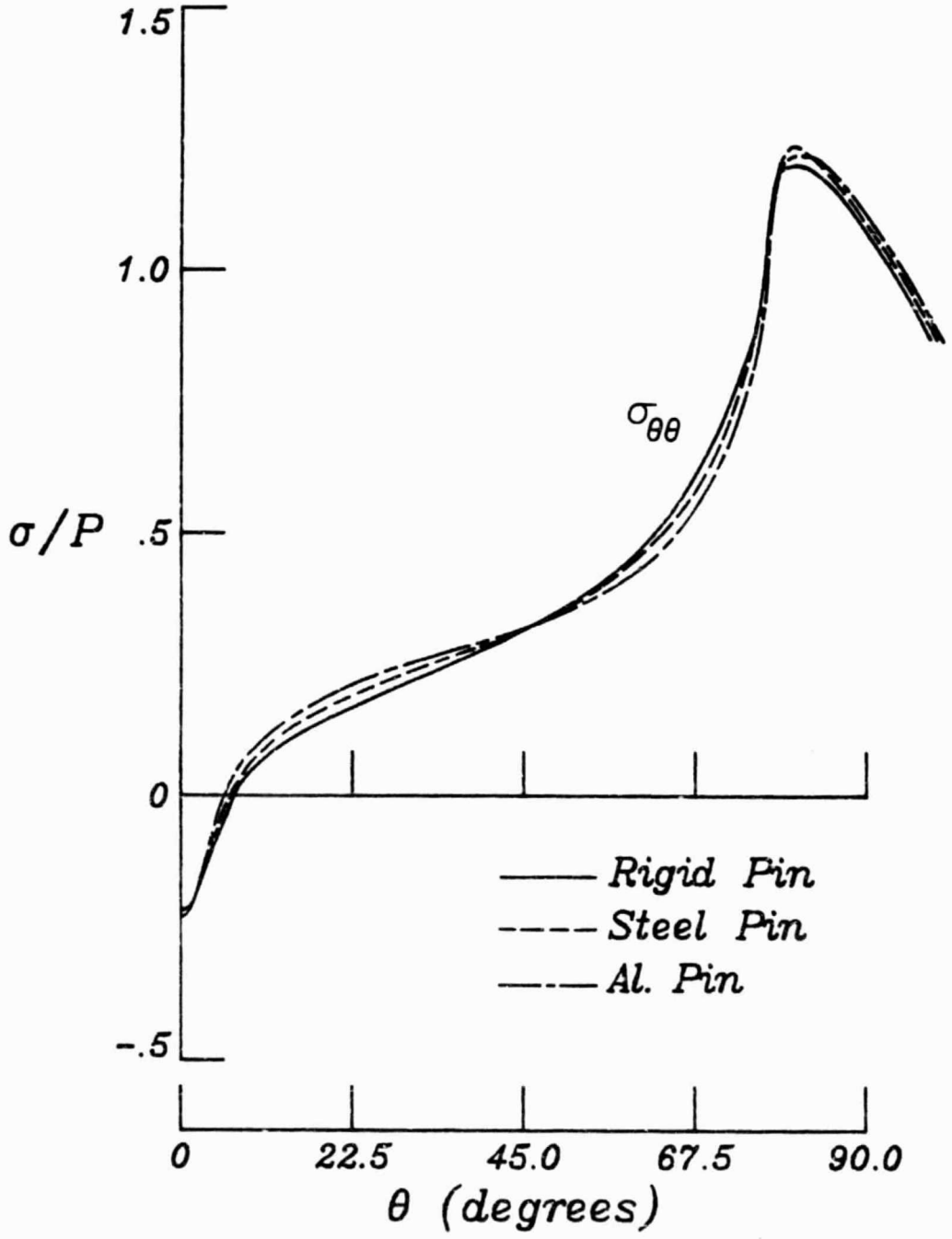

FIG. 29 HOOP STRESSES AT R = 1 FOR THE STANDARD CASE WITH VARIABLE PIN MODULII.

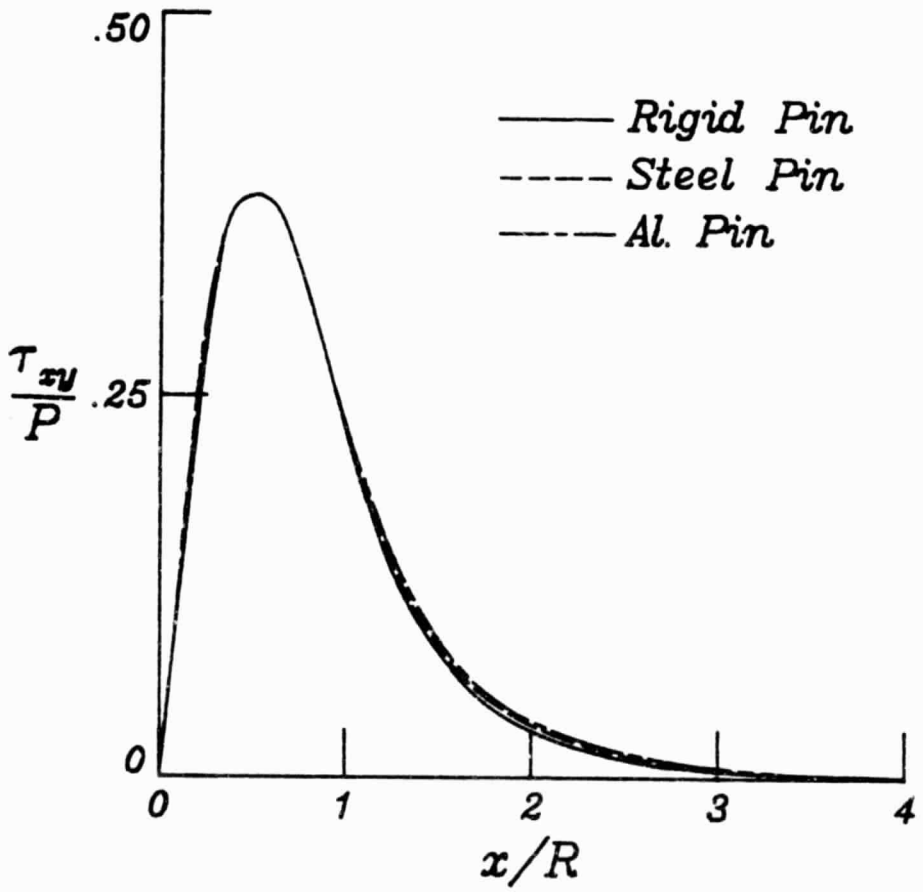

FIG. 30 SHEAR-OUT STRESSES FOR THE STANDARD CASE WITH VARIABLE PIN MODULII.

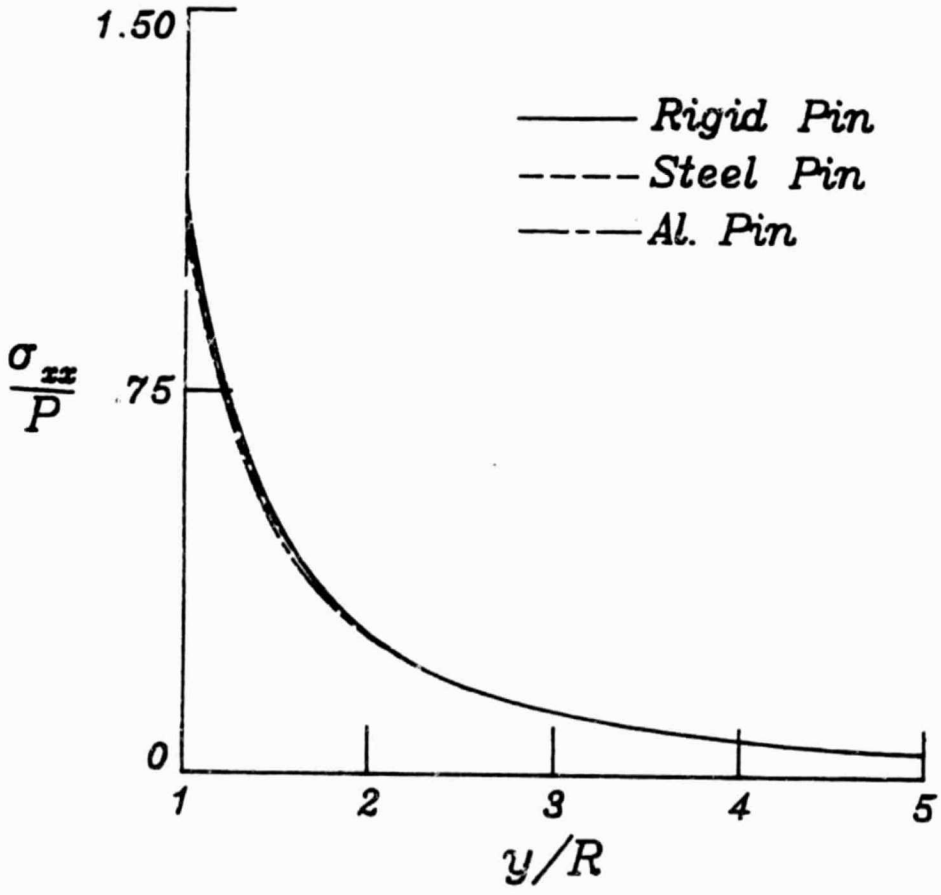

FIG. 31 NET-SECTION STRESSES FOR THE STANDARD CASE WITH VARIABLE PIN MODULII.

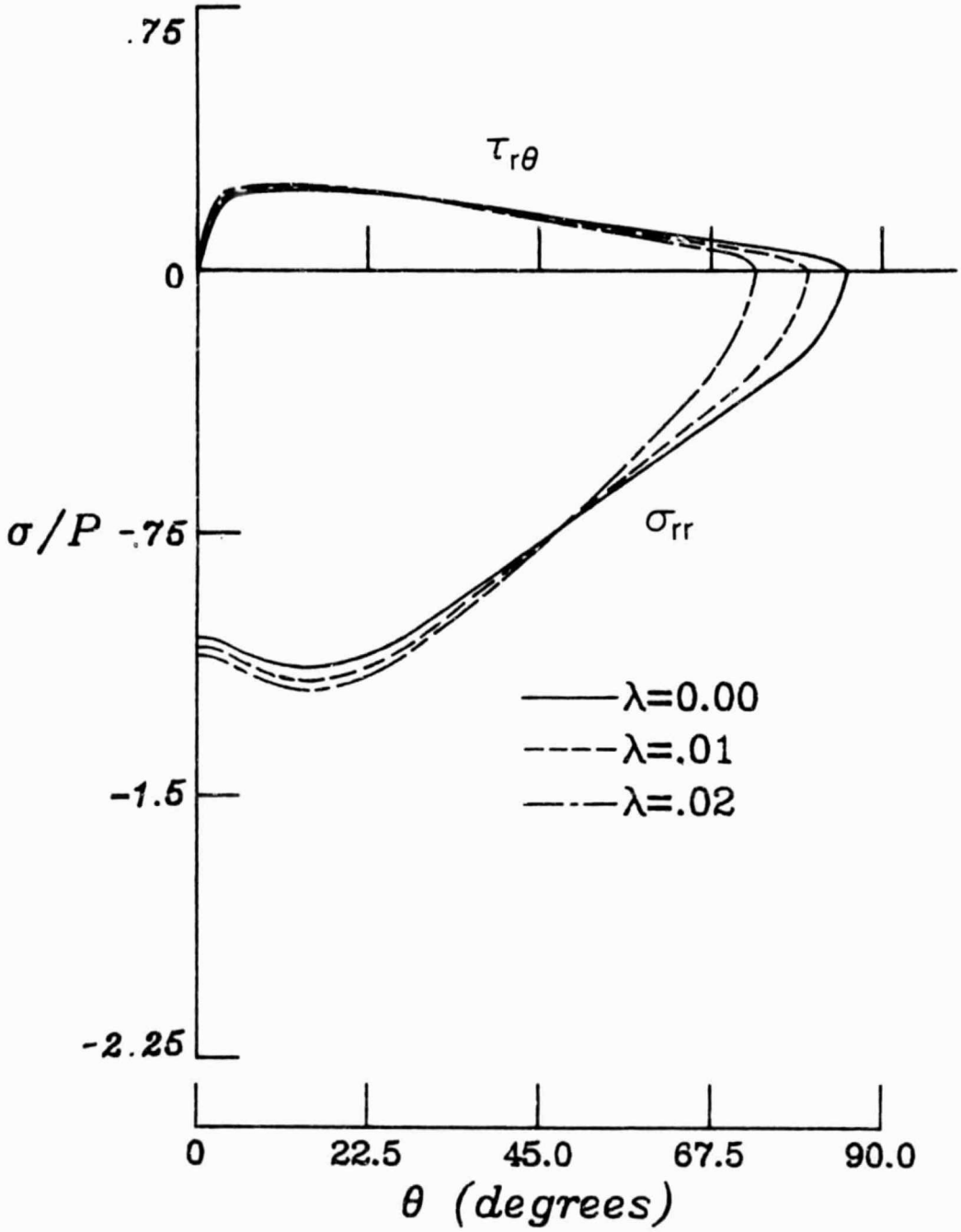

FIG. 32 CONTACT STRESSES AT R = 1 FOR THE STANDARD CASE WITH VARIABLE CLEARANCE, λ.

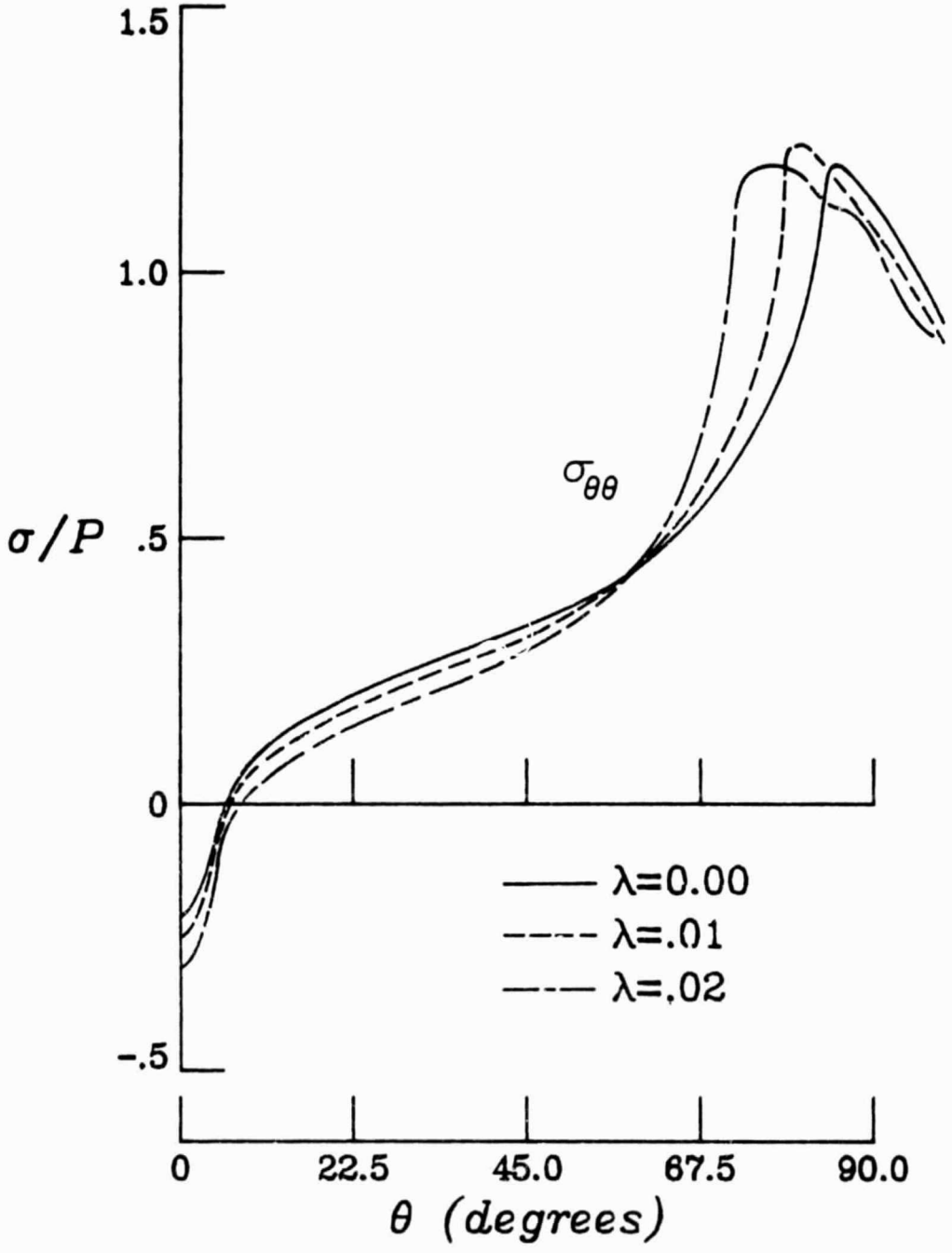

FIG. 33 HOOP STRESSES AT R = 1 FOR THE STANDARD CASE WITH VARIABLE CLEARANCE, λ.

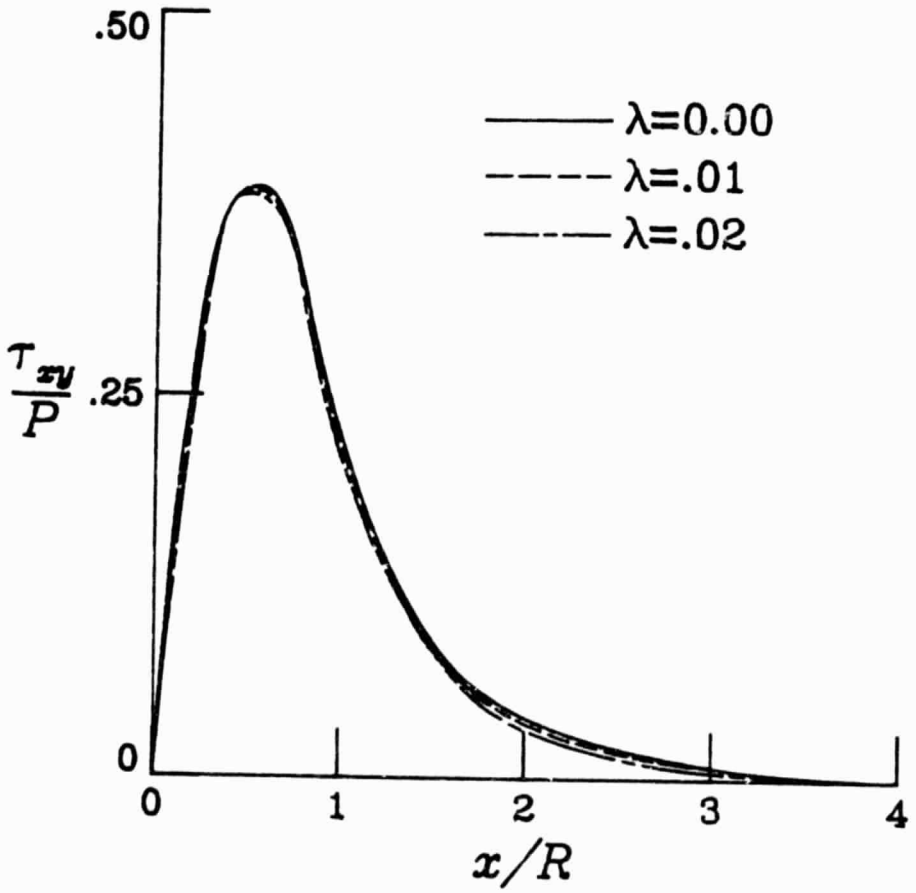

FIG. 34 SHEAR-OUT STRESSES FOR THE STANDARD CASE WITH VARIABLE CLEARANCE, λ.

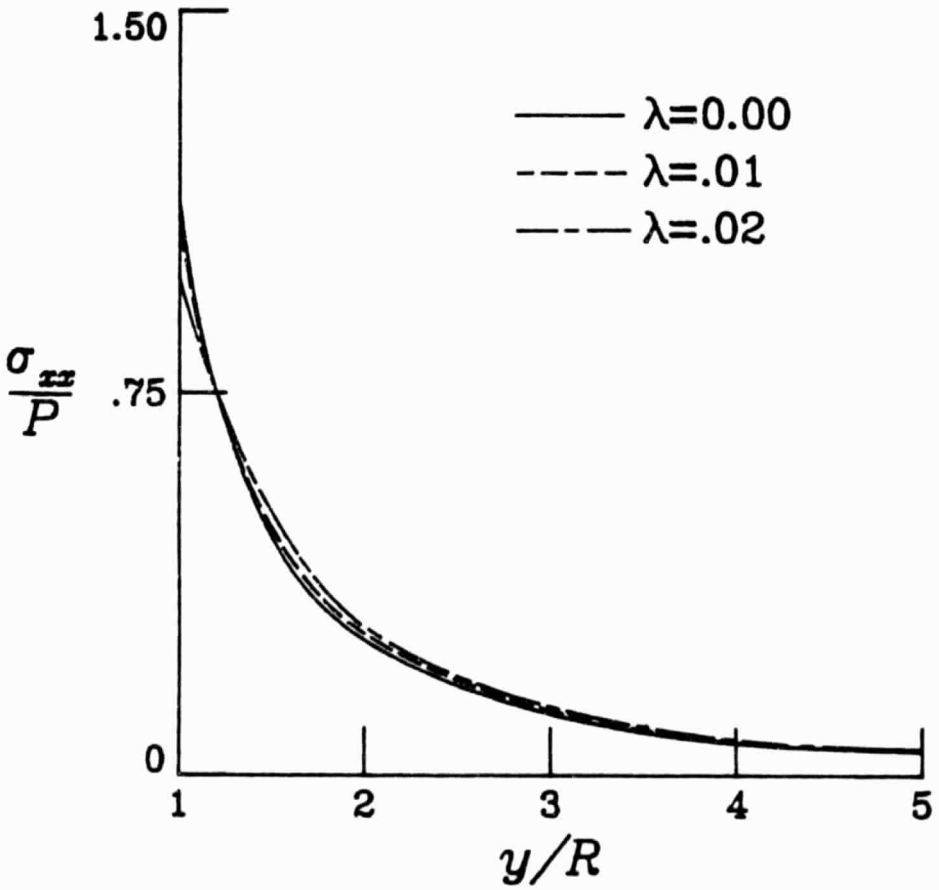

FIG. 35 NET-SECTION STRESSES FOR THE STANDARD CASE WITH VARIABLE CLEARANCE, λ.

easily observed. In fig. 32 it is obvious that the contact angle decreases with increasing clearance. This causes the location of the maximum hoop stress in fig. 33 to vary for these cases. This may have a direct effect on the initial damage location in composite panels.

The coefficient of friction, μ, is varied in figs. 36-39. The sign of the coefficient is negative, indicating monotonic loading for each case. From these figures it is apparent that the magnitude of the coefficient of friction plays an important role in the stress distribution of pin-loaded joints. For example, the hoop stress at the origin actually changes size due to the presence of friction. Also note, the contact angle, β, changes very little, however, the no-slip angle, α, changes substantially for these cases.

A comparison of interference, push, and clearance fits is shown in figs. 40-43. As with the case described in figs. 32-35, the value of the clearance parameter causes the maximum hoop stress to change locations on the inside of the hole.

Finally, in figs. 44-47, the load direction is varied. In these figures, $\mu = +0.2$ corresponds to a joint which has been loaded past $\delta = 0.07$ and monotonically returned to this value of pin displacement. The negative value of μ indicates a panel that has been monotonically loaded from $\delta = 0$ to $\delta = 0.07$. Load reversal is seen to have a significant effect on the stress distribution in the plate. Obviously the nonconservative nature of friction tends to lock in the stresses associated with the higher load level. As has been obvious, the effects of clear-

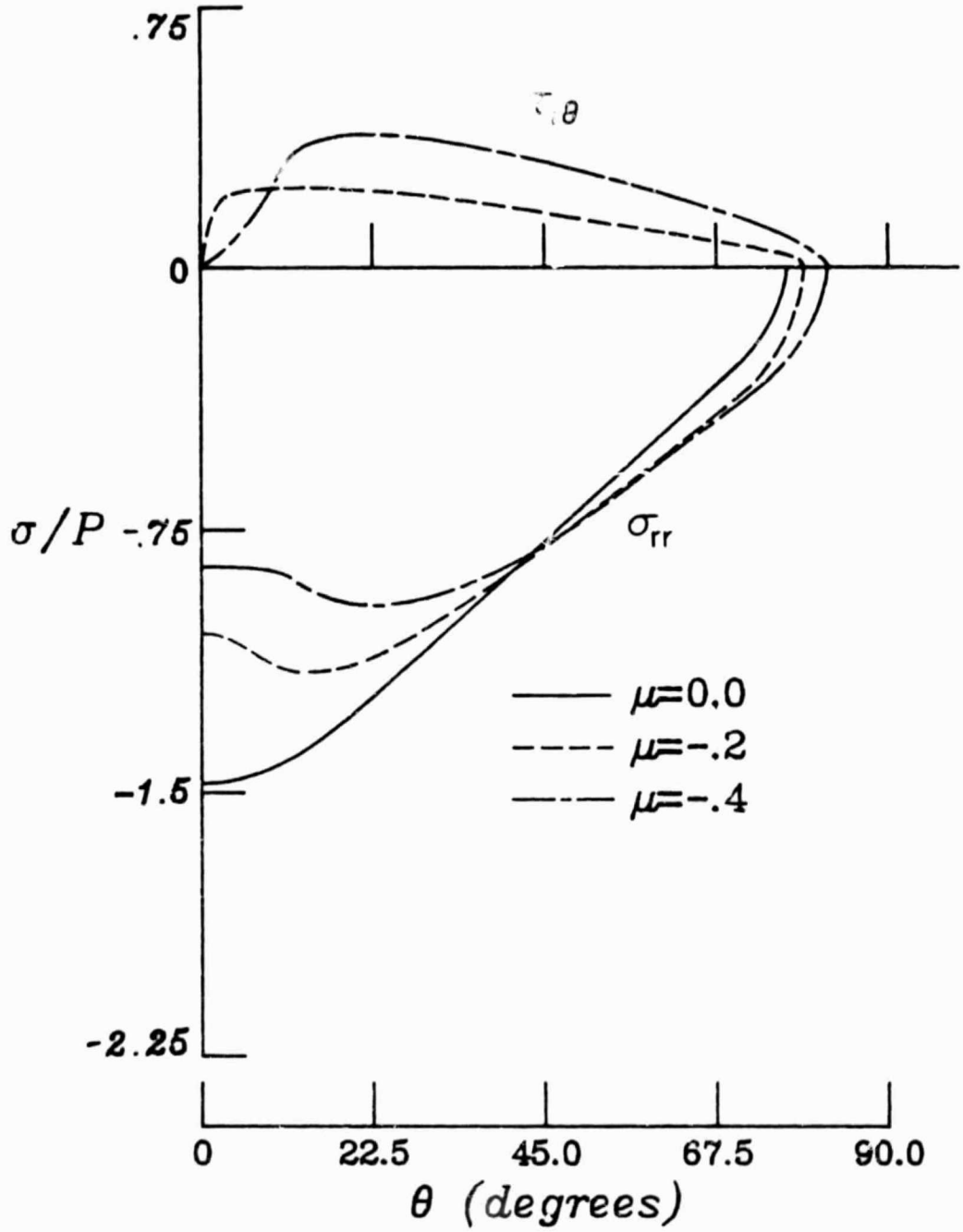

FIG. 36 CONTACT STRESSES AT R = 1 FOR THE STANDARD CASE WITH VARIABLE FRICTION COEFFICIENT, μ.

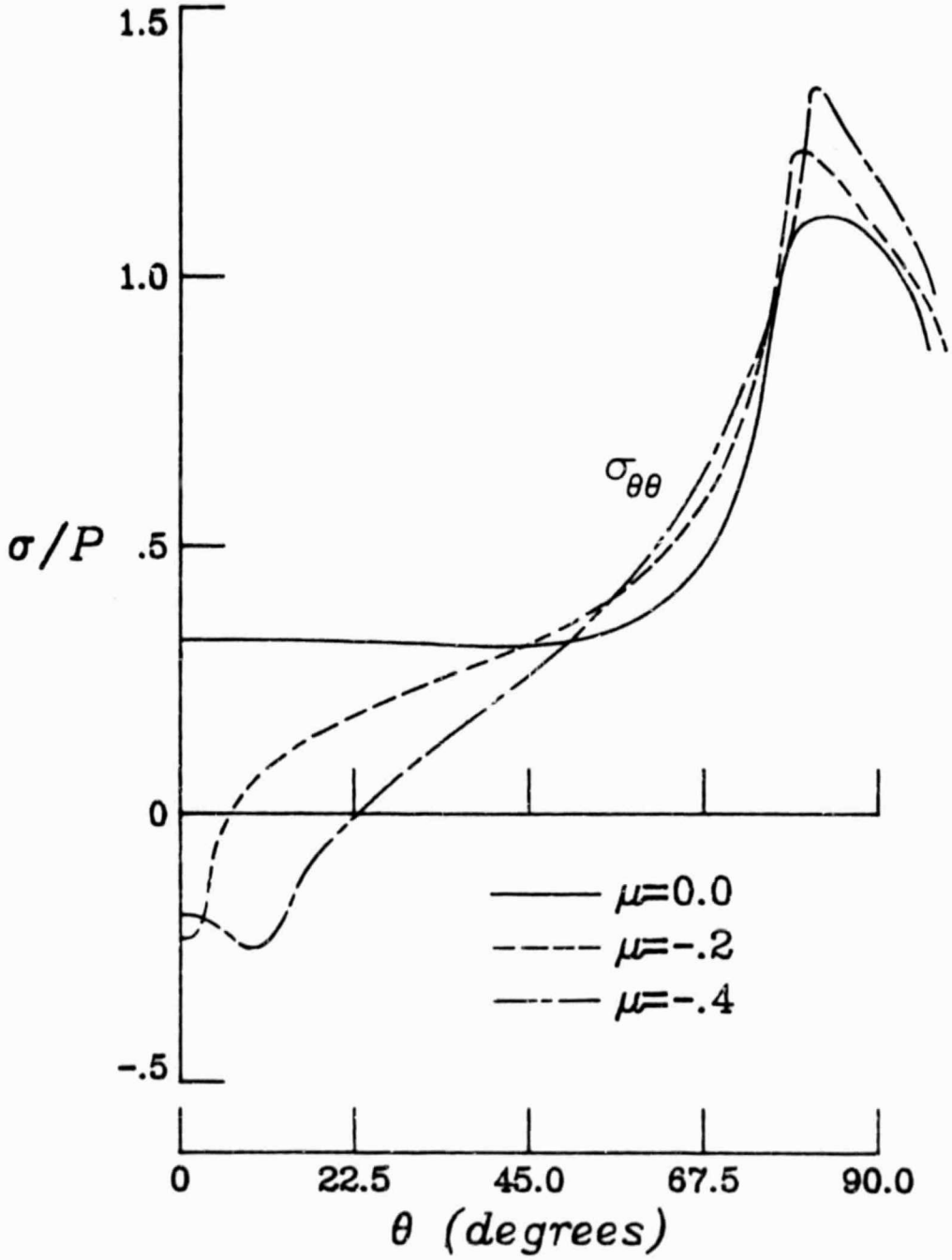

FIG. 37 HOOP STRESSES AT R = 1 FOR THE STANDARD CASE WITH VARIABLE FRICTION COEFFICIENT, μ.

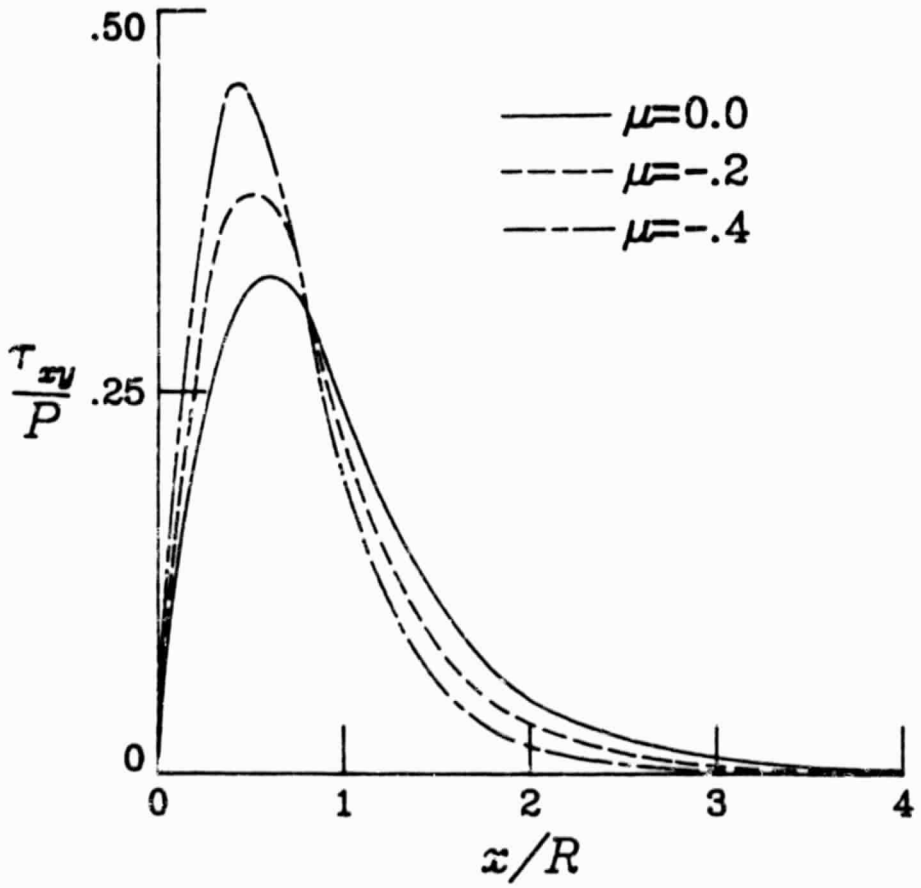

FIG. 38 SHEAR-OUT STRESSES FOR THE STANDARD CASE WITH VARIABLE FRICTION COEFFICIENT, μ.

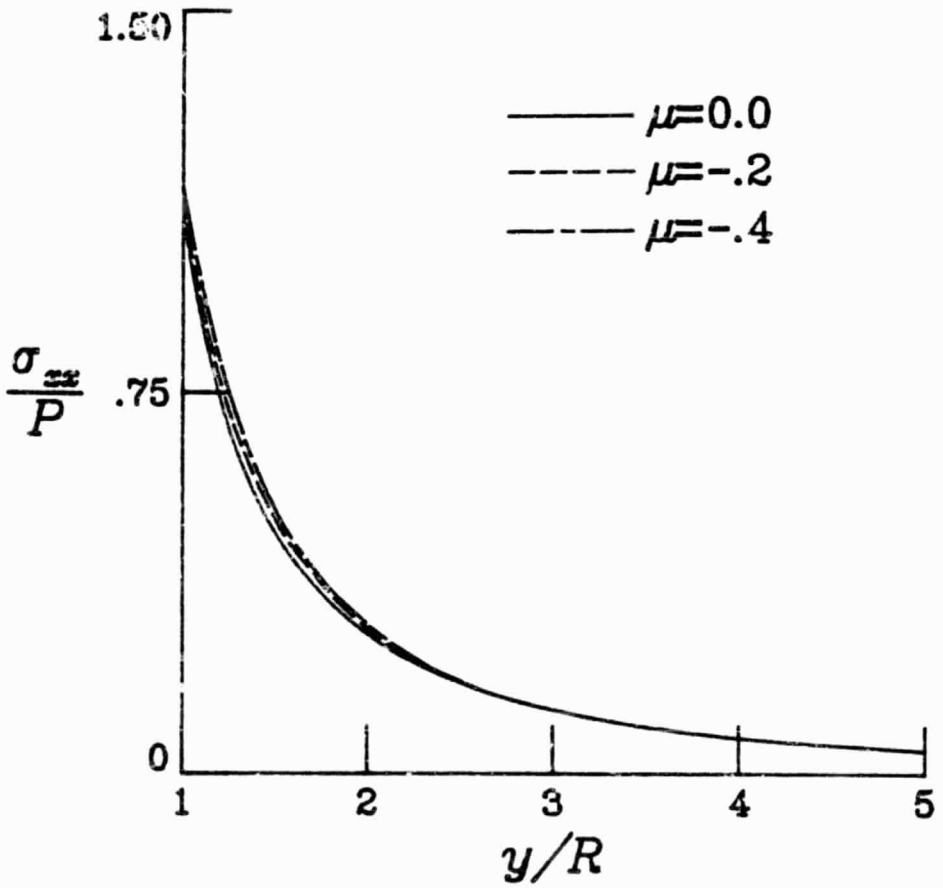

FIG. 39 NET-SECTION STRESSES FOR THE STANDARD CASE WITH VARIABLE FRICTION COEFFICIENT, μ.

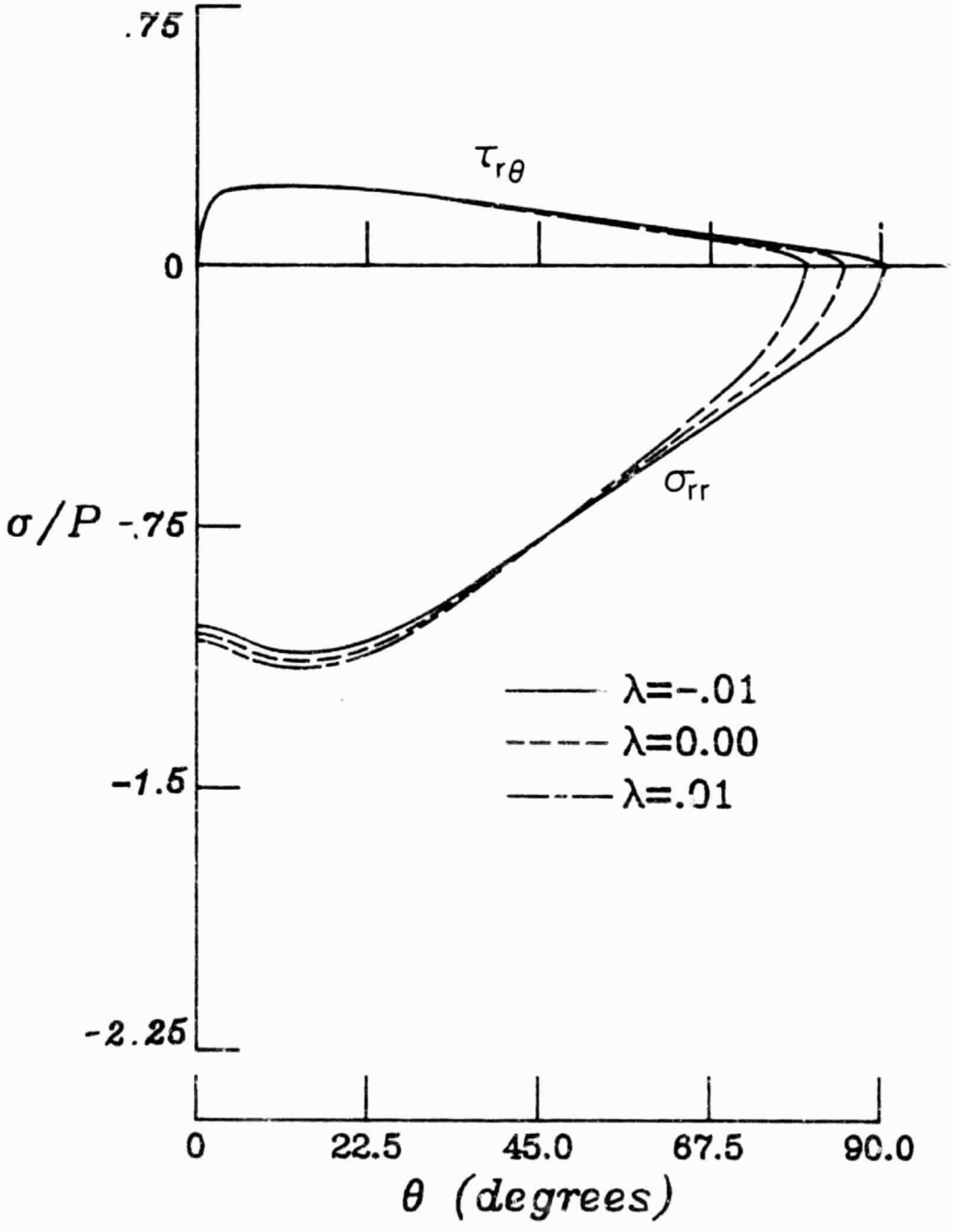

FIG. 40 CONTACT STRESSES AT R = 1 FOR THE STANDARD CASE WITH INTERFERENCE, PUSH, AND CLEARANCE FITS.

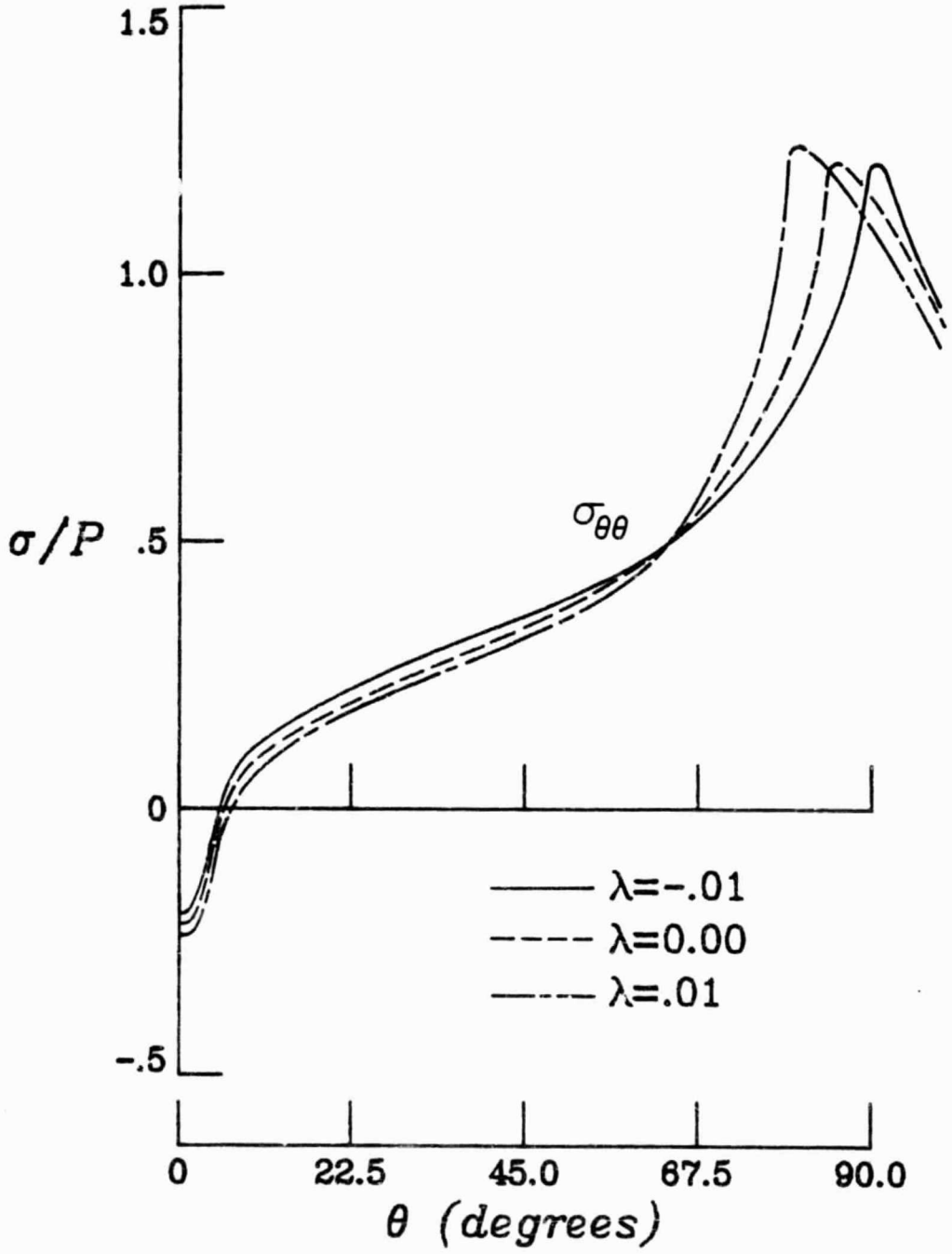

FIG. 41 HOOP STRESSES AT R = 1 FOR THE STANDARD CASE WITH INTERFERENCE, PUSH, AND CLEARANCE FITS.

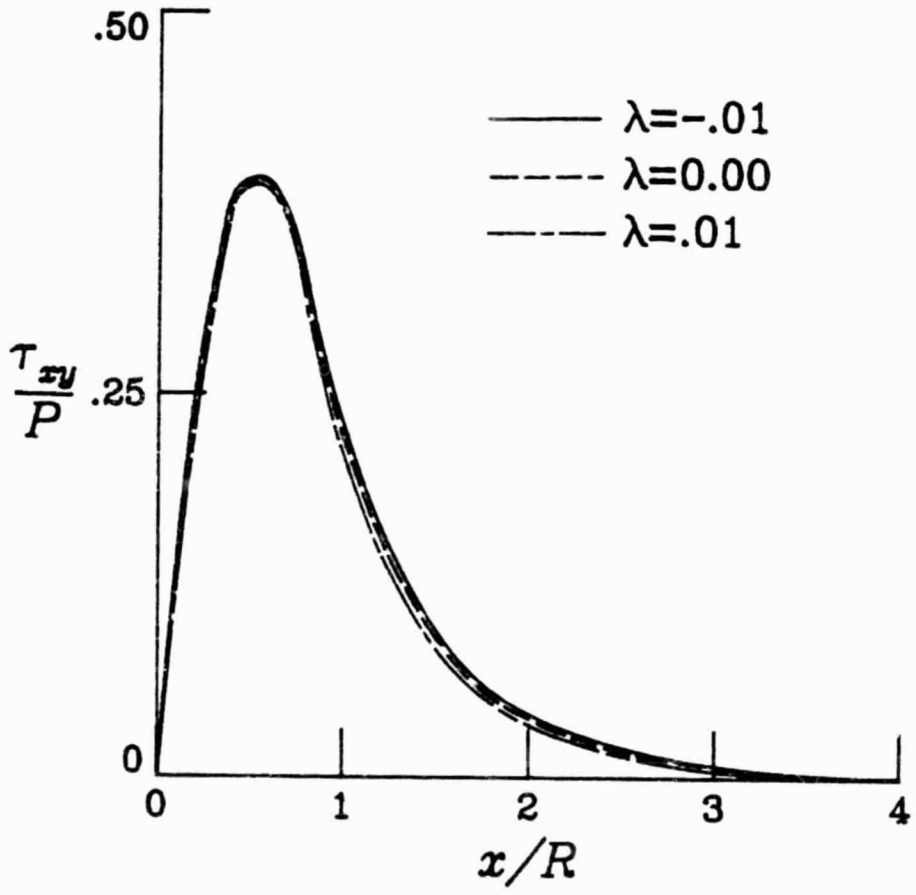

FIG. 42 SHEAR-OUT STRESSES FOR THE STANDARD CASE WITH INTERFERENCE, PUSH, AND CLEARANCE FITS.

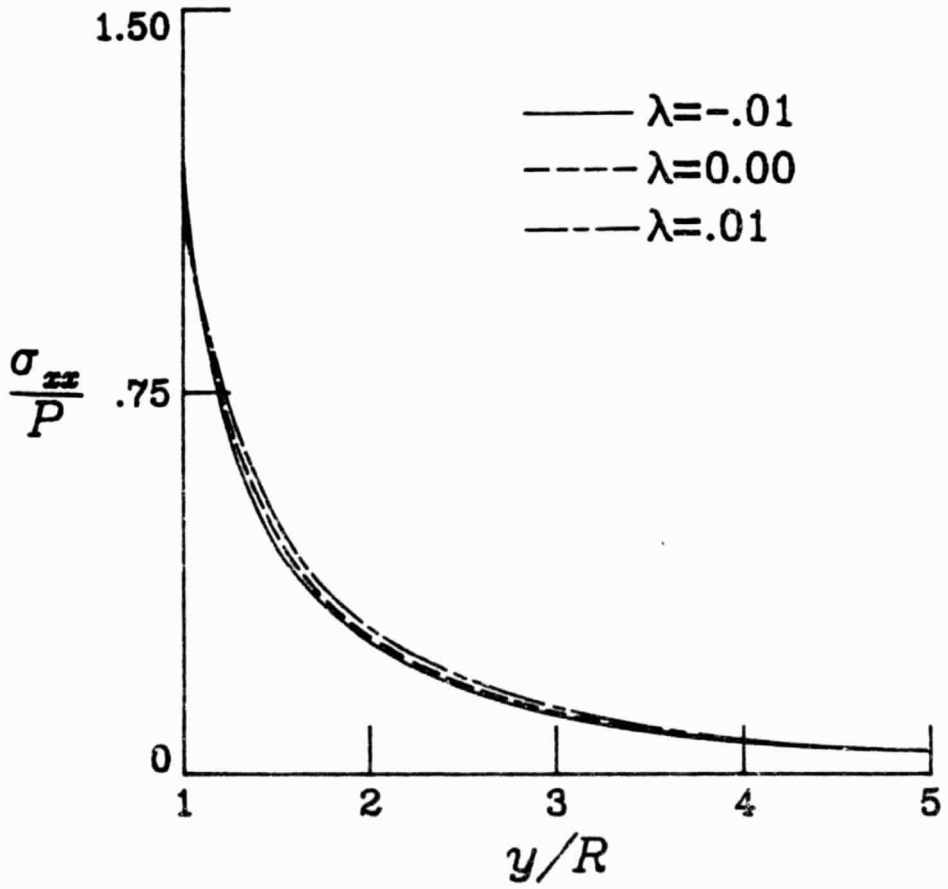

FIG. 43 NET-SECTION STRESSES FOR THE STANDARD CASE WITH INTERFERENCE, PUSH, AND CLEARANCE FITS.

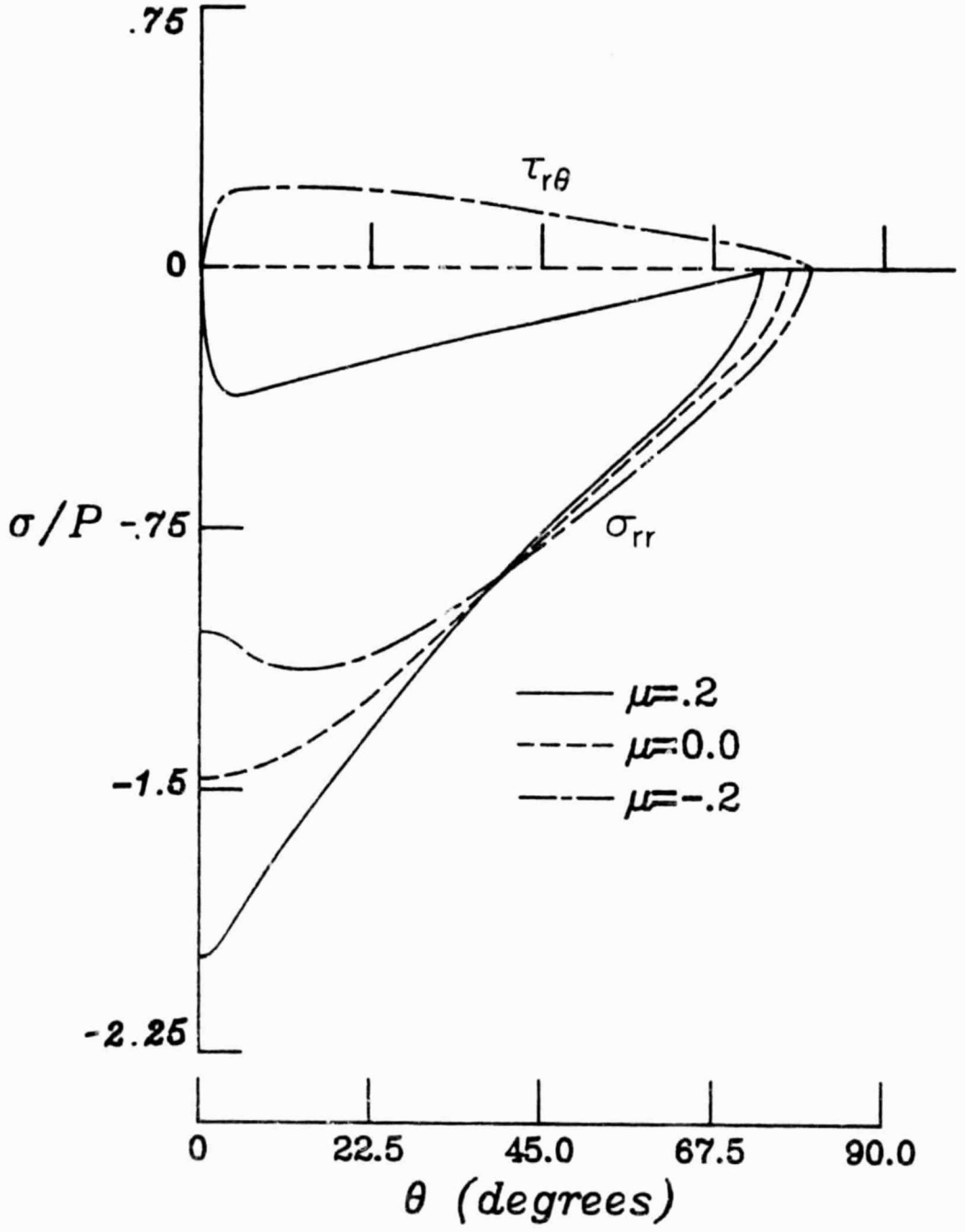

FIG. 44 CONTACT STRESSES AT R = 1 FOR THE STANDARD CASE WITH UNLOADING, ZERO FRICTION, AND LOADING CONDITIONS.

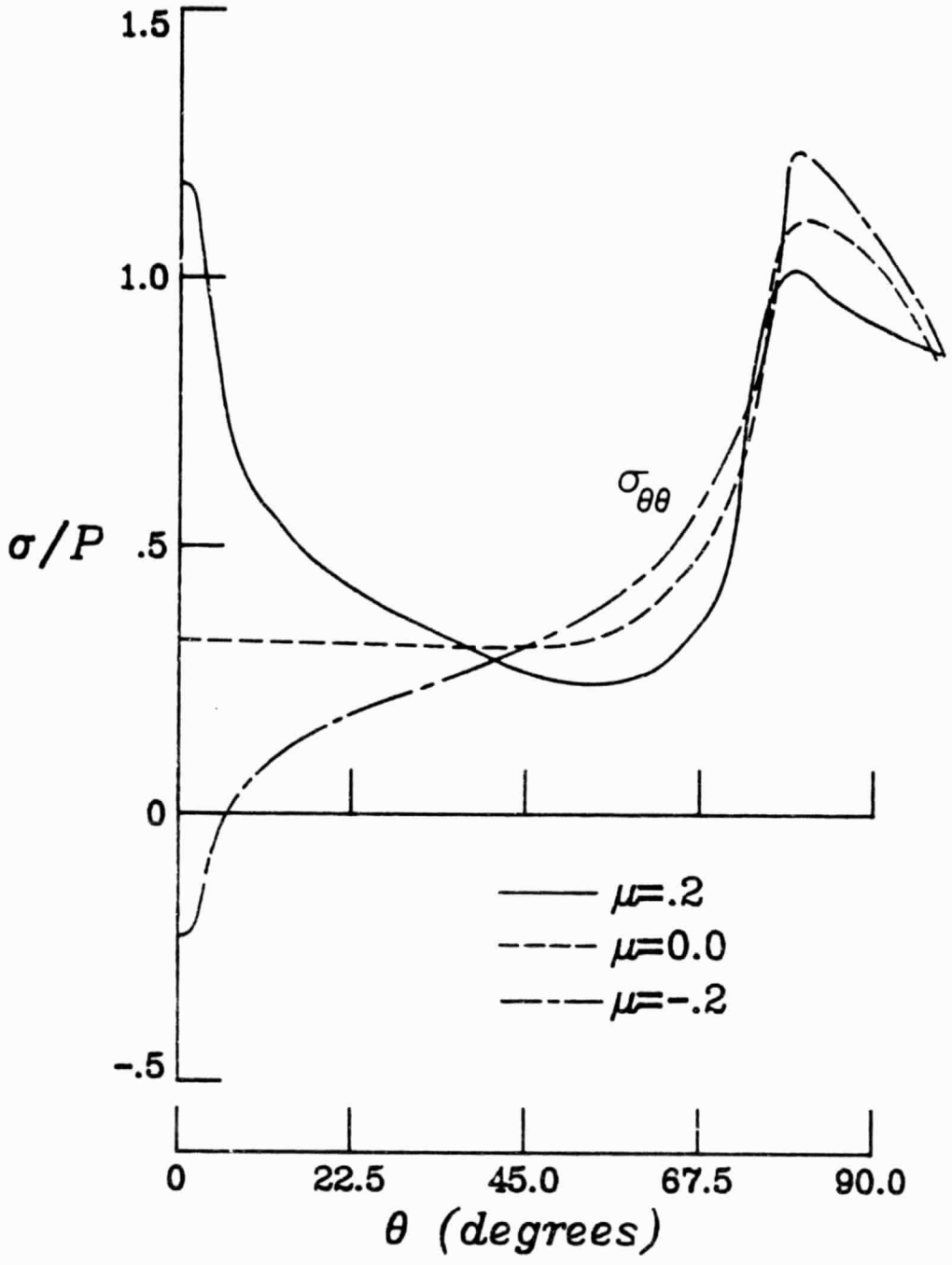

FIG. 45 HOOP STRESSES AT R = 1 FOR THE STANDARD CASE WITH UNLOADING, ZERO FRICTION, AND LOADING CONDITIONS.

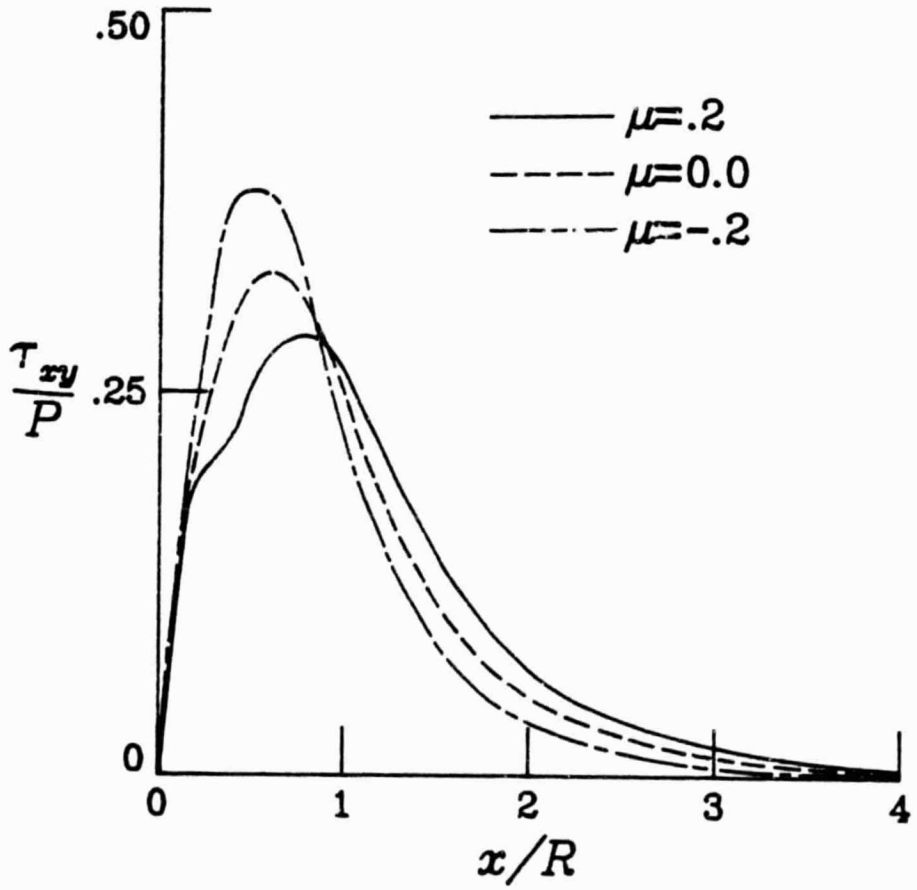

FIG. 46 SHEAR-OUT STRESSES FOR THE STANDARD CASE WITH UNLOADING, ZERO FRICTION, AND LOADING CONDITIONS.

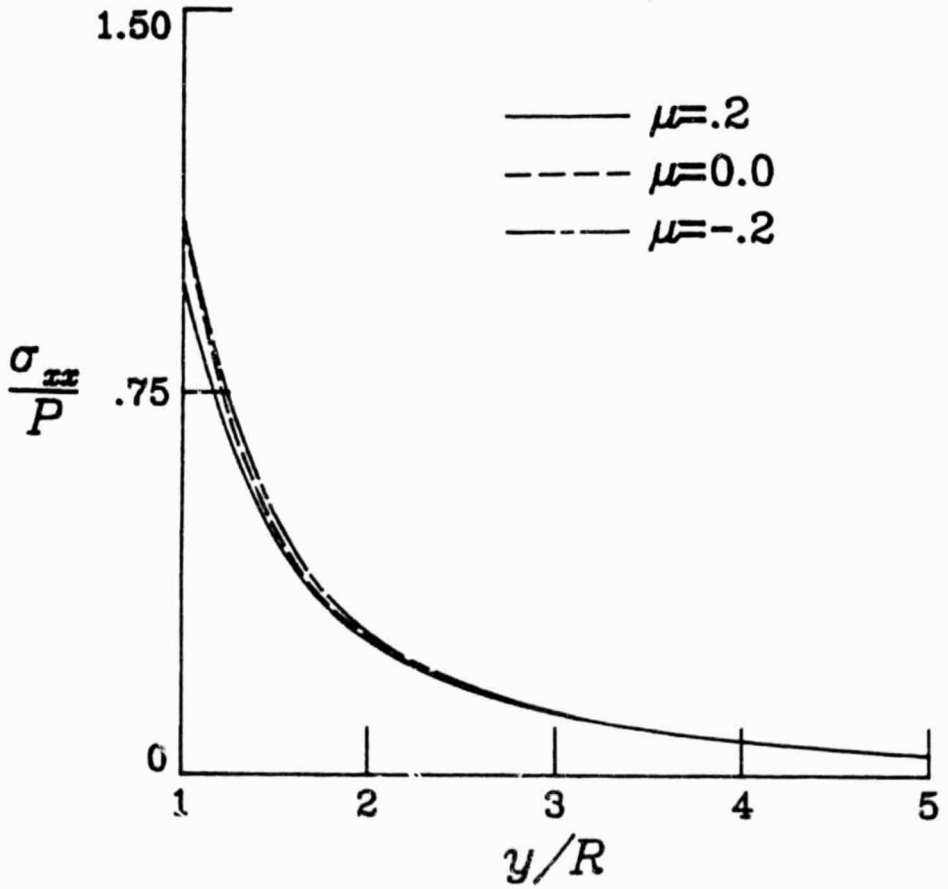

FIG. 47 NET-SECTION STRESSES FOR THE STANDARD CASE WITH UNLOADING, ZERO FRICTION, AND LOADING CONDITIONS.

ance, friction, and pin elasticity on the net section stress and the shear-out stress, for all cases considered is negligible.

The cases presented in this chapter are a sample of the analysis's capability. These figures have demonstrated the flexibility of the analysis and give a limited study of the parameters which effect the stress distribution in pin-loaded joints. This study should help define the importance of these parameters when future design analyses are made.

Isotropic plate

The Appendix presents the analysis and numerical results for the case of an isotropic rather than an orthotropic plate. Although not directly related to the analysis of composites, the pin-loaded isotropic plate is an interesting mechanics problem. Hence the results for this case, which were derived during the course of this investigation, are presented. In fact, the isotropic plate can be used, with a high degree of accuracy, to represent a quasi-isotropic plate.

Chapter 7

CONCLUSIONS & RECOMMENDATIONS

The work presented in this thesis has been directed towards a better understanding of the stresses in composite pin-loaded joints. The results of some simple cases were compared with those of previous researchers. More importantly, new results which represent an advance in the state of the art were presented. From this analysis, the following conclusions are drawn.

1) The algorithm developed has been shown to be accurate and efficient.
2) The material properties of the plate in pin-loaded joints strongly influence the stress distributions.
3) The magnitude of the coefficient of friction has a large effect on the stress distribution in the plots.
4) Loading direction greatly alters the stresses.
5) Clearance (or interference) can cause the location of the maximum hoop stress to vary.
6) Pin elasticity has almost no effect on the stress distributions for the cases studied here.

Although this analysis has produced a better understanding of the state of stress in pin-loaded joints, more work can be done in this area. Specifically the following recommendations are made:

1) Study finite width and end effects.
2) Study multiple-pin configurations.

3) Develop a failure theory to use in conjunction with the stress analysis.

4) Include the cases where the loading direction and the principle material directions do not coincide.

5) Possibly reformulate the problem so that the pin load is the independent parameter rather than the pin displacement.

6) Verify the results with an experimental investigation.

REFERENCES

1. T. A. Collings, "The Strength of Bolted Joints in Multi-Directional CFRP Laminates", Composites, Vol. 8, Jan. 1977, pp. 43-55.

2. W. G. Bickley, "The Distribution of Stress Round a Circular Hole in a Plate", Philos. Trans. R. Soc. London, Ser. A, Vol. 227, Aug. 1928, pp. 383-415.

3. T. de Jong, "Stresses Around Pin-Loaded Holes in Elastically Orthotropic or Isotropic Plates", J. Comp. Mat., Vol. 11, July 1977, pp. 313-331.

4. P. S. Theocaris, "The Stress Distribution in a Strip Loaded in Tension by Means of a Central Pin", J. Appl. Mech., Vol. 23, No. 1, March 1956, pp. 85-90.

5. D. W. Oplinger, K. R. Gandhi, "Stresses in Mechanically Fastened Orthotropic Lamintes", 2nd Conf. of Fib. Comp. in Flight Vehicle Design, May 1974, pp. 813-841.

6. T. de Jong, H. A. Vuil, "Stresses Around Pin-Loaded Holes in Elastically Orthotropic Plates with Arbitrary Load Direction", Report LR-333, Dept. of Aerospace Engr., Delft Univ. Tech., Sept. 1981.

7. D. W. Oplinger, K. R. Gandni, "Analytical Studies of Structural Performance in Mechanically Fastened Fiber-Reinforced Plates", Army Symp. on Solid Mech., Sept. 1974, pp. 211-240.

8. V. A. Eshwar, B. Dattaguru, A. K. Rao, "Partial Contact and Friction in Pin Joints", Rep. No. ARDB-STR-5010, Dept. Aeronaut. Engr., Ind. Inst. Sci., Dec. 1977.

9. S. P. Ghosh, B. Dattaguru, A. K. Rao, "Analysis of Joints with Elastic Pins", Rep. No. AE-3555, Dept. Aeronaut. Engr., Ind. Inst. Sci., Dec. 1978.

10. P. D. Mangalgiri, B. Dattaguru, "Elastic Analysis of Pin Joints in Composite Plate", Rep. No. ARDB-STR-5014, Dept. Aeronaut. Engr., Ind. Inst. Sci., Nov. 1980.

11. T. de Jong, "The Influence of Friction on the Theoretical Strength of Pin-Loaded Holes in Orthotropic Plates", Rep. No. LR-350, Dept. of Aerospace Engr., Delft Univ. Tech., March 1982.

12. J. P. Waszczak, T. A. Cruse, "Failure Mode and Strength Predictions of Anisotropic Bolt Bearing Specimens", J. Comp. Mat., Vol. 5, July 1971, pp. 421-425.

13. B. L. Agarwal, "Static Strength Prediction of Bolted Joint in Composite Materials", AIAA Journal, Vol. 18 No. 11, Nov. 1980, pp. 1371-1375.

14. F. K. Chang, R. A. Scott, G. S. Springer, "Strength of Mechanically Fastened Composite Joints", J. Comp. Mat., Vol. 16, Nov. 1982, pp. 470-494.

15. S. P. Garbo, J. M. Ogonowski, "Effect of Variances and Manufacturing Tolerances on the Design Strength and Life of Mechanically Fastened Composite Joints", AFWAL-TR-81-3041, Vols. 1-3, April 1981.

16. J. H. Crews, C. S. Hong, "Stress-Concentration Factors for Finite Orthotropic Laminates with a Pin-Loaded Hole", NASA TP 1862, May 1981.

17. T. L. Wilkinson, "Stresses in the Neighborhood of Loaded Holes in Wood with Applications to Bolted Joints", Ph.D. Dissertation, Univ. of Wisc.-Madison, Available through Univ. Microfilms, 1978.

18. R. E. Rowlands, M. U. Rahman, T. L. Wilkinson, Y. I. Chiang, "Single- and Multiple-Bolted Joints in Orthotropic Materials", Composites, Vol. 13, No. 3, July 1982, pp. 273-278.

19. F. L. Matthews, C. M. Wong, S. Chryssafitis, "Stress Distribution Around a Single Bolt in Fibre-Reinforced Plastic", Composites, Vol. 13, No. 3, July 1982, pp. 316-322.

20. N. P. Humphris, "Migration of the Point of Maximum Stress in a Laminated Composite Lug Structure--A Stepwise Approach", Jointing in Fibre Reinforced Plastics, Imperial College, London, Sept. 1978, pp. 79-86.

21. S. R. Soni, "Inplane Stress Analysis of Multidirectional Composite Laminates with a Loaded Fastener Hole Using Stress Distribution in the Constituent Angle Ply Laminates", 6th Annual Mech. of Comp. Review, AFWAL-TR-81-4001, Feb. 1981, pp. 85-89.

22. C. M. S. Wong, F. L. Matthews, "A Finite Element Analysis of Single and Two-Hole Bolted Joints in Fibre-Reinforced Plastic", J. Comp. Mat., Vol. 15, Sept. 1981, pp. 481-491.

23. G. S. Ansell, R. G. Loewy, S. E. Wiberley, "Composite Structural Materials", Semi Annual Progress Report for Sept. 30, 1981 through April 30, 1982, Rensselaer Poly. Inst., July 1982.

24. M. M. Frocht, H. N. Hill, "Stress-Concentration Factors Around a Central Circular Hole in a Plate Loaded Through Pin in the Hole", Trans. ASME, J. Appl. Mech., Vol. 62, March 1940, pp. A-5-A-9.

25. M. M. Frocht, Photoelasticity Vol. II, John Wiley & Sons, 1948.

26. M. Nisida, H. Saito, "Stress Distributions in a Semi-Infinite Plate Due to a Pin Determined by Interferometric Method", Experimental Mechanics, Vol. 6, No. 5, op. 233-279.

27. T. L. Wilkinson, E. A. Fuchs, R. E. Rowlands,"Photomechanical Determination of Stresses in the Neighbourhood of Loaded Holes in Anisotropic Media", Proc. 6th Int'l. Conf. of Exp. Stress Anal., 1978, pp. 121-126.

28. R. Prabhakaran, "Photoelastic Investigation of Bolted Joints in Composites", Composites, Vol. 13, No. 3, July 1982, pp. 253-256.

29. M. W. Hyer, D. Liu, "Stresses in a Quasi-Isotropic Pin-Loading Connector Using Photoelasticity," submitted to Experimental Mechanics for consideration of publication.

30. T. H. Lambert, R. J. Brailey, "The Influence of the Coefficient of Friction on the Elastic Stress Concentration Factor for a Pin-Jointed Connection", Aeronautical Quarterly, Vol. 13, Feb. 1962, pp. 17-29.

31. W. J. Quinn, F. L. Matthews, "The Effect of Stacking Sequence on Pin-Bearing Strength in Glass Fibre Reinforced Plastic", J. Comp. Mat., Vol. 11, April 1977, pp. 139-154.

32. J. H. Stockdale, F. L. Matthews, "The Effect of Clamping Pressure on Bolt Bearing Loads in Glass Fibre-Reinforced Plastics", Composites, Vol. 7, Jan. 1976, pp. 34-38.

33. K. N. Snivakumar, J. H. Crews, "An Equation for Bolt Clampup Relaxation in Transient Environments", Comp. Tech. Review, Vol. 4, No. 4, 1982, pp. 132-135.

34. J. R. Eisenmann, J. L. Leonhardt, "Improving Composite Bolted Joint Efficiency by Laminate Tailoring", Joining of Composite Materials, ASTM STP 749, 1981, pp. 117-130.

35. T. A. Collings, "The Strength of Bolted Joints in Multi-Directional CFRP Laminates", Composites, Vol. 8, Jan. 1977, pp. 43-55.

36. G. R. Pyner, F. L. Matthews, "Comparison of Single and Multi-Hole Bolted Joints in Glass Fibre Reinforced Plastic", J. Comp. Mat., Vol. 13, July 1979, pp. 232-239.

37. M. W. Hyer, M. C. Lightfoot, "Ultimate Strength of High-Load-Capacity Composite Bolted Joints", Composite Materials: Testing and Design, ASTM STP 674, 1979, pp. 118-136.

38. M. W. Hyer, J. C. Perry, M. C. Lightfoot, "Load Transfer in Composite Bolted Joints", Paper # 80-0779-CP, presented at AIAA 21st SDM Conference, Seattle, WA,, May 1980.

39. E. W. Godwin, F. L. Matthews, P. F. Kilty, "Strength of Multi-Bolt Joints in GRP", Composites, Vol. 13, No. 3, July 1982, pp. 268-272.

40. G. R. Wichorek, "Experimental Data on Single-Bolt Joints in Quasi-Isotropic Graphite/Polyimide Laminates", NASA TP 2015, May 1982.

41. J. M. Whitney, R. J. Nuismer, "Stress Fracture Criteria for Laminated Composites Containing Stress Concentrations", J. Comp. Mat., Vol. 8, July 1974, pp. 253-265.

42. L. J. Hart-Smith, "Bolted Joints in Graphite-Epoxy Composites", NASA CR 144899, June 1976.

43. T. A. Collings, "On the Bearing Strengths of CFRP Laminates", Composites, Vol. 13, No. 3, July 1982, pp. 241-252.

44. E. W. Godwin, F. L. Matthews, "A Review of the Strength of Joints in Fibre-Reinforced Plastics", Composites, Vol. 11, July 1980, pp. 155-160.

45. D. W. Oplinger, "On the Structural Behavior of Mechanically Fastened Joints in Composite Structures", Fibrous Comp. in Structural Design, 1980, pp. 575-602.

46. N. I. Muskhelishvili, Some Problems of the Mathematical Theory of Elasticity, Trans. J.R.M. Radok, Noordnoff, 1977.

47. I. S. Sokolnikoff, Mathematical Theory of Elasticity, 2nd Ed., McGraw-Hill, 1956.

48. L. M. Milne-Thomson, Plane Elastic Systems, 2nd Ed., Springer-Verlag, 1968.

49. S. G. Lekhnitskii, Anisotropic Plates, Trans. S. W. Tsai and T. Cheron, Gordon & Breach, 1968.

Appendix

ISOTROPIC PLATE ANALYSIS

The research presented in this thesis is primarily concerned with the development of an algorithm which predicts the stress distribution in pin-loaded orthotropic plates. The mathematics change however when the plate material is isotropic. Quasi-isotropic laminates can be treated successfully with an orthotropic analysis, but to remain rigorous in the mathematical development, the truly isotropic case must be treated separately. The mathematics for this case is presented in this appendix to complete the analysis of pin-loaded joints.

The case of an elastically pin-loaded isotropic plate was actually developed before that of the orthotropic plate in the current research program. This was done because the analysis of the isotropic plate parallels that of the isotropic pin. None of the complicated mappings required for the orthotropic case are required for the isotropic case. With the simpler analysis of the isotropic case, the problems associated with the analysis method described in Chapter 2 were solved before the orthotropic case was undertaken. Enough differences exist between these cases, however, to warrant a separate description of the isotropic case in this appendix.

The pin analysis technique remains the same for pin-loaded isotropic plates. The same is true for the overall method of analysis discussed in Chapter 2. The only difference in the problem formulation is the analysis of the plate. Thus, this appendix will be concerned only with the development of the analysis for an isotropic plate. The

governing equations for the pin and plate are similar, therefore an abbreviated version of their development will be presented here.

The constitutive, compatibility, and strain-displacement equations remain the same as they appear in Chapter 3. The equilibrium equations, however, contain no body force for the analysis of the plate. This similifies the governing biharmonic equation to the following form

$$\frac{\partial^4 F}{\partial x^4} + 2\frac{\partial^4 F}{\partial x^2 \partial y^2} + \frac{\partial^4 F}{\partial y^4} = 0 \tag{A1}$$

Integrating eq. A1 yields the following Goursat equation

$$F = \frac{1}{2}\left[z\bar{\phi} + \bar{z}\phi + \chi + \bar{\chi}\right] \tag{A2}$$

Note that eqs. 47 and 63 of Chapter 3 become eqs. A1 and A2 when the body forces are set to zero.

The fundamental stress combinations can now be found in terms of the two stress functions. These combinations are defined by eqs. 65 and 66 of Chapter 3. With the body forces set to zero these equations become

$$\sigma_{yy} + \sigma_{xx} = 2\left[\Phi(z) + \overline{\Phi(\bar{z})}\right] \tag{A3}$$

$$\sigma_{yy} - \sigma_{xx} + 2i\tau_{xy} = 2\left[\bar{z}\Phi'(z) + \Psi(z)\right] , \tag{A4}$$

where $\psi(z) \equiv \chi'(z)$

$\Psi(z) \equiv \psi'(z)$

$\Phi(z) \equiv \phi'(z)$.

Using the appropriate transformations, these combinations can be written in the r-θ coordinate system as

$$\sigma_{\theta\theta} + \sigma_{rr} = 2[\Phi(z) + \overline{\Phi(\overline{z})}] \tag{A5}$$

$$\sigma_{\theta\theta} - \sigma_{rr} + 2i\tau_{r\theta} = 2\sigma^2[\overline{z}\Phi'(z) + \Psi(z)] , \tag{A6}$$

where $\sigma \equiv e^{i\theta}$.

Combining eqs. A5 and A6 yields the required traction boundary condition:

$$N\text{-}iT = \Phi(z) + \overline{\Phi(\overline{z})} - \sigma^2[\overline{z}\Phi(z) + \Psi(z)] . \tag{A7}$$

The form of the stress functions must now be defined. As before, these functions are expanded in Laurent series

$$\Phi(z) = \sum_{-\infty}^{\infty} a_n z^n \tag{A8}$$

$$\Psi(z) = \sum_{-\infty}^{\infty} b_n z^n . \tag{A9}$$

In Chapter 4, the infinite orthotropic plate was required to satisfy the following conditions:

1) The stresses at infinity remain bounded, and,

2) The plate must remain in equilibrium.

When these conditions are enforced for the isotropic plate, the following restrictions are imposed on the form of the stress functions

$$a_n = 0 \qquad n \geq 0 \tag{A10}$$

$$b_n = 0 \qquad n \geq 0 \tag{A11}$$

Thus the following forms for the stress functions remain

$$\Phi(z) = \sum_{n=1}^{\infty} \frac{\alpha_n}{z^n} \tag{A12}$$

$$\Psi(z) = \sum_{n=1}^{\infty} \frac{b_n}{z^n} . \tag{A13}$$

Substituting these forms into eq. A7 and noting that $z = \sigma$ on the boundary, the following equation is obtained

$$N\text{-}iT = \sum_{-\infty}^{\infty} A_n \sigma^n = \sum_{n=1}^{\infty} a_n \sigma^n + \sum_{n=1}^{\infty} \bar{a}_n \sigma^n + n \sum_{n=1}^{\infty} \frac{\alpha_n}{\sigma^n} - b_1 \sigma - \sum_{n=0}^{\infty} \frac{b_n+2}{\sigma^n} . \tag{A14}$$

As before, like powers of σ are compared to find the coefficients a_n and b_n. This procedure is summarized in Table A1.

Table A1

Coefficients for the Stress Functions Φ and Ψ for the Isotropic Plate.

Load	a_n	b_n
$A_0 = 1$	$a_n = 0$	$b_2 = -1$
$A_{-1} = 1$	$a_n = 0$	$b_3 = -1$
$A_{+1} = 1$	*	*
$A_{-2} = 1$	$a_n = 0$	$b_4 = -1$
$A_{+2} = 1$	$a_2 = 1$	$b_4 = 3$
.	.	.
.	.	.
.	.	.
.	.	.
$A_{-k} = 1$	$a_n = 0$	$b_{(k+2)} = -1$
$A_{+k} = 1$	$a_k = 1$	$b_{(k+2)} = k+1$

*See text

The equations which result from setting $A_{+1} = 1$ and all other $A_n = 0$ are

$$\sigma = \bar{a}_1\sigma - b_1\sigma \tag{A15}$$

$$0 = a_1\sigma^{-1} - b_3\sigma^{-1} . \tag{A16}$$

Thus, there are only two equations but three unknowns for $A_{+1} = 1$. A third equation is obtained when restrictions on the displacement field are imposed. The derivation of the displacement equation follows that of Chapter 3 with one modification. This modification is the result of the fact that the plate is assumed to be in a state of generalized plane stress, while the pin was assumed to be in a state of plane strain. With this difference accounted for, the displacement equation becomes

$$u - iv = \frac{1}{2G}[\kappa_1\bar{\phi} - \bar{z}\Phi - \psi] , \tag{A17}$$

where $\kappa_1 \equiv \frac{3-4\nu}{1-\nu}$.

Recall that

$$\phi \equiv \int \Phi \, dz \tag{A18}$$

$$\psi \equiv \int \Psi \, dz . \tag{A19}$$

These integrations yield a logarithmic term similar to that of eqs. 115 and 116 of Chapter 4. The logarithmic terms are multivalued and must be accounted for in this analysis. Examining the displacements at $\theta = 0$ and $\theta = 2\pi$ yields the following

$$(u - iv)_{\theta=2\pi} = 2\pi i(-\kappa_1 \bar{a}_1 - b_1) + (u - iv)_{\theta=0} . \tag{A20}$$

If the displacements are to be single-valued, then the following must be true

$$\kappa_1 \bar{a}_1 + b_1 = 0 . \tag{A21}$$

Using equations A15, A16 and A21, the value for a_1, b_1, and b_3 can be found. These are

$$a_1 = \frac{1}{1+\alpha_1} , \tag{A22}$$

$$b_1 = -\frac{\kappa_1}{1+\kappa_1} , \tag{A23}$$

$$b_3 = \frac{2}{1+\kappa_1} . \tag{A24}$$

With these results, the elastic response of the plate due to the $e^{ik\theta}$ loads is completely defined. The analyses of Chapters 2 and 3 can now be combined with this appendix to produce an algorithm capable of predicting the stresses in pin-loaded isotropic plates. The results

of this procedure will now be discussed.

A standard case has been chosen to present the results for the isotropic case. Variations of the pin modulus, clearance, and the coefficient of friction will be made on the standard case. The parameters adopted for the standard case are

plate - Aluminum ($E = 10^7$ psi, $\nu = 0.25$)

pin - Aluminum ($E = 10^7$ psi, $\nu = 0.25$)

friction coefficient - 0.3

loading direction - positive (i.e., $\mu = -0.3$)

clearance - $\lambda = 0.01$

rigid body pin displacement - $\delta = 0.05$

All of these properties are felt to accurately represent actual values which may be encountered in typical aerospace applications. Variations on the standard case will now be presented.

Figures A1 and A2 show the stresses at R = 1 for the standard case with variable pin modulii. Rigid, steel, and aluminum pins are compared. It is evident that pin modulus plays a small role in the results presented here. A rigid pin assumption appears to be well justified based on these findings.

The stresses at R = 1 for the standard case with variable pin/plate clearance are presented in figs. A3 and A4. The changing contact angle is seen to alter the location of the peak hoop stress for these cases. This may affect the location of first damage in isotropic plates.

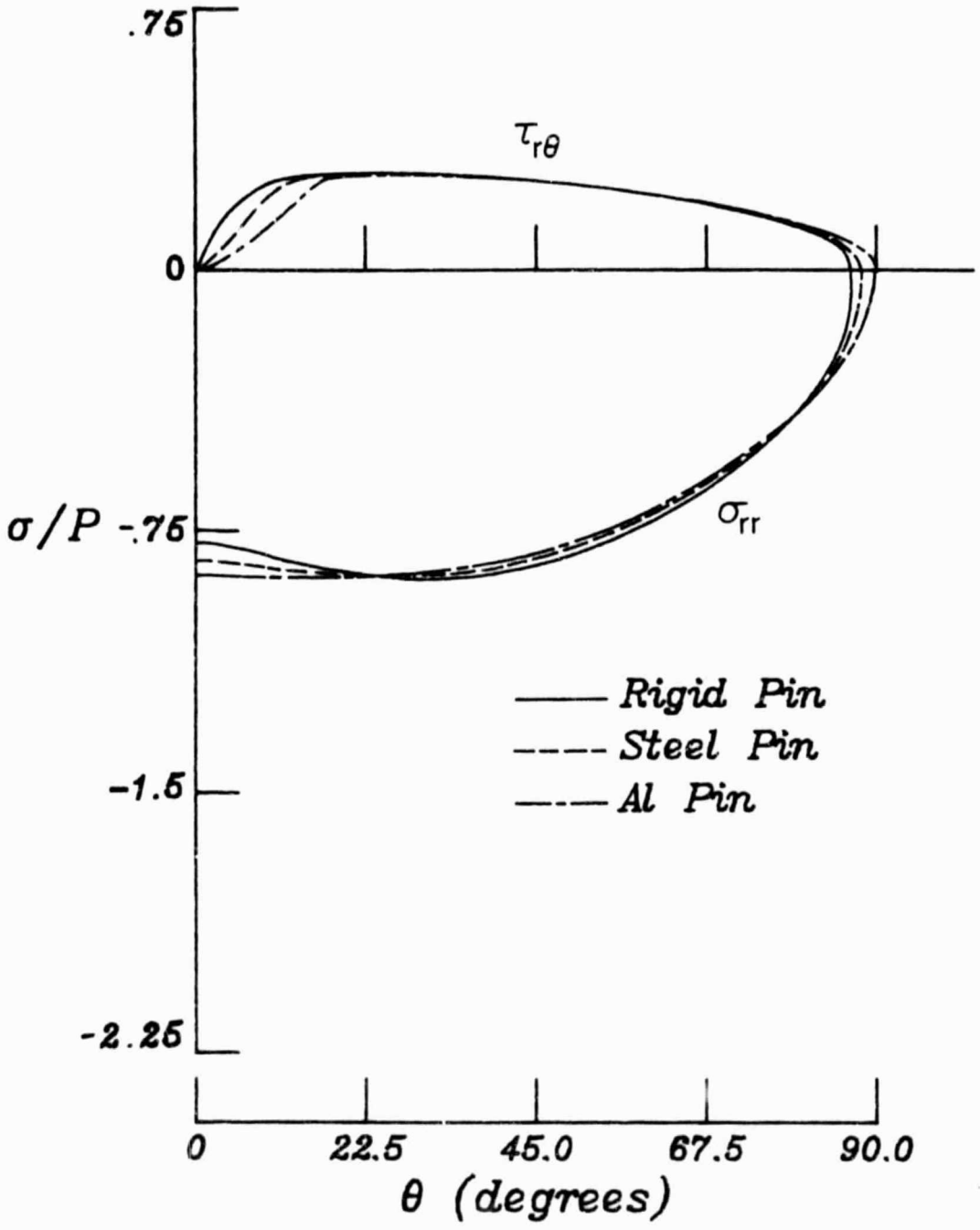

FIG. A1 CONTACT STRESSES AT R = 1 FOR THE STANDARD ISOTROPIC CASE WITH VARIABLE PIN MODULII.

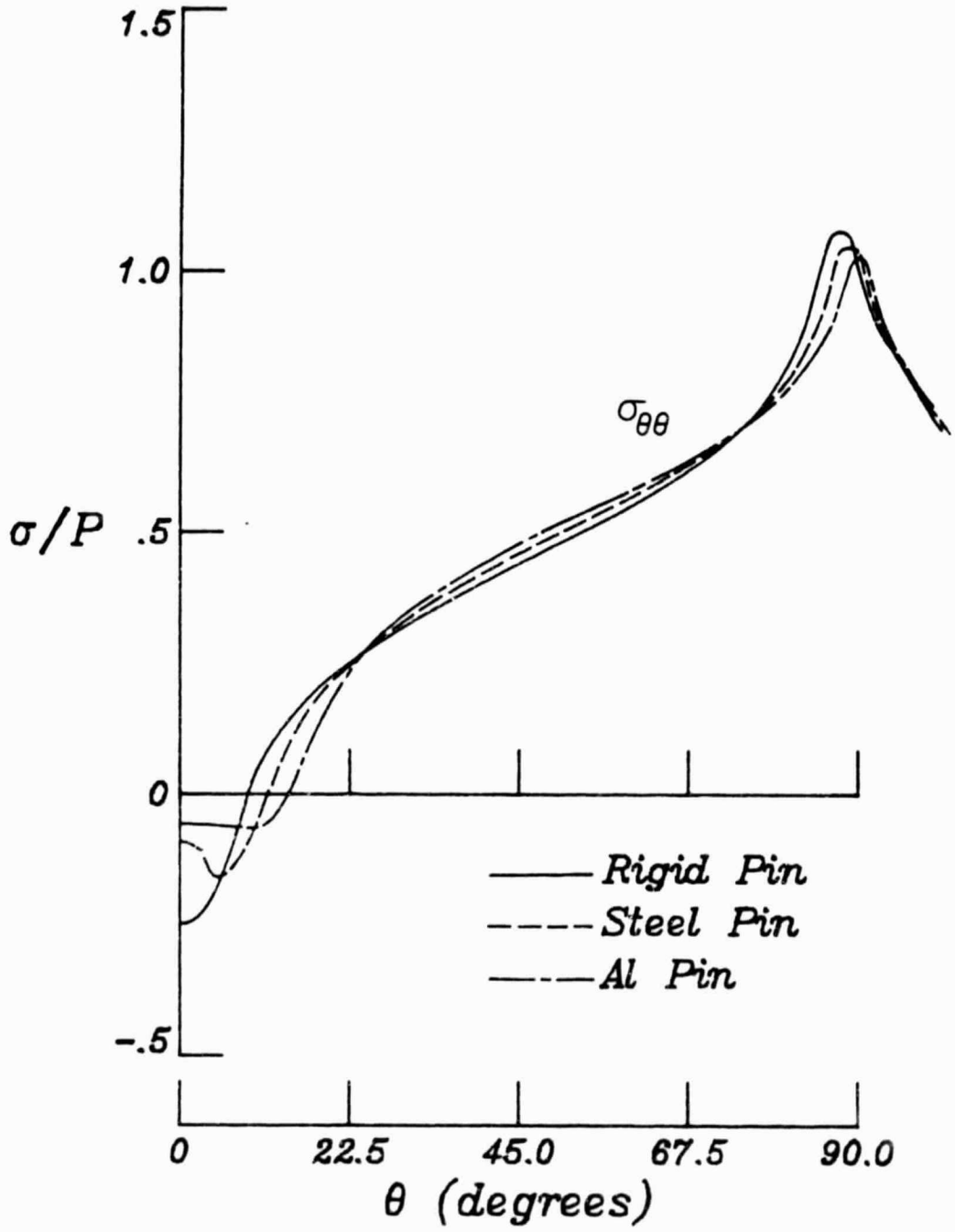

FIG. A2 HOOP STRESSES AT R = 1 FOR THE STANDARD ISOTROPIC CASE WITH VARIABLE PIN MODULII.

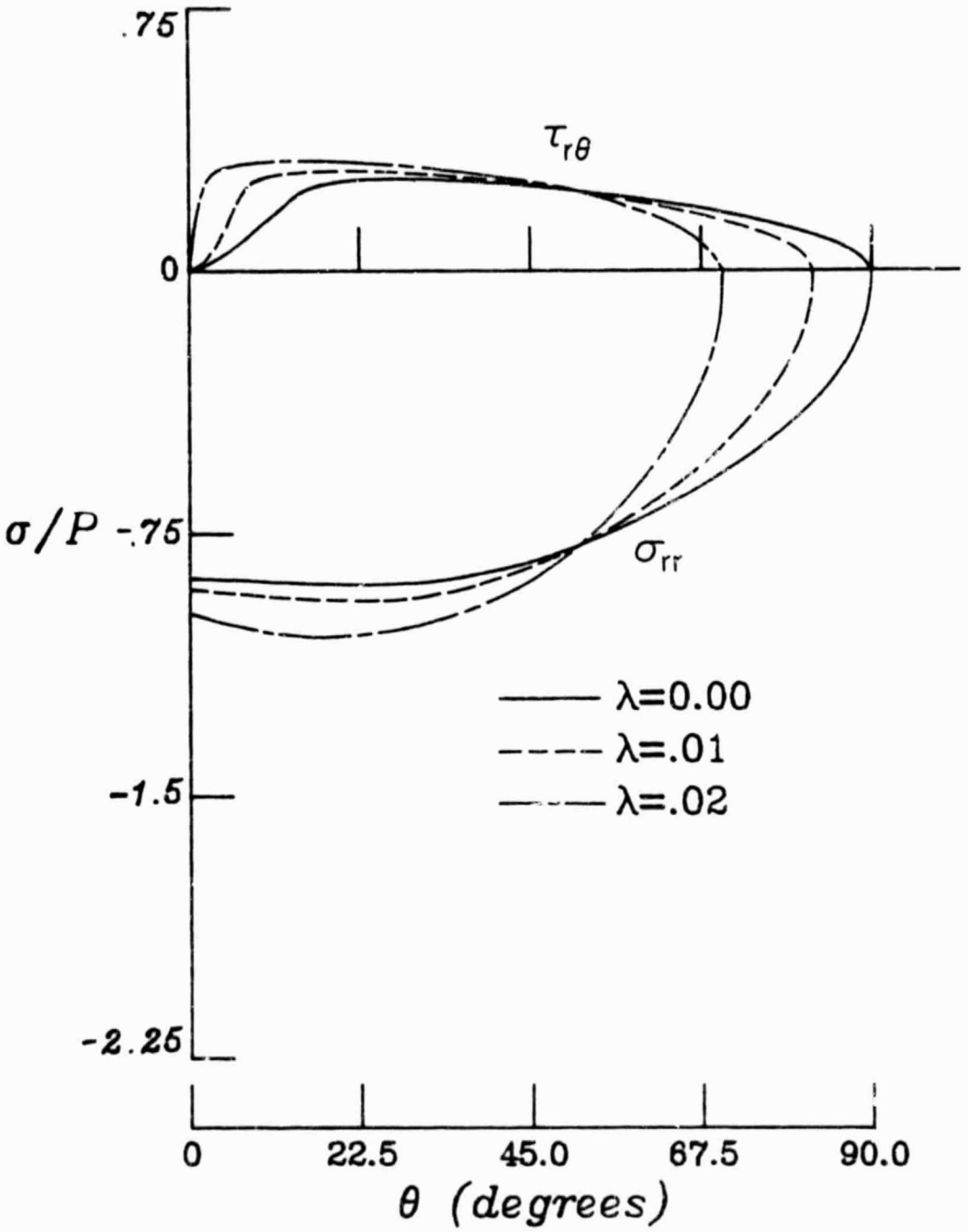

FIG. A3 CONTACT STRESSES AT R = 1 FOR THE STANDARD ISOTROPIC CASE WITH VARIABLE CLEARANCE, λ.

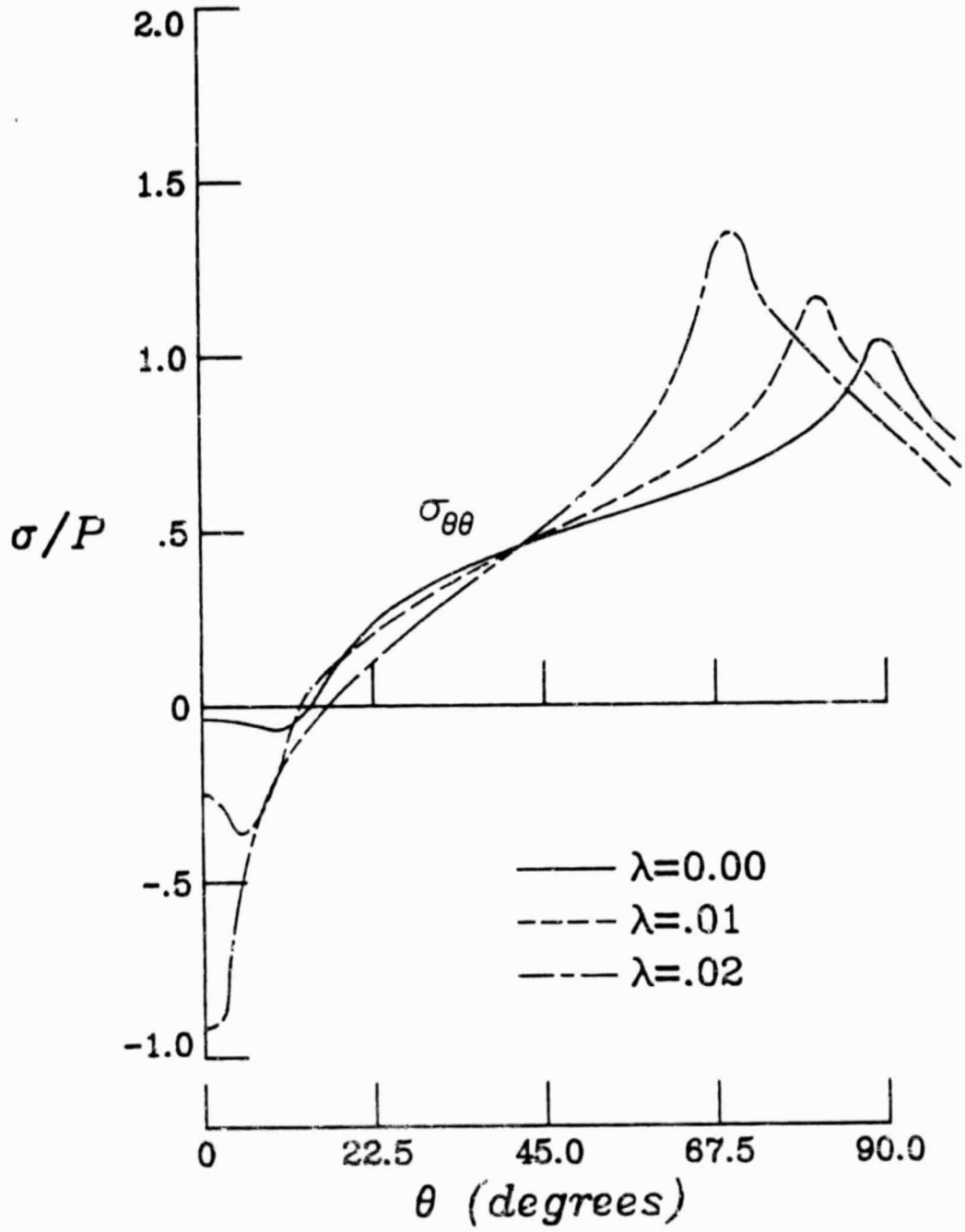

FIG. A4 HOOP STRESSES AT R = 1 FOR THE STANDARD ISOTROPIC CASE WITH VARIABLE CLEARANCE, λ.

Finally, figs. A5 and A6 show the stresses for the standard case with variable friction coefficients. In each case, the plate is assumed to be under monotonically increasing loads (i.e., μ is negative). Friction is seen to alter the normal stress distribution and it causes the hoop stress to change from tensile to compressive at $\theta = 0°$.

Other variations on the standard case will not be presented here due to their similarity with the results presented in Chapter 6. In fact the conclusions drawn for the orthotropic case appear to be valid for the isotropic case as well.

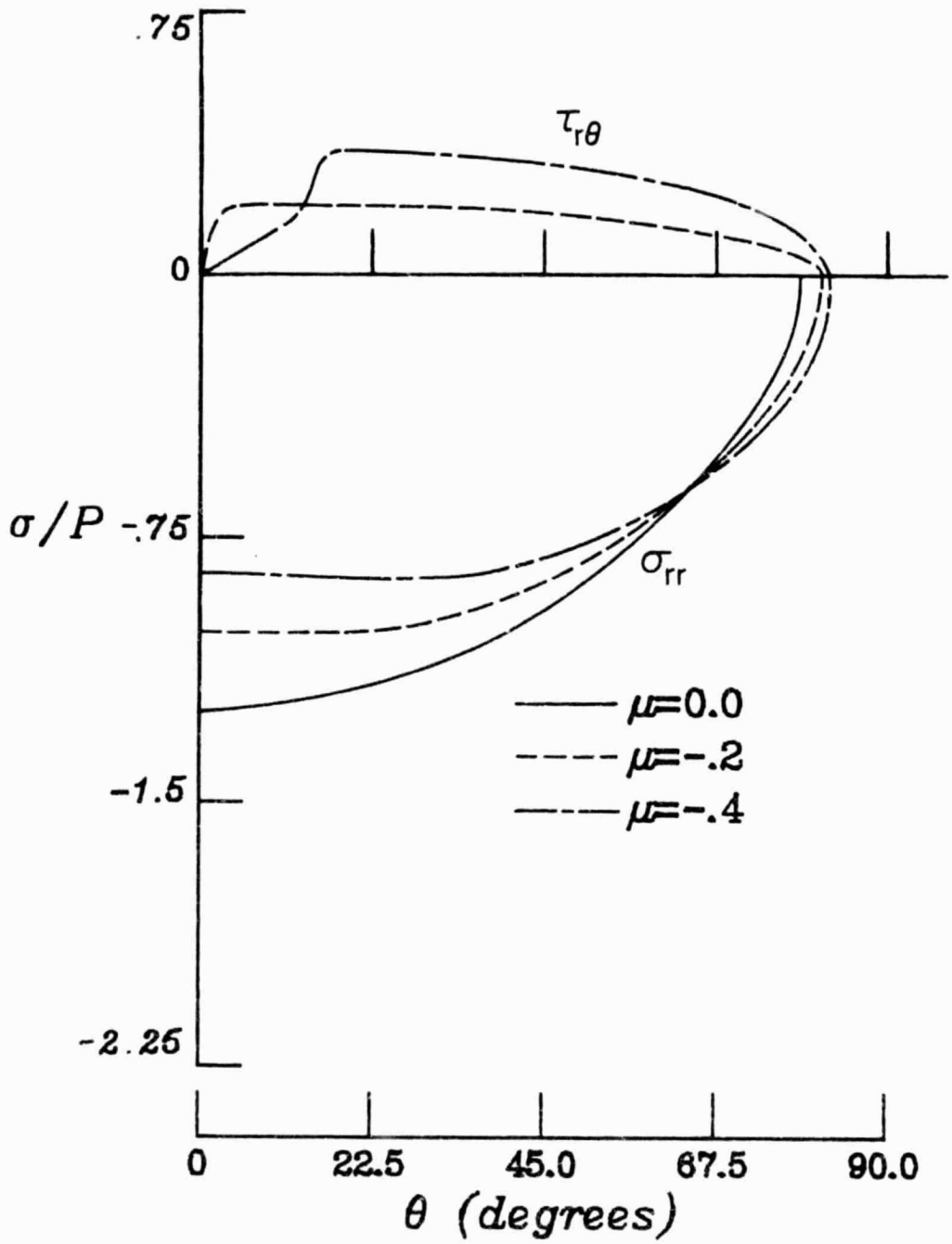

FIG. A5 CONTACT STRESSES AT R = 1 FOR THE STANDARD ISOTROPIC CASE WITH VARIABLE FRICTION COEFFICIENT, μ.

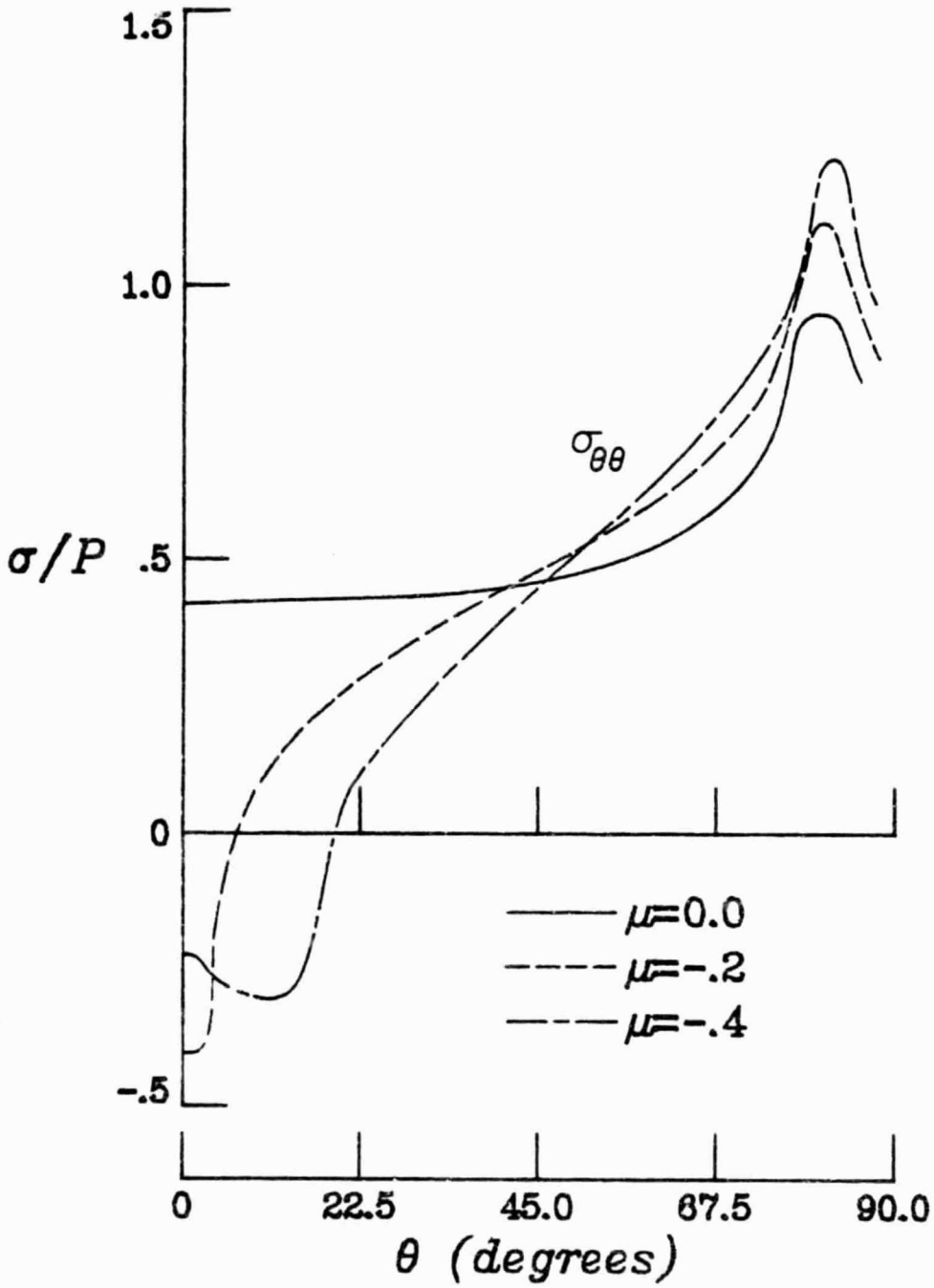

FIG. A6 HOOP STRESSES AT R = 1 FOR THE STANDARD ISOTROPIC CASE WITH VARIABLE FRICTION COEFFICIENT, μ.

BIBLIOGRAPHIC DATA SHEET	1. Report No. CCMS-85-05	2. VPI-E-85-13	3. Recipient's Accession No.

4. Title and Subtitle

The Stress Distribution in Pin-Loaded Orthotropic Plates

5. Report Date: June, 1985

6.

7. Author(s): E. C. Klang and M. W. Hyer

8. Performing Organization Rept. No. CCMS-85-05 VPI-E-85-13

9. Performing Organization Name and Address

Virginia Polytechnic Institute & State University
Engineering Science and Mechanics
Blacksburg, Virginia 24061

10. Project/Task/Work Unit No.

11. Contract/Grant No. NAG-1-343

12. Sponsoring Organization Name and Address

National Aeronautics and Space Administration
Langley Research Center
Hampton, Virginia 23665

13. Type of Report & Period Covered

14.

15. Supplementary Notes

16. Abstracts

The performance of mechanically fastened composite joints was studied. Specifically, a single-bolt connector was modeled as a pin-loaded, infinite plate. The model that was developed used two dimensional, complex variable, elasticity techniques combined with a boundary collocation procedure to produce solutions for the problem. Through iteration, the boundary conditions were satisfied and the stresses in the plate were calculated. Several graphite epoxy laminates were studied. In addition, parameters such as the pin modulus, coefficient of friction, and pin-plate clearance were varied.

Conclusions drawn from this study indicate: 1) The material properties (i.e., laminate configuration) of the plate alter the stress state and, for highly orthotropic materials, the contact stress deviates greatly from the cosinusoidal distribution often assumed; 2) Friction plays a major role in the distribution of stresses in the plate; 3) Reversing the load direction also greatly effects the stress distribution in the plate; 4) Clearance (or interference) fits change the contact angle and thus the location of the peak hoop stress; 5) A rigid pin appears to be a good assumption for typical material systems.

17. Key Words and Document Analysis 17a. Descriptors

orthotropic elasticity, contact stresses, friction, complex variables, bolted joints, composites, stress concentrations, orthotropic plates

17b. Identifiers/Open-Ended Terms

17c. COSATI Field Group 24-01, 39-02, 39-07

18. Availability Statement	19. Security Class (This Report)	21. No. of Pages
Distribution unlimited	UNCLASSIFIED	168
	20. Security Class (This Page) UNCLASSIFIED	22. Price